Remote Sensing of Suspended Sediment in Mayagüez Bay associated with Inland Soil Erosion Rates

by

VILMALIZ RODRÍGUEZ-GUZMÁN

A thesis submitted in partial fulfillment of the requirements for the degree of

MASTER OF SCIENCE
in
Geology

UNIVERSITY OF PUERTO RICO
MAYAGÜEZ CAMPUS
2009

Approved by:

_____	_____
Hernán Santos, Ph.D. Member, Graduate Committee	Date
_____	_____
Eric Harmsen, Ph.D. Member, Graduate Committee	Date
_____	_____
Fernando Gilbes Santaella, Ph.D. President, Graduate Committee	Date
_____	_____
Ana J. Navarro Rodríguez, Ph.D. Representative of Graduate Studies	Date
_____	_____
Fernando Gilbes Santaella, Ph.D. Chairperson of the Department	Date

ABSTRACT

This study combined *in situ* optical measurements, satellite derived reflectance and geospatial data to evaluate total suspended sediment (TSS) spatial and temporal variations in Mayagüez Bay and their relationship with inland soil erosion rates. Several analyses were developed using *in situ* remote sensing reflectance (R_{rs}), backscattering (b_b) and TSS data collected on research cruises carried out between January 2004 and October 2006. These analyses identified the range between 589 nm to 645 as the target spectral region of the electromagnetic spectrum to estimate TSS, and showed the potential of using red to green ratios to improve these estimations. Positive relationships were observed between these parameters and MODIS band 1 reflectance data, however, more data corresponding to high TSS conditions are necessary to better define and validate the results. Three algorithms to estimate TSS were generated for the study area. Best validation results (RMSE= 4.76 mg/l) were observed when using an exponential equation defining relationship between field R_{rs} at 645 nm and MODIS band 1 data. This study incorporated an innovative methodology which used satellite derived TSS products to estimate suspended sediment load in order to compared coastal variation with inland soil erosion estimations. Geographic Information Systems techniques were incorporated in this analysis by applying the Revised Universal Soil Loss Equation (RUSLE) to Mayagüez Bay watershed. Annual spatially variable soil erosion rates and sediment yield estimations were produced for this basin in a five years period (2001-2005), and compared with data collected at the Rio Rosario USGS gauge station. Results of this study represent an important advancement in the development and application of Remote Sensing and GIS based studies in tropical coastal waters.

RESUMEN

Este estudio combinó medidas ópticas *in situ*, medidas de reflectancia colectadas en plataformas satelitales y datos geo-espaciales para la evaluación de variaciones espaciales y temporales del total de sedimentos suspendidos (TSS) en la Bahía de Mayagüez y su relación con tazas de erosión terrestres. Varios análisis fueron desarrollados utilizando reflectancia teledetectada *in situ* (R_{rs}), retrodispersión (b_b), y datos de TSS que fueron colectados en cruceros de investigación llevados a cabo entre enero del 2004 y diciembre del 2006. Estos análisis identificaron el rango entre 589 nm y 645 nm como la región espectral clave al momento de derivar estimados de TSS. Además, se mostró el potencial de utilizar la razón de bandas verde y rojo para mejorar estos estimados. Relaciones observadas entre estos parámetros y datos de la banda 1 de MODIS fueron todas positivas, sin embargo más datos representativos de condiciones predominadas por valores altos de TSS son necesarios para lograr definir mejor y validar estos resultados. Tres algoritmos para estimar TSS fueron generados para el área de estudio. Los mejores resultados de validación (RMSE- 4.76 mg/l) se observaron cuando se utilizó una ecuación exponencial para definir la relación entre medidas de campo de R_{rs} a 645 nm y valores de la banda 1 de MODIS. Este estudio incorporó una metodología innovadora la cual utilizó productos de TSS, derivados de datos de satélite, para generar estimados de descarga de sedimentos a la bahía y luego relacionarlos con estimados de erosión de suelo terrestre. Técnicas de sistemas de información geográfica fueron incorporadas en este análisis a través de la aplicación de la Ecuación Universal de Pérdida de Suelos Revisada (RUSLE, por sus siglas en Inglés) a la cuenca hidrográfica de la Bahía de Mayagüez. Para el área de estudio se generaron tazas de erosión anuales espacialmente variables y estimados de producción de sedimentos correspondientes a un periodo de cinco años (2001-2005), estos estimados fueron comparados con datos colectados en la estación del USGS localizada en el Río Rosario. Los resultados de este estudio representan un avance importante en el desarrollo y aplicación de estudios basados en Percepción Remota y Sistemas de Información Geográfica en aguas costeras tropicales.

To the roots of my existence and the past that brought me here …

"Where the world ceases to be the scene of our personal hopes and wishes,
where we face it as free beings admiring, asking and observing,
there we enter the realm of Art and Science"

-Albert Einstein

ACKNOWLEDGEMENTS

I will always be grateful for the great amount of help and support I received during this journey. My most sincere gratitude to all the people and organizations that contributed to this study and make this accomplishment possible.

Special thanks to:

Dr. Fernando Gilbes Santaella

…who offered me this wonderful opportunity. Thanks for your valuable guidance, patience and strong commitment.

Dr. Hernán Santos and Dr. Eric Harmsen

…for your willingness to be part of this effort, and all the time and knowledge shared.

Dr. Carlos Ramos and Dr. Ramón López

...your great advice and support during this process will always be greatly appreciated.

Patrick Reyes and Dr. Marcos Rosado

…who participated in many of the research cruises, processed part of the field data and provided good recommendations.

Dr. Hamed Parsiani, Yakaira Pérez and all participants of the NOAA-CREST Program

… for their great contribution to the progress of Remote Sensing Sciences.

Faculty, staff and fellow students at the Geology Department.

…who made me feel welcome and made this a great and rewarding graduate school experience.

My adoring family, specially my parents and brother.

…for your unconditional support and love.

My friends Bayrex Rosa, Maridaira Cruz, Johana Córdova, Erika Sanabria and the Colón Carrión family.

…who were always around and helped me in so many levels.

All my colleagues at the USDA APHIS PPQ Plant Inspection Station, especially to the Port Director Norma Rosario and my Supervisor Mildred Sosa

…for your understanding and letting me continue my student life while working.

Diana L. Ortega, Deborah Abrams, Marsha Irizarry, Catherine Pérez, William Hernández, Alejandra Rojas, Roy Ruiz, Joaquín Trinanes, Dr. Ariel Diaz, Dra. Deborah Parilla, Dr. Pérez-Alegría and Dr. Raúl Machiavelli

...who always made themselves accessible to me.

NOAA, NASA, USGS and the PRWRERI

…for making helpful data and information available for researchers

This research was supported by NOAA-CREST grant no. NA06OAR4810162.

TABLE OF CONTENTS

TABLE LIST VIII

FIGURE LIST IX

GENERAL INTRODUCTION 1

STUDY AREA 3
GEOLOGICAL SETTING 4

LITERATURE REVIEW 6

OBJECTIVES 11

CHAPTER 1: REMOTE SENSING OF SUSPENDED SEDIMENT IN MAYAGÜEZ BAY 12

1.1 INTRODUCTION 13
1.2 METHODS 14
1.2.1 Total Suspended Sediments 17
1.2.2 HydroScat-6 18
1.2.3 Remote sensing reflectance 18
1.3 RESULTS AND DISCUSSION 19
1.3.1 Spatial and temporal variability of TSS 19
1.3.2 Spectral and spatial variability of R_{rs} 22
1.3.3 Spectral and spatial variability of b_b and b_{bp} 24
1.3.4 Relationship between b_{bp}, TSS and R_{rs} 26
1.3.5 Effect of TSS on remote sensing reflectance 31
1.3.6 Relationship between MODIS and field data 35
1.4 CONCLUSIONS 39

CHAPTER 2: USING MODIS 250 M IMAGERY TO ESTIMATE TOTAL SUSPENDED SEDIMENT IN MAYAGÜEZ BAY 40

2.1 INTRODUCTION 41
2.2 METHODS 42
2.2.1 In situ measurements 43
2.2.2 MODIS Data 43
2.2.3 Algorithm Development and Validation 45
2.3 RESULTS AND DISCUSSION 46
2.3.1 MODIS Products 46
2.3.2 Total Suspended Sediment Algorithm 47
2.3.3 Total Suspended Sediment Algorithm Validation 49

2.3.4 Total Suspended Sediment Products.....51

2.4. CONCLUSION..... 56

CHAPTER 3: ESTIMATING ANNUAL SUSPENDED SEDIMENT LOAD IN MAYAGÜEZ BAY USING GIS AND REMOTE SENSING TECHNIQUES.....57

3.1 INTRODUCTION..... 58

3.2 METHODS..... 59

3.2.1 Watershed Erosion Modeling.....59

3.2.2 Soil Erodibility factor (K).....62

3.2.3 Cover Management factor (C).....62

3.2.4 Slope Steepness and Length Factor (LS).....63

3.2.5 Rainfall Erosivity factor (R).....64

3.2.6 Support Practice factor (P).....67

3.2.7 Masking Streams.....68

3.2.8 Soil Erosion Products.....68

3.2.9 Sediment Delivery Ratios.....69

3.2.10 Suspended Sediment Load.....71

3.3 RESULTS AND DISCUSSION..... 75

3.3.1 Temporal and Spatial Variability of Soil Erosion Rates.....75

3.3.2 Sediment Yield as the product of Soil Erosion Rates Multiply by Sediment Delivery Ratios.....81

3.3.3. Land-sea interface analysis results.....91

3.4. CONCLUSIONS..... 96

GENERAL CONCLUSIONS.....98

CONCLUSIONES GENERALES.....101

REFERENCES.....104

LIST OF TABLES

Table 1. Details of research cruises within the study period 15

Table 2. Coordinates of all sampled stations, checkmarks indicate permanent stations. 17

Table 3. Regression relationships between backscattering, TSS and R_{rs} at six wavebands. 27

Table 4. Regression relationships between TSS and R_{rs} at 9 single wavebands and four band ratios. 33

Table 5. Pixel values obtained in permanent sampling stations using Method 2 and in situ R_{rs} at 645 nm. 47

Table 6. Eight landuse classes included in the model and their area extent. Defined classes and C factors were based on López et al., 1998.....63

Table 7. Descriptive information of sixteen stations and annual precipitation totals (mm) for five years (2001, 2002, 2003, 2004 and 2005). 66

Table 8. Dates corresponding to good quality MODIS images used in the analysis of suspended sediment load. 72

Table 9. Basic statistics of predicted soil erosion rates in Mayagüez Bay for five years 80

Table10. Results of calculated sediment delivery ratios for five watersheds of different extent associated with Mayagüez Bay. 85

Table 11. GIS model predictions during five simulations corresponding to years 2001, 2002, 2003, 2004 and 2005. 87

Table 12. Summary statistics of suspended sediment discharge data obtained from USGS Río Rosario gauge station (50136400) corresponding to years 2001, 2002, 2003, 2004 and 2005. 89

Table 13. Estimated sediment delivery ratios for five simulated years (2001, 2002, 2003, 2004 and 2005).....90

Table 14. A sensitivity analysis showing hypothetical results (A, Soil Erosion Rate) of the GIS model under six different conditions.....91

LIST OF FIGURES

Figure 1. The Mayagüez Bay illustrating seventeen stations monitored within the study period (January 2004 to October 2006).....16

Figure 2. Box plot indicating variability of TSS concentration associated with three locations in the bay (Inshore, Middle and Offshore).....21

Figure 3. Box plot indicating variability of TSS concentration at inshore, offshore and all stations during the rainy and the dry season.....21

Figure 4. R_{rs} spectra measured during all research cruises from January 2004 to October 2006 at (a) Inshore, (b) Middle and (c) Offshore stations. 23

Figure 5. Spectral variation of the median values for total backscattering (b_b, m-1) and particles backscattering (b_{bp}, m-1) along three regions of the bay (inshore, middle and offshore).....25

Figure 6. Relationship between TSS (mg/l) and b_{bp} (m^{-1}) at six wavebands. 28

Figure 7. Relationship between backscattering (b_b, m^{-1}) and R_{rs} at three different wavelengths (442 nm, 510 nm and 620 nm).....30

Figure 8. Mean measured in situ R_{rs} categorized in four concentration ranges of TSS: >20 mg/l (n=9), 11-20 mg/l (n=9), 6-10 (n=21) and < 5 mg/l (n=33).....32

Figure 9. Relationship between TSS (mg/l) and the R_{rs} red:green ratio 655nm/545nm which presented the best linear relationship defined between these two parameters. 34

Figure 10. Comparison between relationships determined between MODIS band 1 and in situ measurements of (a) TSS (mg/l), (b) b_{bp} at 620 nm (m^{-1}) and (c) R_{rs} at 645 nm (sr^{-1}). 37

Figure 11. Schematic illustration of two methods used to process MODIS data. Method 1 is based in ENVI image processing software and Method 2 uses SeaDAS specialized commands.....44

Figure 12. Seventeen point locations collected along Mayaguez Bay shoreline overlaying two images: October 19, 2005 (left) and December 6, 2005 (right).....45

Figure 13. Data used to develop a TSS algorithm for Mayaguez Bay; 48

Figure 14. Validation results when applying (a) equation 2.1, (b) equation 2.2 and (c) equation 2.3 50

Figure 15 a. TSS products generated using three developed algorithms based on MODIS band 1 data for February 12, 2004.....52

Figure 15 b. TSS products generated using three developed algorithms based on MODIS band 1 data for March 8, 2006.....53

Figure 16. Descriptive statistics and histograms illustrating TSS values distribution for (a) in situ measurements collected within the study period (January 2004-October 2006) and TSS products generated using (b) equation 2.1, (c) eqution 2.2 and (d) algorithm 2.3. 55

Figure 17. Mayagüez Bay and three watersheds associated with this coastal system. Region in red indicates area included in the GIS model. 60

Figure 18. Schematic diagram showing information about the origin of all layers defined in the model. 61

Figure 19. Sixteen weather stations from which precipitation data was obtained to estimate R factor. 65

Figure 20. Output raster layers showing spatial distribution of R factor values for 2004 using three of the evaluated interpolation methods: Inverse Distance Weight, Spline using tension option and Spline using regularized option 67

Figure 21. Stream mask layer incorporated in the GIS model in order to exclude erosion estimations corresponding to channels. 68

Figure 22. Subwatershed associated with USGS gauge station 50136400 70

Figure 23. Vertical profiles of TSS concentration derived from particle backscattering at 620 nm. a) all stations, b) offshore stations and c) inshore stations 73

Figure 24. Illustrative description of methodology used to extract pixel values with higher effect of rivers discharge. 74

Figure 25 a. Raster layers generated to use as input data for the GIS model 76

Figure 25 b. Additional raster layers of the Rainfall factor generated to perform soil erosion simulations representative of years: a) 2001 b) 2002, c) 2003 d) 2005 77

Figure 26. Soil Erosion, A, (Mg/ha*yr) as predicted using GIS model for 2004. Similar spatial variations were observed in all additional years evaluated (2001, 2002, 2003 and 2005). 80

Figure 27. Zoom in of Yaguez R. and Rosario R. subwaterheds showing variation in landuses occurring in these areas. 83

Figure 28. Comparison of sediment yield results (Mg/yr) for simulated years (2001, 2002, 2003, 2004 and 2005) by applying three equations based on Boyce,, 1975, Vanoni et al., 1975, and USDA, 1972. 89

Figure 29. Validation results of GIS model using estimation sediment yield after applying Boyce equation and observed suspended sediment discharge at USGS gauge station (50136400) 91

Figure 30. Suspended sediment load for the twenty dates included in the land-sea interface analysis.. 93

Figure 31. Regression analysis between discharge data collected during dates used for analysis at two USGS gauge stations (50144000 in Añasco watershed and 50138000 in Guanajibo watershed). 93

Figure 32. Image at top is the product of suspended sediment load product generated for Puerto Rico coastal waters in October 19, 2004.. 94

Figure 33. Relationship between Añasco river mean daily discharge (USGS gauge station 50144000) and estimations of suspended sediment load derived from MODIS data.. 95

GENERAL INTRODUCTION

The description of temporal and spatial dynamics of total suspended sediment (TSS) is crucial to better understand sedimentation processes and their impact to the geology, ecology and economy of a water flow system. In a larger scale, sedimentation patterns control the formation of petroleum reservoirs and stratigraphic sequences, which indicate relative sea level changes (Jordan & Flemings, 1991). At local scales, concentration of suspended sediment is considered one of the most important water quality parameters (Wang et al., 2005) and produces non-point source pollution. Some environmental problems associated with the abundance of sediment are reduction of sunlight penetration through the water column, and therefore reduction of primary production, which can affect the habitat condition. In addition, runoff of terrestrial sediments has been suggested as a possible source of coral reef pathogens (Weil, 2004). Consequently, this parameter has been reported as one of the most important factors affecting stress condition of coral reef communities in the Caribbean (Hubbard, 1987; Gardner et al., 2003, Warne et al., 2005). This study has two general objectives: (1) to describe the dynamics of suspended sediment in Mayagüez Bay, and (2) to provide baseline analyses that promote the use of Remote Sensing (RS) and Geographic Information Systems (GIS) techniques to develop advanced water quality and coastal processes assessments in Puerto Rico.

Mayagüez Bay represented an ideal area for the development of this study being located in the western part of Puerto Rico where many biological, chemical and geomorphological processes are affected by the distribution and abundance of suspended sediment. As with other water constituents, TSS is also responsible for changes in the underwater light field by affecting the inherent optical properties (IOPs) and the apparent optical properties (AOPs). This study includes a detailed analysis of *in situ* optical data (backscattering, b_b, and Remote Sensing Reflectance,

R_{rs}), including a description of spatial and temporal patterns of these properties and their relationship with TSS measurements and satellite derived data. This component of the study is fundamental to validate analyses and interpretation of satellite derived data.

As many other coastal environments, this bay is highly affected by inland processes including sediment and nutrient fluxes and anthropogenic derived discharges. Field studies of these processes, and other factors associated with coastal dynamics, are expensive and time consuming. This limitation is reduced when incorporating RS and GIS technologies, which provide many functions and tools which facilitate in the evaluation of broader scales from remotely derived data and geographically defined data layers. This study combined both technologies by integrating results of a GIS model, which predicts soil erosion rates and sediment load values at watershed level, with products derived from water surface reflectance data.

The objectives of this study can be related to three main fields: (1) biogeo-optics, (2) Coastal Remote Sensing and (3) Geographic Information System (GIS) modeling. Following this basis, the main content of this document was structured by developing three chapters that consist of individual but integrated topics. The first chapter includes empirical analyses of biogeo-optical and water color properties of the bay associated with TSS concentration. This type of analysis provides fundamental information for the development of remote sensing based algorithms. Important determinations from the first chapter were incorporated in the second in order to generate TSS products from satellite derived data. Finally, the third chapter describes the use of GIS techniques to predict sediment yield values that are theoretically comparable to TSS products as presented in the second chapter. This integration produced valuable information and new methods that support broader scale studies of

coastal environments. This also represents an innovative effort for developing a better understanding of the Mayagüez Bay using a land-sea interface approach.

STUDY AREA

Mayagüez Bay is a semi-enclosed bay located at the west coast of Puerto Rico between latitude N 18° 09' to 18° 18' and longitude W 67° 09' to 67° 15' (Fig. 1). The west coast of Puerto Rico has presented a mean annual suspended-sediment yield of 1,200 metric tones per square Kilometer (Mg/km^2) (equivalent to 12 Mg/ha) within the period of 1990 to 2000 (Warne et al., 2005). This represents a significant contribution to the total suspended-sediment yield of the island, dominated by the southern area with an annual sediment yield that ranged from 1,000 to 4,300 Mg/km^2 during the same period (Warne et al., 2005). Spatial and temporal variations in TSS abundance can be produced by anthropogenic or natural factors. Therefore, various studies have evaluated and analyzed processes affecting these variations (Grove, 1977; Miller et al., 1994; Gilbes et al., 1996). Abundance and composition of TSS in Mayagüez Bay is highly affected by fresh water input of Añasco, Yagüez, and Guanajibo rivers (Fig. 1). Grain composition of material contributed by these three rivers varies along the area and these differences are noticeable in the composition of beach sands bordering this bay, where the southern part is dominated by dark minerals while the northern part is dominated by quartz and carbonates (Morelock et al., 1983). Spatial extent of associated watersheds are also different in this coastal system; the Añasco River watershed has the higher area of 543.8 Km^2, followed by the Guanajibo River watershed 388.7 Km^2 and the smaller Yagüez River watershed with an area of 41.9 Km^2. Although water turbidity near river mouths are typically associated with storm runoff, previous studies indicate that sediment abundance in this area is primarily controlled by re-suspension of bottom sediments produced by wind-driven events (Morelock et al., 1983; Miller et al., 1994). This area provides an

exceptional field-laboratory to study inshore processes and coastal dynamics that can be used as baseline for the development of biogeo-optical algorithms for tropical coastal waters. Field monitoring and better understanding of coastal processes is extremely labor intensive and very expensive. Therefore, incorporation of resources such as satellite derived data, could provide exceptional information, useful for studying and monitoring TSS dynamics in this type of coastal environment.

GEOLOGICAL SETTING

The study area presents a high variety of geological processes and formations influencing the material deposited into the bay. Topography in the watershed is mainly controlled by fluvial driven processes with the presence of two large valleys, the Añasco and Guanajibo valleys, and a high density of tributaries flowing to the main channels along the entire watershed. Bedrock material was identified and described by Mattson (1960), finding a series of unconformities separating a basal complex, two highly folded sequences composed of igneous and sedimentary rocks, and a younger gently dipped sedimentary strata. Most of the rocks of the southwestern area of Puerto Rico are present in this region:, Yauco Formation, Sabana Grande Formation, Parguera Limestone, Lajas Formation, Cotui Limestone, Melones Limestone, El Rayo Formation and Boqueron Basalt (Volckman, 1983) where the maximum age range has been determined as Santonian to Maestrichtian (Santos, 1999). In the southwest of this area there are exposures of neritic cherts and serpentinites resulted from the subduction of the Caribbean Plate beneath the North America Plate. Many of these rocks are overlain by alluvium deposits from the Quaternary age, which has a thickness that reach 100 feet. Along the Grande de Añasco valley fill material is composed of clay, silt and sand with localized gravel deposits (Veve and Taggart, 1994). The coast is delimited by sandy beaches; the southern area presents dark sand with high amount of lithic fragment compared to

the northern region which is lighter in color by the dominance of carbonates and quartz (Cameron, 2003). Exposed material in this area is composed of swamp and marsh deposits and wide beach deposits which extent up to six miles inland (Álvarez, 2005).

The mineralogy of sediments deposited near the Añasco River is controlled by discharge from the river itself, carbonate production, and diagenesis of marine sediments (Webb et al., 2000). More common types of terrigenous clay sediments that are deposited in the northern area are illite, chlorite, kaolinite and montmorillonite (Piere, 1967). The sediments reaching the southern part of the bay are mainly eroded from serpentinite deposits rich in magnesium, nickel, chromium, cobalt and copper and then transported by the Guanajibo and the Yagüez rivers (Webb et al., 2000).

LITERATURE REVIEW

A complete study of shelf sediments patterns was performed by Morelock et al. (1983). That study gives a valuable description of the shelf sediments and the most important oceanographic features of Mayagüez Bay, such as climate, currents and waves. They also offer information about how variations on these oceanographic features affect the sediment patterns in the bay. They mentioned that wave and tides are the most influential components affecting distribution of these sediments. They described a process where a massive movement of river sediments onto the shelf is slowly redeposited, which was also explained by wave and current action. Additionally, it was highlighted how transportation of sand-sized material onto the shelf occurs only during river flooding. They characterized 6 sediment facies using texture and composition. Terrigenous mud is the most important facies for the proposed study because is highly influenced by inland processes. It has an average of 88 percent silt and clay-sized terrigenous minerals. In terms of their distribution, they indicated that are consistent with surface currents patterns and areas of reduced wave energy. All this information is useful as a preliminary understanding of distribution patterns of Mayagüez Bay shelf sediments associated with its texture and composition properties.

In order to better understand the effect of TSS on sunlight penetration and been able to generate algorithms for quantitative estimations, it is necessary to study how concentration and nature of this material affect optical properties in the area (Bowers and Binding, 2006). Numerous authors have studied these associations for different regions around the world (Rosado, 2000; Wild-Allen et al., 2002; D'Sa and Miller, 2003; Binding et al., 2005; Bowers and Binding, 2006; Tzortziou et al., 2007; Rosado 2008). Wild-Allen et al. (2002) worked on coastal waters highly influenced by fresh water in Netherlands and encountered that vertical mixing was the most important

process controlling suspended sediment dynamics and in-water optical properties in that area. D'Sa and Miller (2003) studied the impact of Mississippi River in bio-optical properties and confirmed the difficulty to retrieve bio-optical variables using global ocean color algorithms in areas highly influenced by rivers. A reference with higher correspondence to the present study was published by Binding et al. (2005). They developed a detailed analysis of optical and particle scattering properties to estimate suspended sediment concentrations in the Irish Sea. The highest correlation coefficient was encountered between irradiance reflectance at 665 nm and mineral suspended sediment concentration. Their conclusions substantiated the difficulty of estimating this water constituent in areas dominated by highly variable particle properties (e.g. grain size). Bowers and Binding (2006) highlighted in their conclusions that variation in scattering per unit concentration, caused by particle physical properties, is the determinant limiting factor for estimations of mineral suspended sediment loads, from remote platforms and field measurements. Tzortziou et al. (2007) studied remote sensing reflectance and inherent optical properties in the mid Chesapeake Bay. Their results encountered that inorganic material was the most dominant water constituent regulating backscattering variability in that area. It was proposed the used of R_{rs} (670 nm) to retrieve non-algal particulate absorption and combine it with UV-blue wavelengths to monitor non-algal suspended particle concentration. All these studies justify the development of this type of study in Mayagüez Bay, a highly complex biogeo-optical system. Synergistic effects of rivers exist within the study area, industrial effluents, and coastal geomorphology which creates a variety of optical provinces in a relatively small geographical area (Rosado, 2000). Rosado (2008) performed Hydrolight simulations for Mayagüez Bay and found that suspended sediments play a key role in the biogeo-optical response of the bay. His work also expressed the need of studying chemical nature, optical properties,

spatial and temporal variability of this parameter to develop accurate Chlorophyll-*a* retrievals from R_{rs} curves.

Cruise and Miller (1994) evaluated spatial, interannual, and seasonal variability of sediment discharges in Mayagüez Bay. They found significant seasonal changes on runoff and sediments discharges. It was also determined that rainfall distribution has an effect on sediment yields. When the rainfall was concentrated in *heavily forested mountainous* areas the sediment yields were lower than in years when rainfall was uniformly distributed. Miller et al. (1994) presented Remote Sensing-based methods and algorithms to monitor short term changes in the source and spatial distribution of Suspended Particulate Matter (SPM) in Mayagüez Bay, this term is equivalent to TSS in the proposed study. To analyze and map this information they used data from the Calibrated Airborne Multispectral Scanner (CAMS). Changes in rivers discharge were detected through variations in spatial distribution of SPM. Several analyses indicated that sediment plumes are mainly affected by wind-driven resuspension events.

Gilbes et al. (1996) evaluated the relationship between phytoplankton Chlorophyll-*a* (Chl-*a*) and SPM in Mayagüez Bay. They described spatial and temporal variations of these two parameters from analyses of data collected from March 1990 to February 1991. Their results indicated a positive spatial correlation between SPM and Chl-*a*, but temporal correlation was not significant. These correlations were also associated with nutrients, and it was suggested that it represents phytoplankton adaptations to changes in light input. Some of these interpretations were expressed in a model that describes Chl-*a* and SPM seasonal dynamics in Mayagüez Bay.

A more recent study developed in the Northern Gulf of Mexico produced an efficient algorithm to estimate Total Suspended Matter (TSM) using remotely sensed data

(Miller and McKee, 2004). They established a significant linear relationship (r^2=0.89; n=52) between band 1 (620-670 nm) of MODIS Terra 250 m data and *in situ* measurements of TSM. This study recognized MODIS Terra instrument data as an effective resource for the study of TSM in small bodies of water (i.e., bays and estuaries).

Many studies were reviewed to determine which model or combinations of models will effectively estimate inland soil erosion rates and sediment yields. López et al. (1998) integrated data layers corresponding to soils, land use, and topography to predict soil erosion in Guadiana watershed, Naranjito, Puerto Rico. The methodology consisted in combining GIS and the Revised Universal Soil Loss Equation (RUSLE) to estimate the sediment yields and soil erosion in a watershed scale. Factors identified as increasing soil erosion were annual rainfall, slope, and land uses with open canopies. They also evaluated the relative effects of different land uses on soil erosion in that area and, in general, it was determined that any land use that reduces vegetation cover increases soil erosion. A temporal analysis showed that the most effective way to reduce soil erosion in this watershed is to reforest areas with higher soil erosion rates (>46 Mg ha^{-1} yr^{-1}). Results of this study supported the integration of RUSLE and GIS as an effective method for estimating soil erosion at the watershed scale.

Villalta (2004) evaluated different sediment transport functions to compare the effectiveness estimating bed and suspended sediment load for the Añasco, Yagüez and Guanajibo rivers. He considered hydraulics geometric and grain size characteristics of the three rivers. It was mentioned that USGS sediment data for this area is not enough to develop studies of sediment transport. Four functions were used to generate simulations of the Añasco River. Results included five and ten years'

estimations of total sediment passing through cross sections that he established. Although the study period was from 1990 to 2000, these estimations provide good reference information to evaluate results of the current study.

Behera and Panda (2006) discussed different models that have been developed to monitor non-point source pollution, including: ANSWERS (Beasly and Hugins, 1982); HSPF (Johanson et al., 1984); EPIC (Williams et al., 1984); AGNPS (Young et al., 1989); SWRRB-WQ (Arnorld et al., 1990); and SWAT (Arnorld et al., 1996).

Cartwright (2002) identified potential sediments sources to Weeks Bay, Alabama, using a remote sensing and GIS analyses. The analysis was made using Landsat satellite images for leaf-on and leaf-off periods of 1990 and 2000. Although the erosion potential model does not give information of the total sediment yield or erosion rates, the author made a spatial analysis within the watershed. A map was presented with five erosion potential classes, which were produced based on slope and Landuse/Landcover (LULC) change. It was also indicated that combination of surface slope changes and LULC had much more impact on the erosion than either of the factors alone. Important recommendations were established for similar projects, as improve the classes quality produced on the LULC classification using specific band combinations. They also recommended addition of a soils data layer to the erosion potential model to add a soil erodability factor.

OBJECTIVES

The main objective of this study was to describe TSS dynamics in Mayagüez Bay and its association to inland soil erosion rates by combining *in situ* measurements, remotely derived data and a GIS based analysis. In order to accomplish this main objective, it was necessary to:

- Study spatial and temporal variations of biogeoptical properties in the study area.
- Develop and validate an algorithm to estimate TSS using satellite derived data.
- Predict soil erosion rates within the Mayagüez Bay watershed applying RUSLE through a GIS based model. This objective included the following sub-objectives:
    - Calculate sediment yields as the product of erosion rates multiply by spatially variable sediment delivery ratios.
    - Use USGS suspended sediment data to calibrate sediment delivery ratios calculations.
    - Estimate annual sediment load to Mayagüez Bay using MODIS images and evaluate results using both GIS and Remote Sensing techniques.

CHAPTER 1:

Remote Sensing of Suspended Sediment in Mayagüez Bay

Abstract

In situ measurements of total suspended sediments (TSS), backscattering (b_b and b_{bp}) and Remote Sensing reflectance (R_{rs}) and MODIS-Terra band 1 reflectance were spatially and temporally compared. Spatial analysis indicated that absolute values of TSS, R_{rs} and b_b increases with proximity to shoreline. It was observed that median values of b_b and b_{bp} vary spectrally, and higher difference in magnitude between these parameters was observed in shorter wavelengths and offshore stations. Good relationships resulted from TSS concentration and b_{bp} linear regression analyses in all six analyzed wavelengths (R^2=0.74-0.76; n=133). Resultant correlation results between b_b and R_{rs} using corresponding wavelength, show significant wavelength dependant variations where best relationship was observed at 620 nm (R^2=0.78; n=61). The relationship between R_{rs} and TSS indicate that the best wavelengths to estimate TSS are between 589 to 645 nm. The analysis of R_{rs} single band and R_{rs} ratio for derivation of TSS indicates that red to green ratio ($R_{rs}655/R_{rs}545$) present the best correlation results (R^2=0.84; n=72). Simultaneous MODIS reflectance band 1 data and *in situ* measurements of TSS concentration, $b_{bp}620$ and $R_{rs}645$ were all positively correlated, but more data are required to better define and validate the results. Sensors with better spatial and spectral resolution are needed in order to generate operational products of TSS in these highly variable optical tropical waters.

1.1 INTRODUCTION

Comprehension of the relationships between water constituents (i.e. IOPs and AOPs) is important for characterizing the marine optical environment, developing ocean color algorithms (D'Sa and Miller, 2003) and interpretation of satellite imagery for case 2 waters (Doxaran et al., 2002a). A better understanding of TSS provide valuable information necessary to interpret and analyze satellite information because in ocean waters satellite sensors essentially recorded images of backscattered light (Dana and Maffione, 2002; Boss et al., 2004b). Scattering is a fundamental process of light propagation in the ocean, where electromagnetic radiation is deflected from its original beam by particles. The optical backscattering coefficient (b_b) indicates the attenuation caused by scattering at angles from 90° to 180°. Considering that this coefficient is representative of the amount of photons scattered backward, it is directly related to reflectance information collected near the water surface with field radiometers or even from satellite sensors (Dana and Maffione, 2002; Boss et al., 2004a). There are many constituents in water that affects the b_b coefficient such as bubbles, organic and inorganic particles, Colloids, and liquid or oil particles. An extensive description of the role and significance of each one of these constituents to b_b are discussed in Stramski et al. (2004).

Although a large amount of optically active water constituents (e.g. algae, Colored Dissolve Organic Matter [CDOM], aquatic vascular plants and oils) are present in this type of waters, scattering of TSS tends to dominates (over Chlorophyll-a [Chl-a] and CDOM absorption) the water leaving signal, specially in wavelengths longer that 500 nm within the visible range of the electromagnetic spectrum (Schalles et al., 2001; D'Sa and Miller, 2003). Several studies have also presented dependence of TSS concentration and reflectance in the near infrared region in highly turbid waters (Moore et al., 1999; Doxaran et al., 2002b; Teodoro et al., 2008). However, the

application of previously formulated ocean color algorithms for estimation of water constituents is generally limited by site-specific factors (Hellweger et al., 2004). These factors make necessary the development of local algorithms to retrieve products of water quality parameters, such as TSS, through remote (Menon et al., 2005) or *in situ* optical measurements. Spatial and temporal changes were associated with optical variability in this area in order to address this limitation.

The main objective of the work presented in this chapter was to derive empirical relationships between TSS concentration, optical backscattering, *in-situ* remote sensing reflectance (R_{rs}) and MODIS data in order to provide a baseline for the development of site specific algorithms to estimate TSS in tropical coastal environments.

1.2 METHODS

Twelve research cruises were carried out between January 2004 and October 2006 (Table 1). A total of 17 stations were monitored within this period for bio-optical properties, remote sensing reflectance (R_{rs}), TSS, Chl-a and CDOM (Fig. 1; Table 2). Six were visited during all cruises and eleven were visited only in 2004. Distribution of stations along the bay aimed to detect variations associated with river discharge by aligning them in transects that extent offshore from the mouths of the Añasco, Yagüez and Guanajibo rivers. Stations were categorized as inshore, middle and offshore stations based on their distance to the shoreline for each transect. Eleven additional sites at the river mouths were monitored for R_{rs} and TSS during June 4, 11, and 16 of 2008. This work was focused on the analysis of TSS concentration, backscattering coefficients (b_b and b_{bp}) and R_{rs}.

Table 1. Details of research cruises within the study period

Dates	Season	No. of stations	Field Data missing	Good quality images available
January 12-14, 2004	Dry	12		2
February 12, 2004	Dry	9	TSS Depth; R_{rs}	1
August 19, 2004	Rainy	10	TSS Depth	0
July 19, 2005	Rainy	6	TSS Depth	0
August 17, 2005	Rainy	6	TSS Depth	1
September 20, 2005	Rainy	6		0
October 19, 2005	Rainy	6		1
December 6, 2005	Dry	6		1
March 8, 2006	Dry	5	R_{rs}	1
April 21, 2006	Dry	5		0
September 26, 2006	Rainy	6		0
October 26, 2006	Rainy	6		0

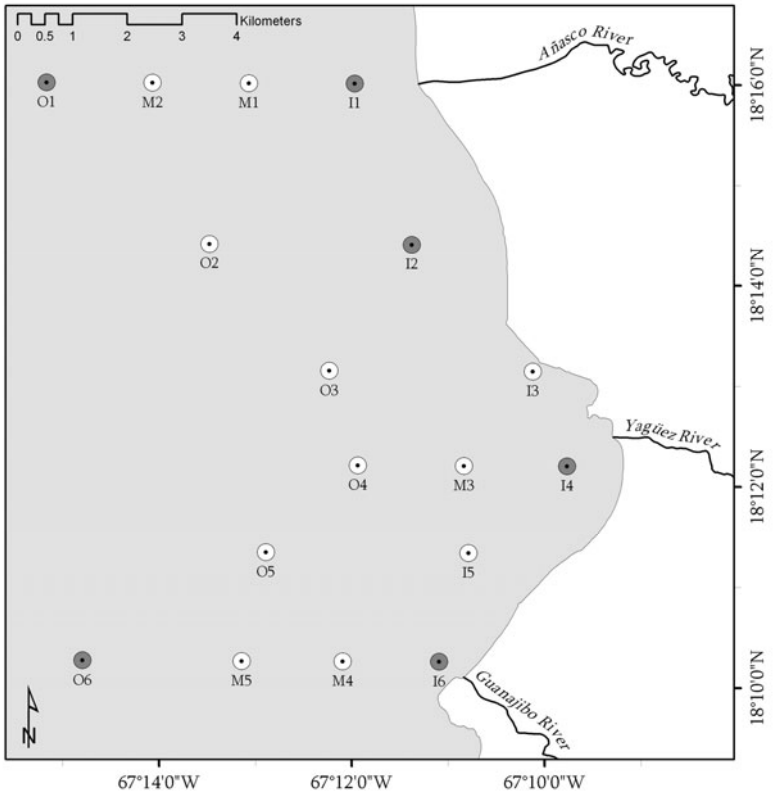

Figure 1. The Mayagüez Bay illustrating seventeen stations monitored within the study period (January 2004 to October 2006). Stations colored in white indicate specific sites that were sampled only during selected dates, while six stations in gray are permanent stations. Letter assigned to station ID refers to the location in terms of their distance to the shoreline (I=inshore, M= middle and O=offshore).

Table 2. Coordinates of all sampled stations, checkmarks indicate permanent stations.

Station ID	Latitude	Longitude
I1*	18º 16.00'	67º 12.00'
M1	18º 16.00'	67º 13.10'
M2	18º 16.00'	67º 14.10'
O1*	18º 16.00'	67º 15.20'
I2*	18º 14.40'	67º 11.40'
O2	18º 14.40'	67º 13.50'
I3	18º 13.14'	67º 10.14'
O3	18º 13.14'	67º 12.25'
I4*	18º 12.20'	67º 09.78'
M3	18º 12.20'	67º 10.85'
O4	18º 12.20'	67º 11.95'
I5	18º 11.33'	67º 10.80'
O5	18º 11.33'	67º 12.90'
I6*	18º 10.25'	67º 11.10'
M4	18º 10.25'	67º 12.10'
M5	18º 10.25'	67º 13.15'
O6*	18º 10.25'	67º 14.80'

1.2.1 Total Suspended Sediments

Water samples for analyses of TSS concentration were collected using a marine pump adapted to a hose that was lowered to 1 m (considered surface at all stations), 4-5 m (considered deep at inshore stations) and 10 meters (considered deep at offshore stations). The water samples, collected in 4 liter plastic containers, were taken in duplicates in each station at surface and deep. The water was filtered through Millipore ® HA 0.45 µm white nylon HNWP 47mm diameter membrane filters. These filters were previously oven-dried over-night at 60ºC and pre-weighed in an analytical balance (±.0001g). The filtered water volumes varied between station samples (depending on the sediment load of each sample). From each water sample, two sub-samples were taken after vigorously shaking the container to homogenize the contents. After filtration the filters were washed three times with distilled water to remove salts. The filters were then dried at 60ºC over-night and re-weighted.

1.2.2 HydroScat-6

Vertical profiles of total backscattering (b_b) and particle backscattering (b_{bp}) at six different wavelengths (442, 470, 510, 579, 620 and 671/675 nm) were measured using a HydroScat-6 (HS-6, elaborated by HOBI Labs). This instrument converts a raw signal to a value of Volume Scattering Function (VSF) around a single fixed angle of 140º (Maffione and Dana, 1997). From these values and other defaults calibration coefficients estimations of b_b and b_{bp} were made using HOBI-Labs processing software (HydroSoft). All raw-files collected during the entire study period were processed using the same version of HydroSoft (v.2.74) to ensure consistency in the data set (D. Dana, personal communication). Since b_b is the sum of b_{bp} and b_{bw} (backscattering by pure water), the difference of estimating b_b and b_{bp} resides in the value assign to b_{bw}. The calculation of b_b was based on pure salt water values given by Morel (1974), and for b_{bp} the b_{bw} was set as 0 (D. Dana, personal communication). Values used for this analysis were corrected using the sigma correction incorporated within the processing options of the software. This correction could account for possible underestimation of backscattering due to attenuation occurred between the instrument and the detection volume (HS-6 User Manual, 2007). Although conditions in local areas suggest that this effect should be low. Finally, full resolution vertical profiles (entire downcast) were used to generate binned profiles of b_b and b_{bp} with a 0.5 m resolution.

1.2.3 Remote sensing reflectance

Above water remote sensing reflectance (R_{rs}) was measured in each station using the GER 1500 portable spectroradiometer, which has 512 spectral channels, following SeaWiFS protocols (Mueller and Austin, 1995). Three replicates of total water radiance, $L_0(\lambda)$, sky radiance, $L_s(\lambda)$, and downwelling irradiance, $E_d(0^+, \lambda)$, were measured to calculate the R_{rs}. $L_0(\lambda)$ was measured by pointing the instrument to the water at 45º from the vertical plane and 90º from the solar plane to avoid sun glint

effect. $L_s(\lambda)$ was measured using the same geometry but pointing the instrument toward the sky. $E_d(0^+, \lambda)$ was measured by attaching a cosine collector to the spectroradiometer lens and pointing the instrument directly up toward the sky. The collected data were plotted for evaluation and any curve with anomalous peaks (produced by clouds, sun glint or boat shadow) was not included in the dataset. Subsequently, mean values were calculated for each parameter and then used to calculate R_{rs} with the following equation:

$$R_{rs} = \frac{L_0(\lambda) - (f * L_s(\lambda))}{E_d(0^+, \lambda)} \quad (1.1)$$

Where f is the Fresnell coefficient equal to 0.028 at 45° (Austin, 1974). The curves were corrected for sky-light reflection subtracting the minimum measured value between 900-920 nm, in a few cases the curves were corrected at lower regions (730-900 nm). It was not possible to select a specific wavelength because stations monitored include both clear and turbid waters and these conditions affect the determination of the most appropriate wavelength for this correction (Mueller et al., 2003).

1.3 Results and Discussion

1.3.1 Spatial and temporal variability of TSS

TSS concentration in surface and deep waters ranged from 1.1 to 28.4 mg/l with a mean of 5.6 mg/l, a median of 3.7 mg/l and a positive skewed distribution. The highest value was obtained in station I6 in August 17, 2005 and the lowest value was found on station O6 during August 19, 2004. This highest TSS value was associated to a significant rain event that was recognized using USGS gauges discharge data. During that day the mean daily discharge of Guanajibo River was around six times higher than estimated mean value for that same day in a period of 33 years (USGS, 2008). On the other hand, the lowest TSS value was also measured in the southern

area at station O6, which is characterized for very clear waters influenced by coral reefs (Morelock et al., 1983). It is inquiring that both extreme values were observed during August which is considered the rainy season (Carter et al., 1997). Magnitude and variability of TSS values increases with proximity to shoreline (Fig. 2). Overall mean values from inshore, middle and offshore stations were 7.5, 3.6 and 2.7 mg/l, respectively. Minimal differences of magnitude and variability associated with seasons were detected (Fig. 3). During dry season mean concentration of TSS was 5.9 mg/l, while in the rainy season was 5.2 mg/l. A high value was detected during dry season at O4 (8.9 mg/l), which is considered an offshore station. However, this is the closest station to the shoreline from all offshore stations and this result suggests that it could be affected by inshore processes. Minimum values always ranged between 1.1 to 1.8 mg/l independently of the location and sampling season. A similar analysis was performed using surface measurements only and the same tendency was observed as presented by results in both depths. Spatial analysis indicates that magnitude of TSS in Mayagüez Bay is positively related to shoreline proximity. This association is not only explained with river discharge, but also with the effect of re-suspension in shallow waters (Morelock et al., 1983; Miller et al., 1994). The general magnitude of TSS in the bay is relatively low compared to other areas where similar studies have taken place (i.e., Miller and McKee, 2004; Doxaran et al., 2002a), this represents a challenge for TSS estimations in Mayagüez Bay since the signal will be more difficult to detect.

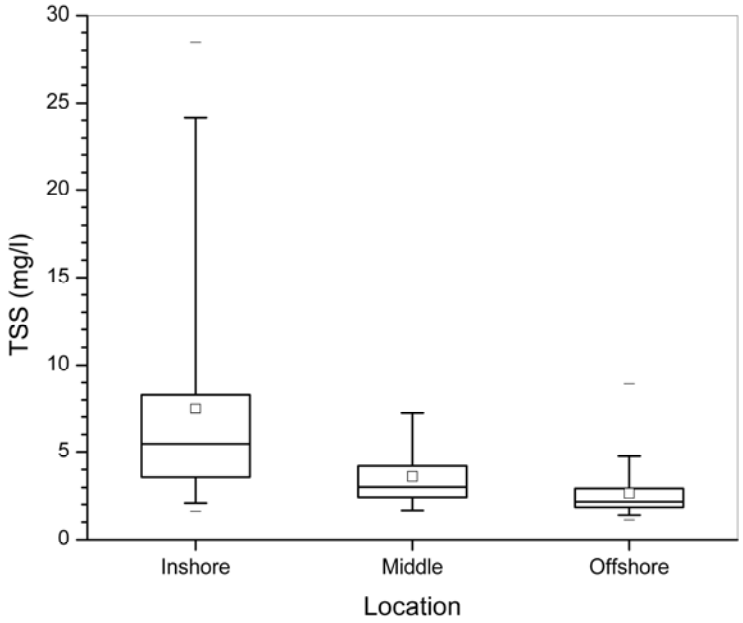

Figure 2. Box plot indicating variability of TSS concentration associated with three locations in the bay (Inshore, Middle and Offshore). The presented data represent the distribution of values collected at surface and deep waters. Each box illustrates the range and distribution of the values. Base and top of the boxes represents the 25th and 75th percentile, respectively. Line and empty small square inside the boxes indicates median and mean values, respectively. While extended lines enclosed all values in the data range and the small line individually dispalyed (-) corresponded to outliers.

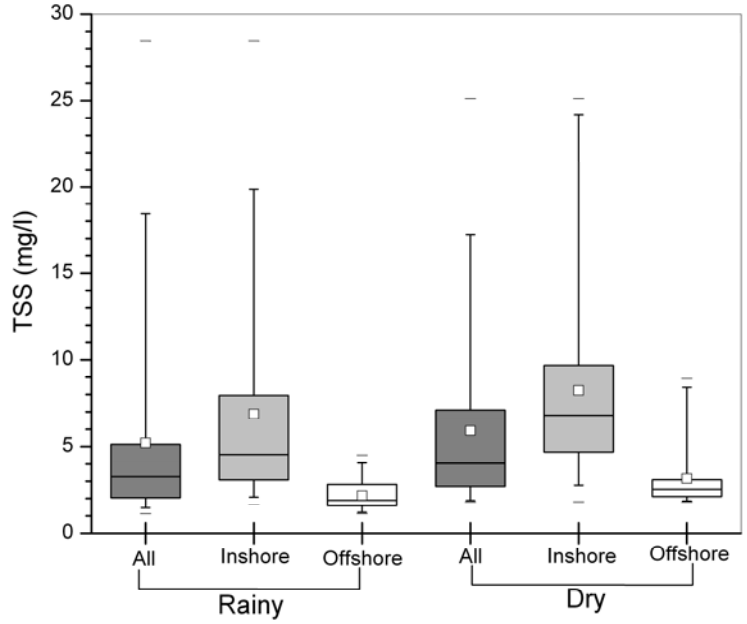

Figure 3. Box plot indicating variability of TSS concentration at inshore, offshore and all stations during the rainy and the dry season. The presented data represent the distribution of values collected at surface and deep waters.

1.3.2 Spectral and spatial variability of R_{rs}

A total of 61 R_{rs} spectral curves were obtained from all research cruises; 35 corresponded to inshore stations, 23 to offshore stations, and 3 to middle stations (Fig. 4). Middle stations were not permanent stations and there was not R_{rs} data for February 2004 cruise (due to problem with the instrument) when most of these stations were sampled. Spectral R_{rs} showed magnitude and shape variations between 400 to 890 nm associated with location. Maximum R_{rs} values observed at inshore stations ranged from 0.006 to 0.058 sr^{-1} (at 400 and 585 nm). These values were higher than observed in middle and offshore stations that ranged from 0.005 to 0.026 sr^{-1} and 0.005 to 0.020 sr^{-1} (400-550 nm), respectively. The region of maximum R_{rs} for inshore stations was near to 565 nm and then shifted to 490 nm at offshore stations, while in middle stations both conditions were observed. Offshore stations generally presented lower R_{rs} between 600 and 700 nm and values were more closed to 0 in the NIR region than those detected at middle and inshore stations. Most of offshore stations presented a R_{rs} peak around 490 nm and lower values in the green to red and near-infrared region. In these stations reflectance shape is mainly controlled by relative contribution of backscattering and absorption of water and Chl-a. The spectral shape of O4 station behaves similar to those corresponding to inshore stations, supporting previous statement which suggested that this station is affected by inshore process. Inshore stations are characterized by strong absorption in the red region that forms the highest reflectance peak near 575 nm. It is evident that absorption by phytoplankton and CDOM is stronger in these stations; therefore, backscattering signal from suspended particles (organic and inorganic) is more evident resulting in higher R_{rs} values within the green region (D'Sa and Miller, 2003). Main variations associated with shoreline proximity are: (1) an increase in magnitude, which is attributed to higher scattering by water constituents, and (2) a shifting from 490 nm to 575 nm of the higher peak due to higher absorption by Chl-a and CDOM

combined with higher scattering of TSS in the red region (Bowers et al., 2004). These R_{rs} curves are comparable with previously reported curves in other locations (i.e., Althius, 1998; Froidefond et al., 2002; D'Sa and Miller, 2003).

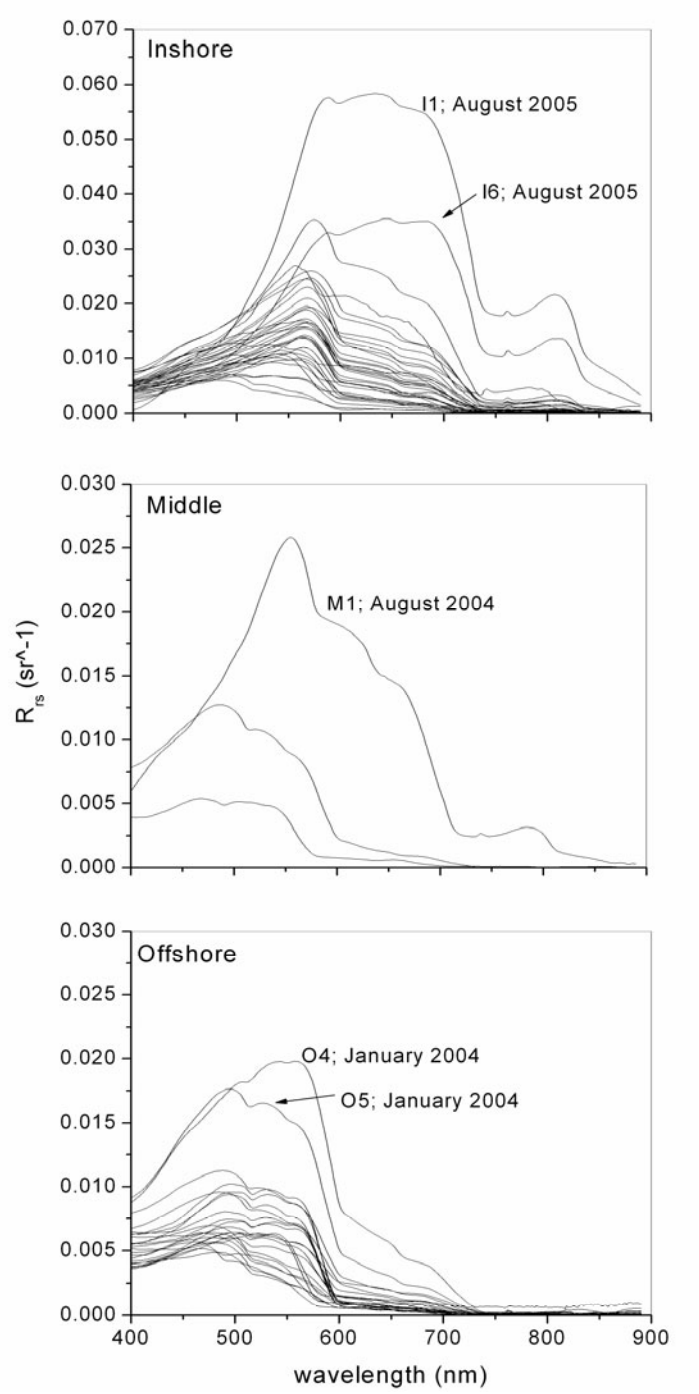

Figure 4. R_{rs} spectra measured during all research cruises from January 2004 to October 2006 at (a) Inshore, (b) Middle and (c) Offshore stations.

1.3.3 Spectral and spatial variability of b_b and b_{bp}

Median values of b_b and b_{bp} showed differences in magnitude and spectral response associated with sampling location (Fig. 5). Values from inshore stations were nearly one order of magnitude higher than those observed in offshore stations. Measurements of b_b in offshore stations presented typical behavior of clear waters where higher values were observed in the blue region continuously decreasing with longer wavelengths (Morel et al., 2007). Middle and inshore stations also had higher b_b values in the blue region but after 470 nm backscattering signal increases, especially at inshore stations where similar values were observed in channel 589 and 620 nm, both higher than observed in 470 nm (Fig. 5). The relative magnitude variations of these coefficients as affected by location are very similar to those by D'Sa and Miller (2003), and where lower values were observed in offshore stations and increasing as it moved closer to shoreline. Figure 5 shows that difference between median values of b_b and b_{bp} varies spectrally and spatially and this difference is more evident in shorter wavelengths and offshore stations. In order to determine variability of these differences, median and MAD (Median Absolute Deviation) of the difference between b_b and b_{bp} were calculated for all pair of values in the dataset (results not shown). Although difference by wavelength was very similar in all locations, offshore stations presented lower deviations indicating higher significance in the differences. In general, the relative contribution of b_{bp} to b_b becomes more important, up to two factors, at inshore and longer wavelengths. Median values obtained in inshore stations are very similar to reported for riverine waters in the Gulf of Mexico (Sydor and Arnone, 1997), which can either mean that concentrations are similar in both locations, or combination of differences in particles properties resulted in similar b_b values. Contribution of particle backscattering to total backscattering is higher at inshore stations than in middle and offshore stations due to usual turbidity of this type of waters. High backscattering values at 589 nm and 620

nm correspond to target wavelengths to estimate TSS because they reach ideal conditions where there is a dominance of TSS in the backscattering signal and the Chl-a fluorescence effect is reduced.

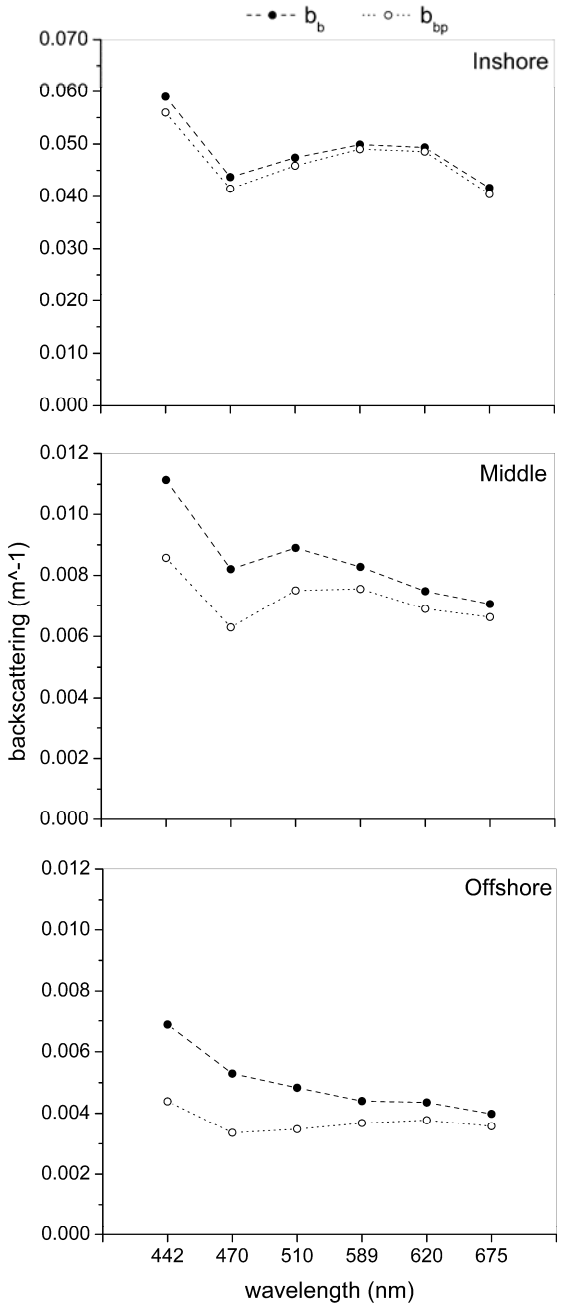

Figure 5. Spectral variation of the median values for total backscattering (b_b, m-1) and particles backscattering (b_{bp}, m-1) along three regions of the bay (inshore, middle and offshore). Dotted lines joining data points were included for illustration purposes and do not represent any spectral interpolation.

1.3.4 Relationship between b_{bp}, TSS and R_{rs}

The relationship between b_{bp}, TSS, and R_{rs} was determined with linear regression analyses in similar wavelengths for all measured parameters; that were 442, 470, 510, 589, 620 and 675 nm (Table 3). Good relationships for TSS and b_{bp} were found in all six wavelengths (R^2=0.74-0.76; n=133; P<0.0001 for all cases). Although there were not major differences in regression results between bands based on the square correlation coefficient (R^2) they tended to increase with longer wavelengths. Nearly identical regression results were obtained with b_b, with a slightly decrease in coefficients of determinations for all wavelengths (results are not presented here). Similar correlations results in both b_b and b_{bp} indicate that TSS dominates backscattered signal in all six wavelengths. It was determined that b_{bp} has a higher potential for TSS estimations over b_b, especially because it responds better to TSS variations and it does not incorporate the water effect. The best relationship between TSS and b_{bp} were obtained at 675 nm (R^2=0.76; n=133; P<0.0001) and 620 nm (R^2=0.75; n=133; P<0.001), Figure 6 shows three examples of linear regression for 442, 510 and 620 nm. Three points located farther of linear fit in all wavelengths correspond to station I6, showing a high variability contributed by this station. Sediment in the southern part of the Bay, where station I6 is located, are different in composition to the northern part of the bay due to material sources, physical processes, and inshore sand transport (Morelock et al., 1983). Beaches near Guanajibo River are dominated by igneous fragments, Magnetite and other dark minerals, while Quartz and Feldspars are more common near the Añasco River. In the regression analysis of b_{bp} and TSS the only variable considered was concentration. However, it is known that the volume scattering function, ß(θ), is also dependant of particle size, shape, and index of refraction (Baker et al., 2001). Waters condition in station I6 should be analyzed independently in terms of b_b response to TSS and compare to other regions of the bay because these waters appear to be optically different. This

presents an inconvenience not only to do estimations of TSS using the b_{bp} coefficient, but also in the development of algorithms based on satellite derived data.

Table 3. Regression relationships between backscattering, TSS and R_{rs} at six wavebands.

wavelength (λ)	Regression relationship; n=133; TSS =	R^2	Regression relationship; n=61; $R_{rs}(\lambda)$ =	R^2
442	70.616 * (b_{bp}442) + 2.1996	0.74	0.0157 * (b_b442) + 0.0062	0.14
470	81.786 * (b_{bp}470) + 2.3444	0.74	0.0272 * (b_b470) + 0.0073	0.24
510	71.632 * (b_{bp}510) + 2.4213	0.73	0.0593 * (b_b510) + 0.0075	0.54
589	59.066 * (b_{bp}589) + 2.6036	0.74	0.1337 * (b_b589) + 0.0022	0.77
620	64.895 * (b_{bp}620) + 2.5188	0.75	0.1415 * (b_b620) + 5E-06	0.78
675	79.089 * (b_{bp}675) + 2.391	0.76	0.1356 * (b_b675) - 0.0008	0.67

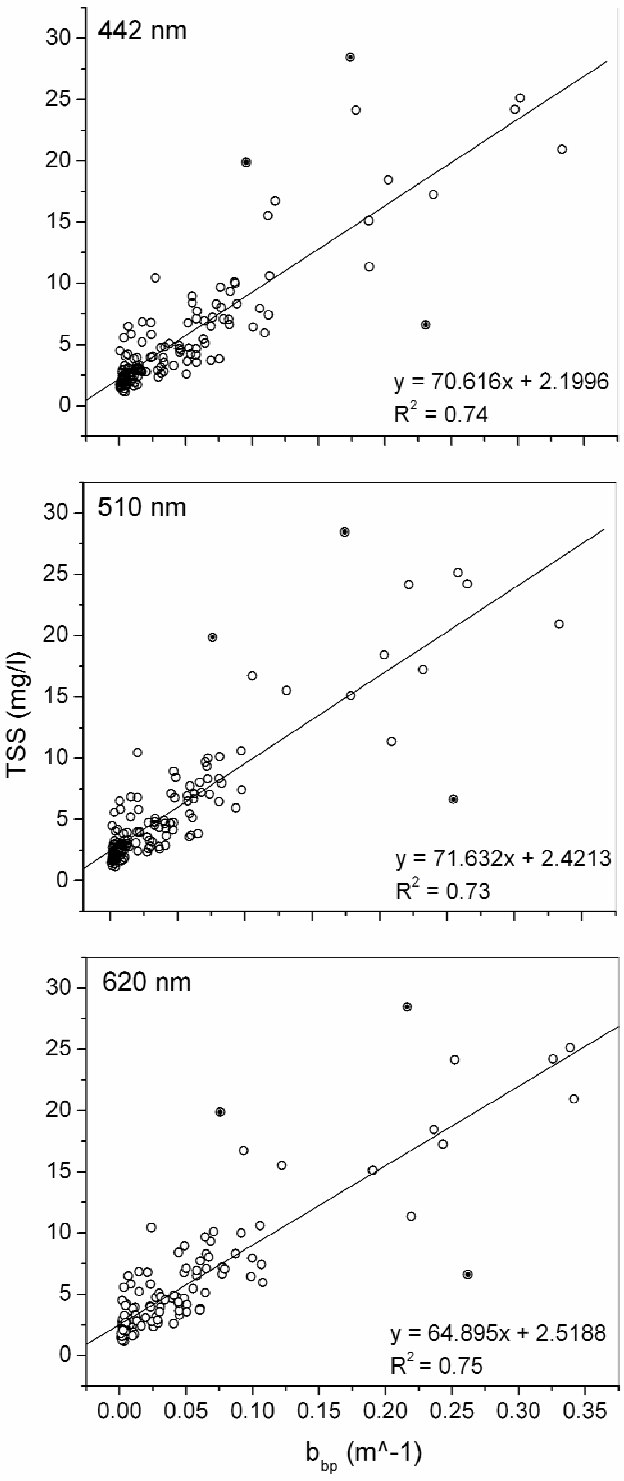

Figure 6. Relationship between TSS (mg/l) and b_{bp} (m^{-1}) at six wavebands. Filled circles identified three data points farther to linear equations; all these points corresponded to station I6.

Selection of the best channel for TSS estimation based on b_{bp} measurements involves evaluation of correlation results between these parameters. Although best correlation result was observed at 675 nm, it is well known that this channel is highly affected by Chl-*a* fluorescence (McKee and Cunningham, 2006; Huot et al., 2007) and it should not be consider for TSS estimation. On the other hand, numerous studies have identified an important contribution of TSS to water leaving signal at 620 nm (Ritchie et al., 1976; Witte et al., 1982; Doxaran et al., 2002a; Karabulut and Ceylan, 2005), therefore it is suggested to use the 620 nm channel to estimate TSS in regions similar to Mayagüez Bay.

Surface measurements (~0.5 m) of b_b were related with R_{rs} at same wavelength in order to determine the contribution of backscattering to water-leaving signal in this area. Regression results showed significant wavelength dependant variations, where square correlation coefficients increased with longer wavelengths (Fig. 7). The best regression was found at 620 nm (R^2=0.78; n=61), followed by 589 nm (R^2=0.77; n=61) and 675 nm (R^2=0.67; n=61). All these regression had a significance P value of <0.0001. In short wavelengths, values of R_{rs} showed higher variability than b_b, which resulted in not significant relationships in 442 nm, 470 nm and 510 nm (R^2= 0.14, R^2=0.24, R^2= 0.54, respectively; n=61). Pattern observed in regression analyses of R_{rs} and b_b occurred because in the red region pure water has an important contribution to total absorption, therefore variations detected in R_{rs} are mainly influenced by total backscattering (Tzortziou et al., 2007). Tzortziou et al. (2007) explain that in shorter wavelengths, R_{rs} is affected by both, total backscattering of suspended particles and absorption by non-covarying particles and dissolved components due to the minimal contribution of pure water absorption. Based on this, poor correlations in short wavelengths suggest not only the influence of both parameters, but also dominance of absorption over backscattering.

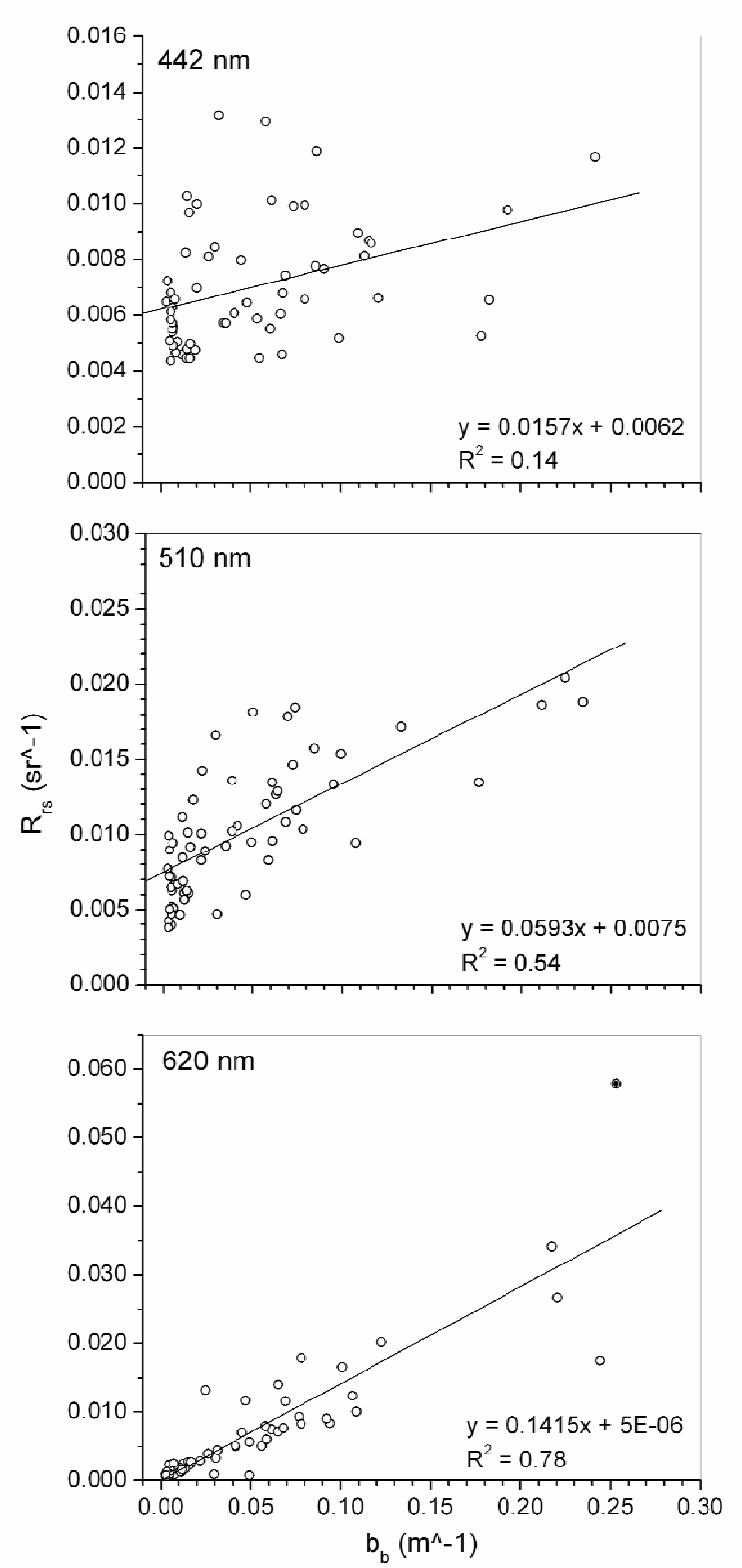

Figure 7. Relationship between backscattering (b_b, m^{-1}) and R_{rs} at three different wavelengths (442 nm, 510 nm and 620 nm). Filled circled in the third plot corresponds to station I1 in August 17, 2005, a day of a significant rain event.

1.3.5 Effect of TSS on remote sensing reflectance

Eleven measurements taken at river mouths during June of 2008 were incorporated in the database in order to have more values of high TSS concentration. Remote sensing reflectance curves were plotted using all collected data and calculating mean values of R_{rs} associated with four different ranges of TSS concentrations (<5 mg/l, 6-10 mg/l, 11-20 mg/l and > 20 mg/l). Figure 8 shows variations in magnitude and spectral shape as affected by concentration of TSS. The highest difference in R_{rs} magnitude due to TSS was observed from 550 nm to 700 nm. A clear peak was observed in the near-infrared region (775 nm to 825 nm) for concentrations higher than 20 mg/l, this signal is lost in lower concentrations suggesting that this region is highly affected by high concentrations of TSS. Previous studies have shown similar results for relationship between TSS and R_{rs} (Ritchie et al., 1976; Doxaran et al., 2002a; Doxaran et al., 2003, Schalles et al., 2001), even when observed TSS concentrations are significantly lower than other used in this type of analyses. In highly turbid waters, reflectance in the near-infrared can be successfully incorporated when developing algorithms for TSS estimations (Doxaran et al., 2002b; Moore et al., 1999). Mayagüez Bay, however, is dominated by waters with relatively low concentrations of TSS, thus the signal in this region is normally weak. Additionally, low water-leaving radiance cannot be distinguished from the effect of atmosphere during satellite monitoring applications.

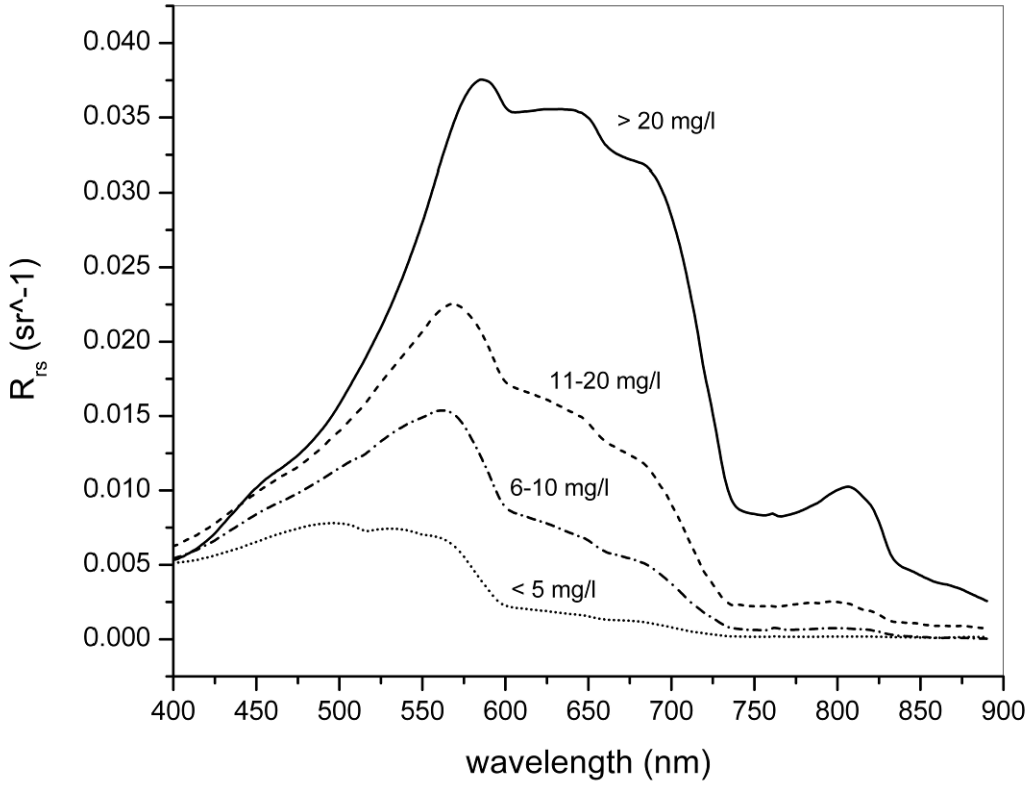

Figure 8. Mean in situ R_{rs} categorized in four concentration ranges of TSS: >20 mg/l (n=9), 11-20 mg/l (n=9), 6-10 (n=21) and < 5 mg/l (n=33). These values include all measurements obtained within the study period and data collected at mouth of the rivers during June 2008.

Table 4. Regression relationships between TSS and R_{rs} at 9 single wavebands and four band ratios. Comparison between ratios of R_{rs} at 560nm/620nm, 412nm/670nm (evaluated by Wernand et al., 1998 as in SeaWiFS and MERIS algorithms), 665nm/555nm (evaluated by Binding et al., 2005) and 655nm/545nm, which presented the best correlation results from present analysis.

R_{rs} parameter (X)	Regression relationship; n=72; TSS =	R^2
$R_{rs}(442)$	1357.9 * (X) - 1.512	0.17
$R_{rs}(470)$	1331.6 * (X) - 3.4123	0.24
$R_{rs}(510)$	1153.2 * (X) - 4.2096	0.45
$R_{rs}(589)$	579.58 * (X) + 1.6079	0.73
$R_{rs}(620)$	599.3 * (X) + 2.7821	0.73
$R_{rs}(645)$	602.63 * (X) + 3.1481	0.73
$R_{rs}(665)$	634.34 * (X) + 3.5357	0.71
$R_{rs}(675)$	641.76 * (X) + 3.6363	0.71
$R_{rs}(859)$	3675.4 * (X) + 5.9588	0.46
$R_{rs}(560)/R_{rs}(620)$	$16.941 * (X)^{-1.232}$	0.75
$R_{rs}(412)/R_{rs}(670)$	$7.7701 * (X)^{-0.5628}$	0.77
$R_{rs}(665)/R_{rs}(555)$	23.943 * (X) - 0.7366	0.81
$R_{rs}(655)/R_{rs}(545)$	20.353 * (X) - 0.3937	0.84

Regression analyses for TSS and R_{rs} using several single wavelengths and ratios of them were performed combining data collected during monthly cruises and river mouths samplings (Table 4). Initially, same wavelengths presented in previous analysis (442, 470, 510, 589, 620, 675 nm) were used to facilitate the comparison with other results. Then, other wavelengths corresponding to spectral bands of ocean color sensors such as MODIS, SeaWiFS, and MERIS were also analyzed to evaluate their applicability over the study area (Table 4). Within the single band analysis, the best regressions were found at 589, 620 and 645 nm with a significant good relationship (R^2 = 0.73; n=72). In longer wavelengths (665 and 675 nm) the square correlation coefficients decreased slightly toward the near-infrared region where a poor correlation was observed at 859 nm (R^2=0.46; n=72); both 645 and 859 nm wavelengths represent the center of MODIS band 1 and 2, respectively. Since color band ratios reduce variability of reflectance associated with changes in particle

characteristics (e.g. size and shape; Doxaran et al., 2002b; Moore et al., 1999) and effect of surface reflection (Doxaran et al., 2004), this approach was included in the analysis in order to compare the relationship from ratios and single wavelengths. Many authors have found that square correlation coefficient increased when using ratios. For instance, Wernand (1998) evaluated band ratios associated with SeaWiFS band 1 (412 nm) and 6 (670 nm) and MERIS bands 5 (560 nm) and 6 (620 nm) for TSS estimation with reasonable results. Same ratios were incorporated in this study and better relationships were found between R_{rs} and TSS (R^2= 0.75 for $R_{rs}560/R_{rs}620$ and R^2=0.77 for $R_{rs}412/R_{rs}670$) than using single wavelengths. After evaluating various combinations within the visible spectral region, it was determined that best relationship was produced by a red:green ratio, specifically at 655 and 545 nm (R^2=0.84; n=72; Fig. 9).

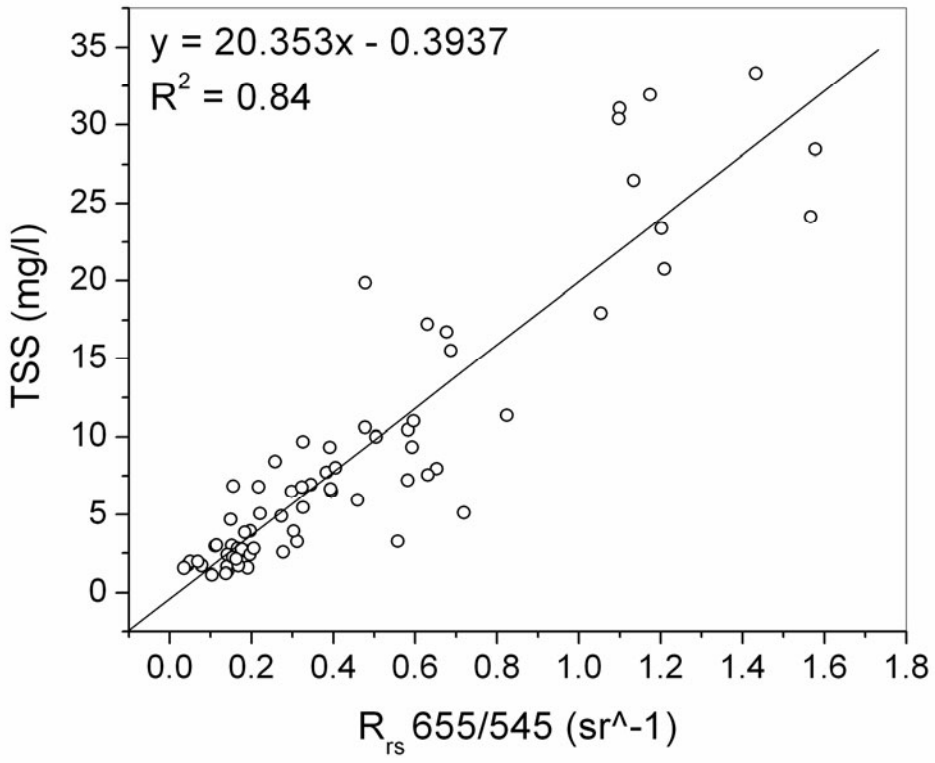

Figure 9. Relationship between TSS (mg/l) and the R_{rs} red:green ratio 655nm/545nm which presented the best linear relationship defined between these two parameters.

The single band regression analysis supports the use of wavelengths 589 or 620 nm to estimate TSS because both showed higher square correlation coefficients. The regression analysis using R_{rs} at 645 nm (center of MODIS band 1) also presented same correlation results, a band previously used for this type of application. On the other hand, present analysis presented a stronger correlation using a R_{rs} red:green ratio (R^2=0.81; n=72). This is different to observations of Binding et al. (2005), which correlate irradiance reflectance (R_{-0}) and mineral suspended sediments and observed a weak red to green ratio (R^2=0.65), compared to when using the single red band (R^2=0.92). Better relationships between red to green reflectance ratios suggest that suspended sediments dominates water optical properties, over the effect of phytoplankton and CDOM substances (Binding et al., 2003). This presents an advantage to generate estimations of TSS from satellite derived data in Mayagüez Bay since the effect of other water constituents in water-leaving signal is reduced. This analysis suggests that combination of bands will be the best approach to estimate TSS in this type of waters; however, the incorporation of bands ratios is restricted to data availability from appropriate sensors in terms of spectral and spatial characteristics.

1.3.6 Relationship between MODIS and field data

Attempts to validate previously published algorithms using MODIS band 1 (Miller and McKee, 2004) were made for the study area with unsuccessful results. One of the major limitations for this approach is the large variability of physical and optical properties in this area; this makes necessary the development of site specific algorithms. Per cent of cloud cover in available MODIS images also presented a significant limitation for this analysis. Out of 13 days of sampling only 7 images could be used (Table 2). Origin and processing methods corresponding to MODIS data used in this analysis are fully described in the second chapter. Normally, remote sensing techniques applied to tropical environments is limited by availability of cloud free

images, and this limitation is overstated during afternoons in west part of Puerto Rico due to the orographic effect (Pico, 1974). Therefore, constant monitoring of TSS or other water constituents using remotely derived data is restricted in this area. *In situ* parameters included in this analysis were TSS concentration, b_{bp} at 620 nm (HydroScat-6) and R_{rs} at 645 nm (GER-1500 spectroradiometer). These two wavelengths were used because other authors have suggested 620 nm for TSS estimation and 645 nm is the center of MODIS band 1. The relationship between TSS, b_{bp}, R_{rs} and MODIS band 1 reflectance is shown in Figure 10. Best regression of MODIS data with *in situ* measurements was observed with R_{rs}. Two relationships were defined between R_{rs} 645 nm and MODIS reflectance because of the presence of an outlier in the dataset (Fig. 10c). This outlier corresponds to station I1 sampled during a high discharge event occurred in August 17 of 2005; mean discharge for that day was equal to 62.3 m^3/sec, while overall mean discharge for the entire month of August was 11.6 m^3/sec (USGS, 2008). The square correlation coefficient when incorporating this point showed a strong relationship (R^2=0.88; n=30; P<0.0001) between these two parameters, indicating a high correspondence between MODIS reflectance and *in situ* R_{rs}. A decrease in both, slope and square correlation coefficient (R^2=0.69; n=29; p< 0.0001) is observed when that point is excluded. This extreme value could be representative of rare, but real conditions; therefore, more sampling associated with high river discharge is necessary to validate this relationship.

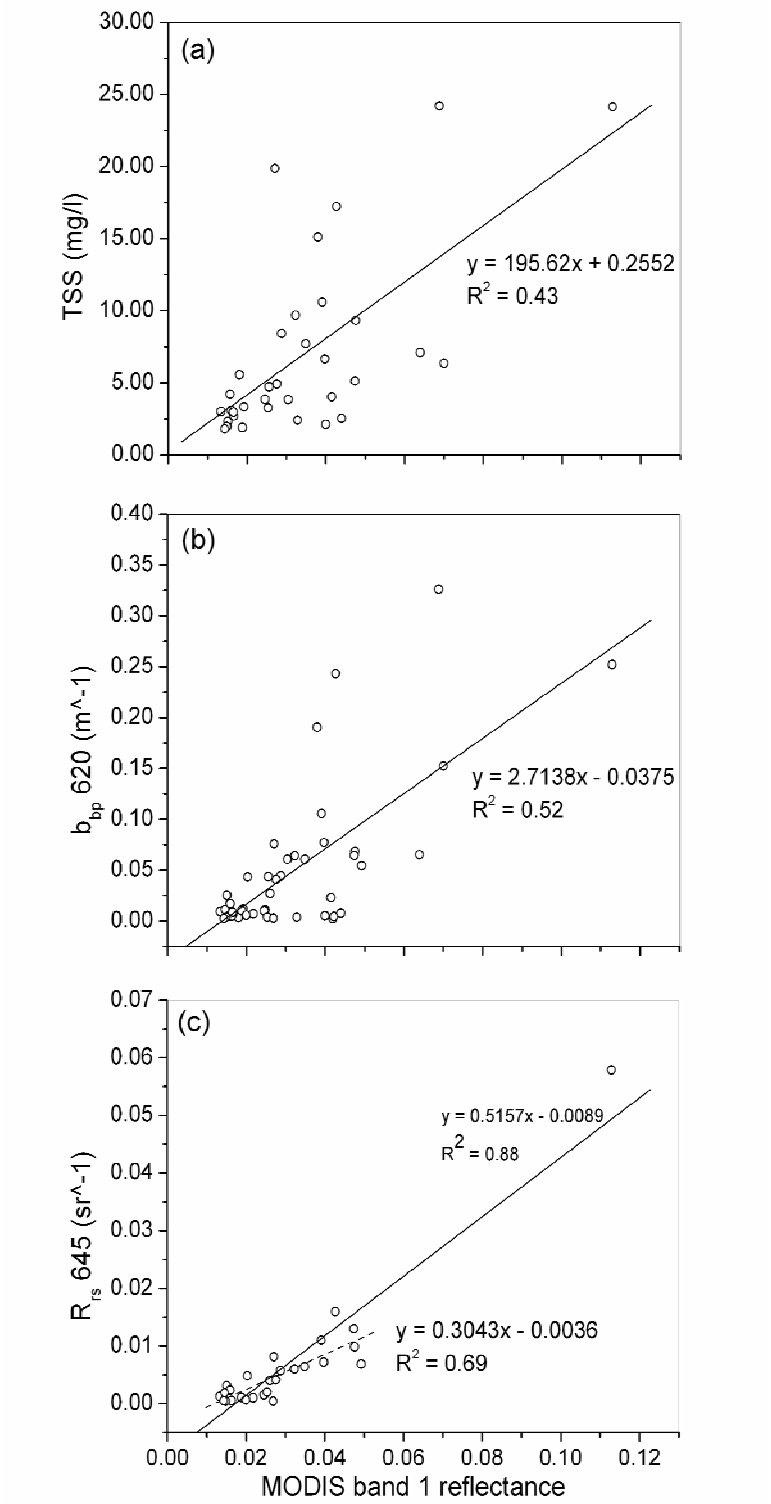

Figure 10. Relationship between MODIS band 1 and in situ measurements of (a) TSS (mg/l), (b) b_{bp} at 620 nm (m^{-1}) and (c) R_{rs} at 645 nm (sr^{-1}). The long line in the last plot included the outlier data point from station I1 during August 17 of 2005 while the short line only included clustered values.

These results indicates how challenging is to define any relationship between MODIS reflectance and *in situ* measurements of optically active components in this area. This difficulty could be diminished by incorporating more observations in the dataset. Some general issues that can introduce additional uncertainty in this analysis are sensors and *in situ* measurement errors and difference in timing between *in situ* measurements and satellite overpasses (Chang et al., 2006). However, there are various factors more specific of this analysis and the study area conditions that can be affecting the analysis such as limited spatial extent and highly disturbed atmospheric conditions. The Mayagüez Bay encompasses a small area (~95 Km^2) where significant variations in turbidity within meters are observed. Working with a relatively small range of TSS values from which extreme values can be found (as shown in station I1) within an area smaller to the size of a pixel (250 m) unavoidably resulted in variability difficult to define. Also, this analysis incorporated the used of the dark-subtract atmospheric correction, which have been previously used for same applications in the Gulf of Mexico (Miller and McKee, 2004). One consideration is an improvement in the atmospheric correction; however, this requires the incorporation of other bands in the infra-red region which have broader spatial resolutions (500 m and 1 Km). Another factor is the signal produced by sea floor (Curran and Novo, 1988). This effect is reduced when account that in the red region the depth of light penetration is smaller than in shorter wavelengths. But, the southern region of this bay is characterized by very clear and shallow waters, which suggests a high bottom effect and higher error in satellite –derived products. In conclusion, a lack of better correlations is attributed to four main factors: (1) high spatial variability of water constituents, (2) the atmospheric effect, (3) sensor limitation and (4) sea floor reflectance.

1.4 CONCLUSIONS

This study provides a baseline for better understanding spatial and spectral variability of remote sensing parameters and their relationship with TSS. No significant difference in TSS values was detected between the rainy and the dry season; therefore, higher concentrations of TSS associated with shoreline proximity were not only attributed to river discharged but also to re-suspension events. The southern part of the bay appears to be optically different to the rest of the area considering that it contributed a large amount of variability when b_{bp} and TSS were related. Regression analyses between b_b and R_{rs} suggest that TSS dominates water-leaving signal between 589- 645 nm making a target region for applications using remote sensors. This is sustained when the incorporation of red to green ratios improved the square correlation coefficient in the linear fit between these parameters. These results support the use of red and green bands in the development of better remote sensing algorithms for tropical waters. On the other hand, the near infrared region is not suitable for these purposes because the signal in this region was only associated with TSS values higher than 20 mg/l and these conditions are limited to waters very closed to the mouth of the rivers, especially in Añasco River. Comparison of MODIS band 1 reflectance with b_{bp} 620 nm and TSS *in situ* measurements presented poor correlations, while a strong correlation between R_{rs} and MODIS was defined. The main limitation of this analysis was MODIS data unavailability due to high percent of cloud cover in most of cruises dates. High spatial variability of optical parameters in the study area in combination with the relative low spatial resolution of MODIS demonstrated that better ocean color sensors are required for coastal studies in tropical open bays.

CHAPTER 2:

Using MODIS 250 m Imagery to Estimate Total Suspended Sediment in Mayagüez Bay

Abstract

Monitoring and better understanding of sediment flux and processes in coastal environments are important to maintain water quality and geomorphologic balance. This chapter describes the development and validation of an algorithm to estimate total suspended sediment (TSS) based on remote sensing reflectance (R_{rs}) and MODIS/Terra band 1 data. Two image processing methods, based on two image analysis packages with predefined routines, were evaluated and compared in order to determine the most suitable method for the study area. Analyses of *in situ* data showed a significant relationship between TSS and *in situ* R_{rs} at 645 nm (R^2=0.73) indicating positive response of this parameter in the interested region of the spectrum. Developed algorithms were evaluated by applying resultant equations to two MODIS images from which *in situ* data were available. In the validation analysis the lower error was encountered when using an exponential equation, however linear equations estimations followed better the tendency of measured values. TSS estimations of all three algorithms presented values within the range of *in situ* observations and spatial patterns characteristic of coastal environments. Additional data and pre-processing parameters should be evaluated in order to improve validation results and produce TSS operational products for tropical coastal waters.

2.1 Introduction

Distribution and abundance of TSS is of great importance when evaluating the condition of a coastal system. However, it is challenging to develop methods that assist in the monitoring and assessment of these processes especially at broad scales (Hu et al., 2004). This limitation is reduced by incorporating remote sensing techniques where desired information can be retrieved from spectral data collected using remote platforms. Satellite technologies are widely used to quantify and monitor water quality parameters in coastal waters. Empirical algorithms are used to derive satellite estimations of water constituents (e.g. Chl-a, CDOM and TSS) which reduce field work and help covering large areas. The development of these algorithms normally involves the establishment of empirical relationships between the satellite derived data and *in situ* measurements. This is based on the principle that variations in spectral response can be associated with specific water constituents. Several studies have used satellite derived data to estimate TSS to monitor water turbidity (Chen and Muller-Karger, 2007), sediment resuspension (Miller et al., 2004), and other novel applications such as the estimations of deposition rates (Peckham, 2007).

Numerous sensors have been developed for different ocean color applications, including water turbidity assessments, such as AVHRR, SeaWiFS, MODIS, IKONOS, Landsat TM and ETM+. Variations in temporal and spectral resolutions, data availability, calibration issues and temporal coverage are some of the most important factors determining the selection of the best instrument for a particular study (Li and Li, 2004). MODIS provides a good temporal resolution (1 day) for monitoring purposes; however, the spectral sensitivity of this sensor decreases as the spatial resolution increases. It is well known that in Case 2 waters the leaving signal is highly dependant of TSS concentration specially in wavelengths longer than 500 nm

(Moore et al., 1999; Doxaran et al., 2003; Teodoro and Veloso-Gomes, 2008). Therefore MODIS band 1 (250 m), which covers the range between 620 to 670 nm, has large potential data to estimate TSS. Although this band was originally created for land applications, previous studies have validated it use for water quality studies in coastal and estuarine waters (Hu et al., 2004; Miller and McKee, 2004; Chen et al., 2007; Nasr et al., 2007). The application of previously formulated ocean color algorithms for the estimation of water constituents is generally limited by site-specific factors (Hellweger et al., 2004), and presently there is no uniform remote sensing based model to estimate TSS (Wang et al., 2005). Limiting factors in Mayagüez Bay are primarily the combination of working in a relatively small area (~95 Km^2), the presence of optically complex waters (Rosado, 2008) and a relatively small range of TSS values. On the other hand, one of the most determinant aspect when using satellite images to retrieve water quality parameters is the atmospheric correction. In this study we have compared and evaluated the results of two atmospheric correction methods available in two different image analysis packages: ENVI and SeaDAS. The present study is focused in the development and validation of site-specific algorithms to estimate TSS with MODIS reflectance band 1.

2.2 METHODS

This study aimed to establish empirical relationship between *in situ* measurements of TSS concentration, MODIS band 1 reflectance and *in situ* remote sensing reflectance (R_{rs}) as measured with a field spectroradiometer. This approach will show the potential of MODIS sensor for TSS estimations and determine the best method to develop an algorithm for this purpose.

2.2.1 In situ measurements

All *in situ* data used in this chapter corresponded to field measurements described in sections 1.2.1 and 1.2.3.

2.2.2 MODIS imagery

Two different processing methods were used to generate functional products derived from the Moderate Resolution Imaging Spectroradiometer (MODIS). One was based on pre-processing routines available in ENVI software and the second used SeaDAS commands (Fig. 11). Images collected by MODIS during the same sampling dates were downloaded through two NASA Internet servers: LAADS Web and OceanColor Web. For the first method the product selected at LAADS Web was MOD02QKM, which includes reflectance and radiance values of MODIS/Terra band 1 and 2. All these images were processed using ENVI (v. 3.4) processing routines: MODIS Georeference and Dark Subtract. The spatial reference system was defined as UTM NAD83 for Puerto Rico region. The georeferencing was validated by overlaying seventeen points corresponding to shoreline limits within the Mayagüez Bay on the georeferenced band 2 images (Fig. 12). The dark subtract atmospheric correction consists in the selection of the darkest value in band 2 and subtract it to all band 1 data. This value was manually identified in each image and then defined in the "User Value" option of this routine. For the second method, L0 data were downloaded at the OceanColor Web browser. These data were processed using SeaDAS MODIS commands from level 0 to level 2. The program L2gen uses as input L1b data and generates level 2 products by applying atmospheric corrections and bio-optical algorithms (OceanColor Webmaster, 2008). Conditions in these waters suggested that the best algorithm for atmospheric correction available in SeaDAS is the one that performs multiscattering switching between Near Infrared (NIR) and Short Wave Infrared (SWI) bands (J. Trinanes, personal communication). However, additional

algorithm corrections, available within L2gen command, were evaluated in order to improve the results. After generating L2 products, the data were projected as UTM NAD83 using SeaDAS Map Projection command.

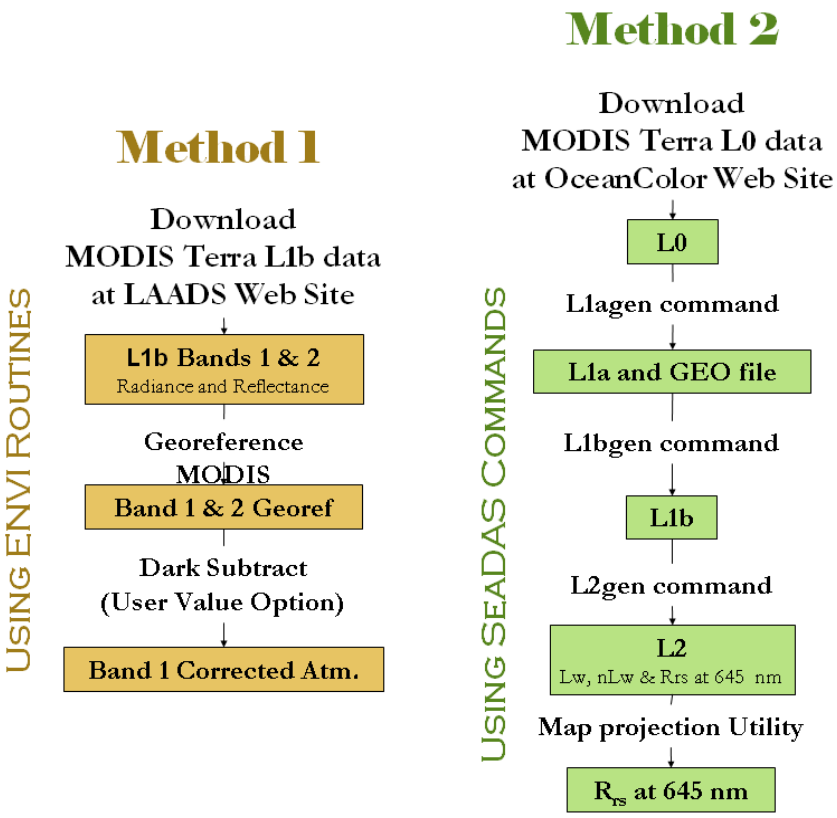

Figure 11. Schematic illustration of two methods used to process MODIS data. Method 1 is based in ENVI image processing software and Method 2 uses SeaDAS specialized commands.

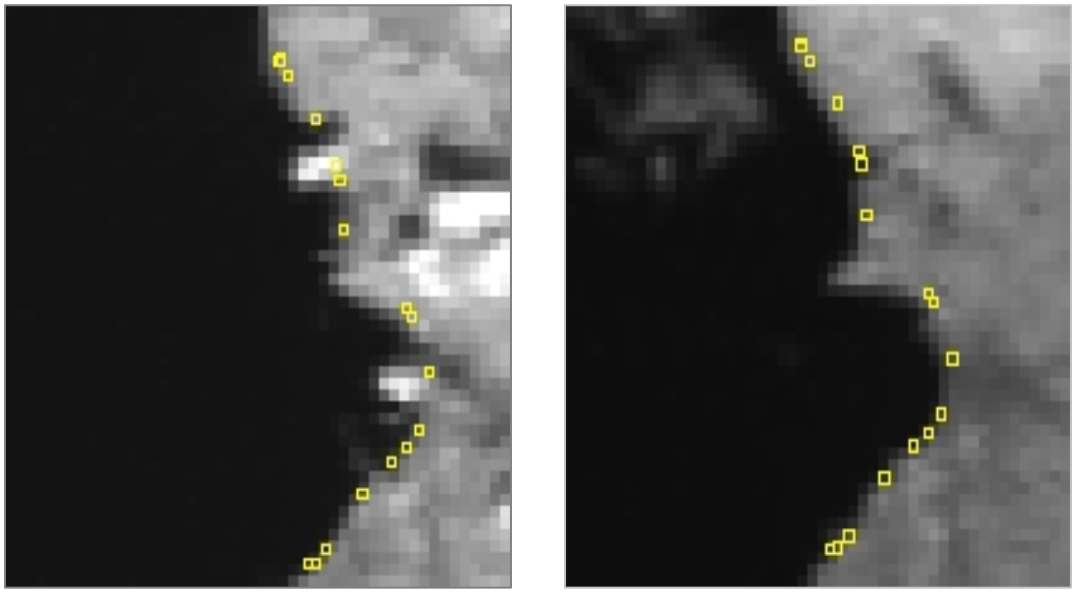

Figure 12. Seventeen point locations collected along Mayagüez Bay shoreline overlaying two images: October 19, 2005 (left) and December 6, 2005 (right).

.2.2.3 Algorithm Development and Validation

The developed algorithm consisted in the combination of two equations, one defining the relationship between field R_{rs} and TSS, and other establishing the relationship between field R_{rs} at 645 nm and MODIS band 1. Data collected during thirteen sampled days were used to develop the first equation, while this number was limited to five for the second equation. This difference was mainly due to the lack of good quality images suitable for analyses, which affected the development of the second equation. MODIS reflectance values were extracted from pixels corresponding to stations monitored for R_{rs}. Developed equations were applied to two images (February 12, 2004 and March 8, 2008), which were not incorporated in the previous analysis and *in situ* data were available in order to validate developed algorithms. Application of the equations was possible using ENVI band math tool, which contains easy to use options to ingrate image bands in mathematical equations.

Proficiency of the algorithms was evaluated by comparing estimated and observed values in a root mean square error (RMSE) analysis. Additionally, obtained TSS products were visually analyzed in order to evaluate and identify spatial patterns associated with this type of environment. Finally, all resultant pixel values within Mayagüez Bay area were extracted for statistical analyses by defining a region of interest (ROI) corresponding to that specific area. This ROI was created from a polygon vector file that was digitalized using visual interpretation of orthorectified aerial photographs (2006) in ArcMap (ArcGIS 9.3, ESRI).

2.3 Results and Discussion

2.3.1 MODIS Products

The first method resulted on seven reflectance products at 645 nm (band 1), one for each research cruise dates. Three different products for each date were generated using the second method: Remote sensing reflectance (R_{rs}), Water-Leaving Radiance (L_w) and Normalized Leaving Radiance (nL_w). For purposes of this study the target product was R_{rs} at 645 nm, however the generated values (and the rest of generated products) were mostly negative and with flagged values. This suggested that the standard method for processing MODIS data in SeaDAS is not suitable for application in this type of waters characterized by relative high concentrations of TSS and other water constituents (like CDOM) in comparison to oceanic waters. Low and negative values indicated that the applied atmospheric correction is overcorrecting by removing also part of the water-leaving signal while flag values in the coast suggest that the processing routine is identifying as errors highly contrasting reflectance values. The variations between Case 1 and Case 2 waters limit the generation of standard satellite products (Guerriero et al., 2007). These processing algorithms are mainly developed for oceanic waters, therefore they are not able to recognize as good

values, patterns that are typical in coastal waters. One potential option to minimize the number of flag values is to adjust the different parameters available in the flags menu option within the L2gen command, but this approach was not included in this analysis because that is topic for another research. Table 5 shows MODIS reflectance and *in situ* R_{rs} 645 nm obtained in sampling stations during October 19, 2005. Comparison between these two parameters showed that satellite derived reflectance is considerably lower than *in situ* R_{rs}. This difference can be mainly attributed to two factors: atmospheric effects and spatial resolution. Radiometric measurements collected by sensors on satellite platforms are not only affected by land or water surface radiance but also atmospheric absorption, scattering and attenuation and these atmospheric effects are not included on field R_{rs} measurements. Additionally, MODIS data is representative of 250 m pixels while the field spectoradiometer gives measurements of as specific point within that area.

Table 5. Pixel values obtained in permanent sampling stations using Method 1 and *in situ* R_{rs} at 645 nm.

Stat. ID	Latitude (N)	Longitude (W)	Method 1 Reflectance at 645 nm	*in situ* R_{rs} at 645 nm
I1	18º 16.00'	67º 12.00'	0.047406	0.0130
O1	18º 16.00'	67º 15.20'	0.018792	0.00118
I2	18º 14.40'	67º 11.40'	0.027528	0.0041
O2	18º 14.40'	67º 11.40'	0.019948	0.0007
O4	18º 12.20'	67º 12.95'	0.016265	0.0005
I6	18º 10.25'	67º 11.10'	0.027037	0.0081
O6	18º 10.25'	67º 14.80'	0.014844	0.0005

2.3.2 Total Suspended Sediment Algorithm

In chapter 1 a significant relationship (R^2=0.73; n=72) was foundz between TSS (mg/l) and *in situ* R_{rs} at 645 (Fig. 12a). This result suggests that this region of the spectrum is

suitable for TSS estimation using remotely sensed data in these waters. However, a large unknown variability was detected in this equation that could be reduced by the incorporation of more observations. Two linear equations were defined to establish the relation between TSS (mg/l) and in *in situ* R_{rs} at 645 nm (Fig. 13b) because of the presence of an extreme value. The higher square correlation coefficient (R^2=0.88; n=30; P<0.0001) was observed when incorporating such extreme value. The strong relationship between these two parameters indicates a high correspondence between MODIS reflectance and *in situ* R_{rs}. A decrease in both, slope and square correlation

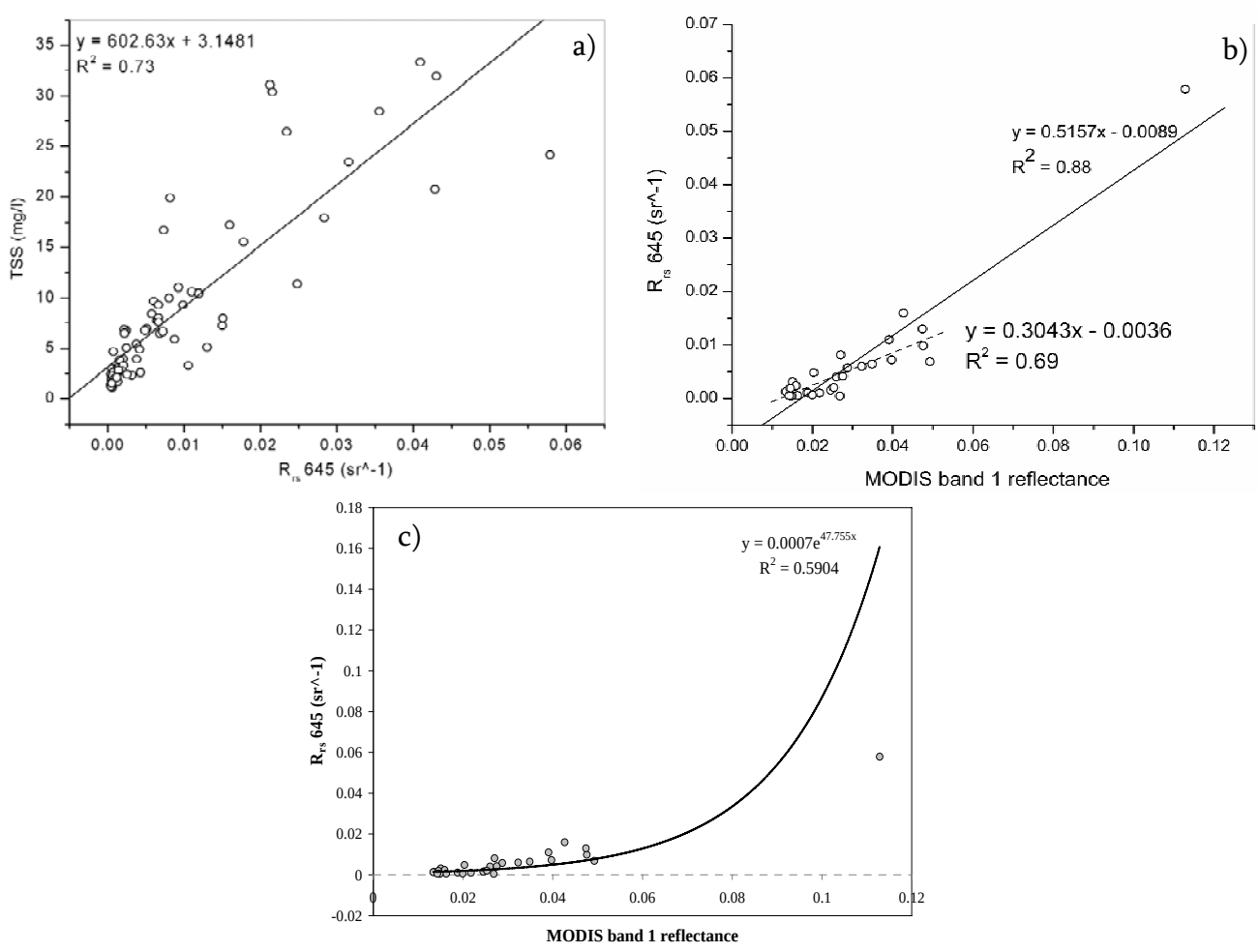

Figure 13. Data used to develop a TSS algorithm for Mayagüez Bay; (a) Relationship between in situ R_{rs} at 645 nm and TSS, (b) Two linear equations and (c) one exponential equation defining the relationship between in situ R_{rs} at 645 nm and MODIS band 1 reflectance.

coefficient (R^2=0.69; n=29; p< 0.0001) is observed when the extreme value is excluded. This value could be representative of rare, but real conditions; therefore, more sampling associated with high river discharge is necessary to validate this relationship. It was observed that when working with low reflectance values resultant estimations tended to be negative or extremely low, therefore an exponential equation was incorporated in this analysis in order to minimize this effect (Fig. 13c). The square correlation coefficient of this equation was lower (R^2=0.59) than when using linear equations. Based on these analyses the following algorithms were implemented and tested:

$$TSS = 602.63 * (0.5157 * (\text{MODIS band 1}) - 0.0089) + 3.1481 \quad (2.1)$$

$$TSS = 602.63 * (0.3043 * (\text{MODIS band 1}) - 0.0036) + 3.1481 \quad (2.2)$$

$$TSS = 602.63 * (0.0007 e^{47.755 * \text{MODISband1}} + 3.1481 \quad (2.3)$$

2.3.3 Total Suspended Sediment Algorithm Validation

For validation purposes, equations (2.1), (2.2) and (2.3) were applied to two images corresponding to cruises dates (Feb 12, 2004 and March 8, 2006) not included in the development of the equations. The first two algorithms resulted in RMSE higher than 5 mg/l (Fig. 14a-b) while the lower RMSE (4.8 mg/l) was encountered when using equation 2.3 (Fig. 14c). Comparison between these validation results indicated that equation 2.3 was able to better estimate TSS in lower concentrations, but during higher concentrations it tended to underestimate this parameter. Although equation 2.1 showed a higher RMSE, estimated values followed better the tendency of observed values. The limitations of these algorithms can be attributed to various factors: (i) limited data of high TSS concentrations, (ii) MODIS band 1 is not capable of detecting TSS signal under low concentrations conditions, (iii) the atmospheric correction method is not appropriate, and (iv) the presence of sea-bottom effect in the signal. Another problem that could be affecting the results is the mixing pixel

phenomenon; which is a common and highly influence problem when trying to derive information from satellite imagery (Roosta et al., 2007). In the case of TSS estimations, the mixing pixel occurs when variations in TSS concentrations or land and water areas are combined within the 250 m cover area of a pixel. Occurrence of this phenomenon can be reduced by using images with higher spatial resolution, but this alternative is limited by current ocean color sensors.

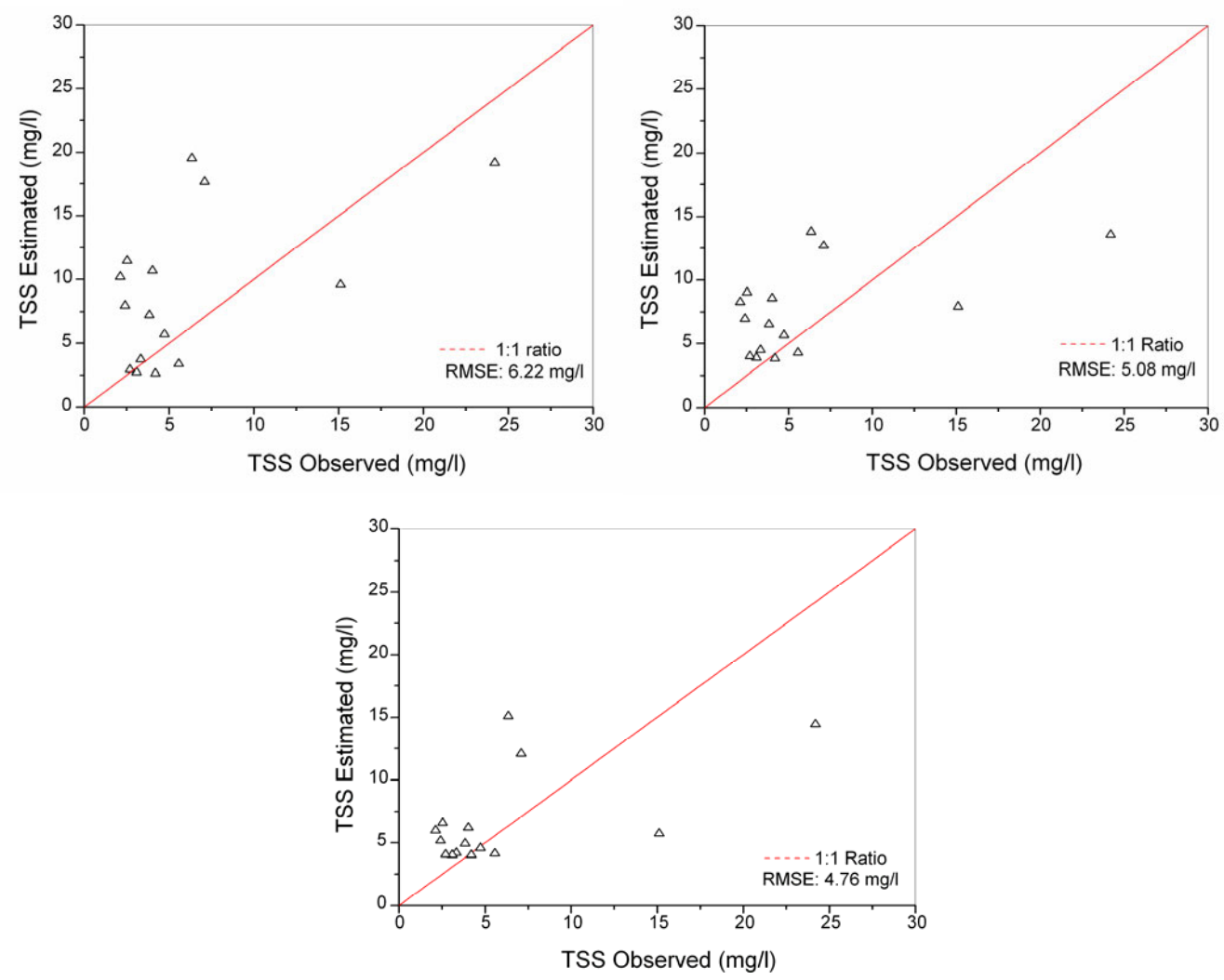

Figure 14. *Validation results when applying (a) equation 2.1, (b) equation 2.2 and (c) equation 2.3.*

2.3.4 Total Suspended Sediment Products

Estimations of TSS were generated using three developed algorithms in order to spatially analyze results and compare efficiency of the equations. Figures 15 a-b show spatial variations associated with TSS concentration in Puerto Rico surroundings areas and Mayagüez Bay for the dates used in the validation analysis. The spatial variability in MODIS-derived TSS appeared to respond by inshore processes showing higher concentrations in areas closer to the shoreline which are typical of coastal environments. In the case of Mayagüez Bay the majority of high values are concentrated in the northern part of the bay where the Añasco River plume is located. Comparison between all three different algorithms does not indicate any significant difference between them; the main difference resides in algorithm 2.1 which range of values is higher than the algorithm 2.2 and 2.3. Therefore, application of algorithm 2.1 resulted on more contrasting spatial variations between values in inshore and offshore areas.

February 12, 2004

Algorithm 2.1

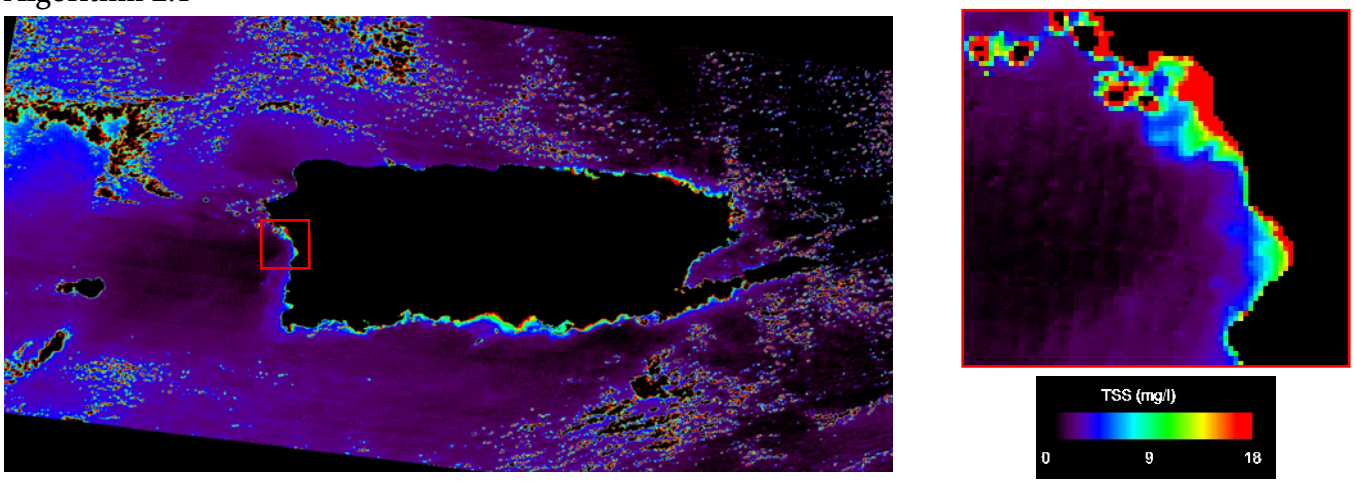

Algorithm 2.2

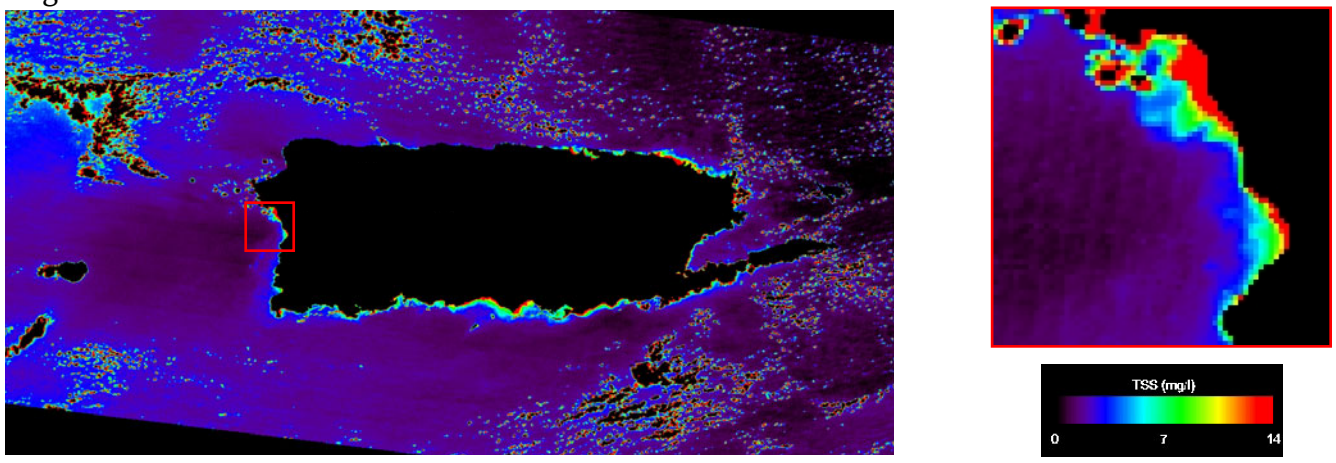

Algorithm 2.3

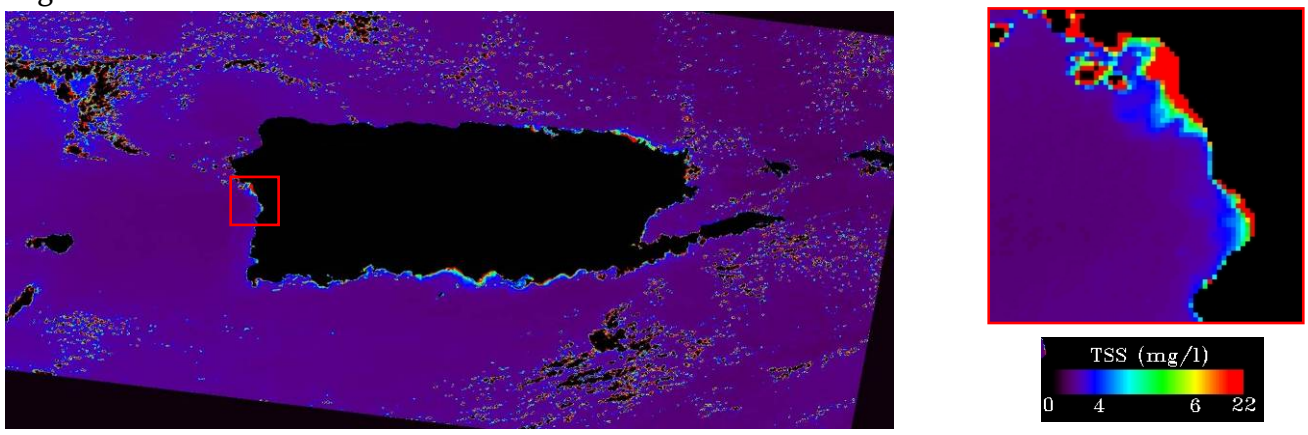

Figure 15 a. TSS products generated using three developed algorithms based on MODIS band 1 data for February 12, 2004. Mayagüez Bay indicated with the red box and a close up is shown on the right side. Note the differences in scale values of the color palettes.

March 8, 2006

Algorithm 2.1

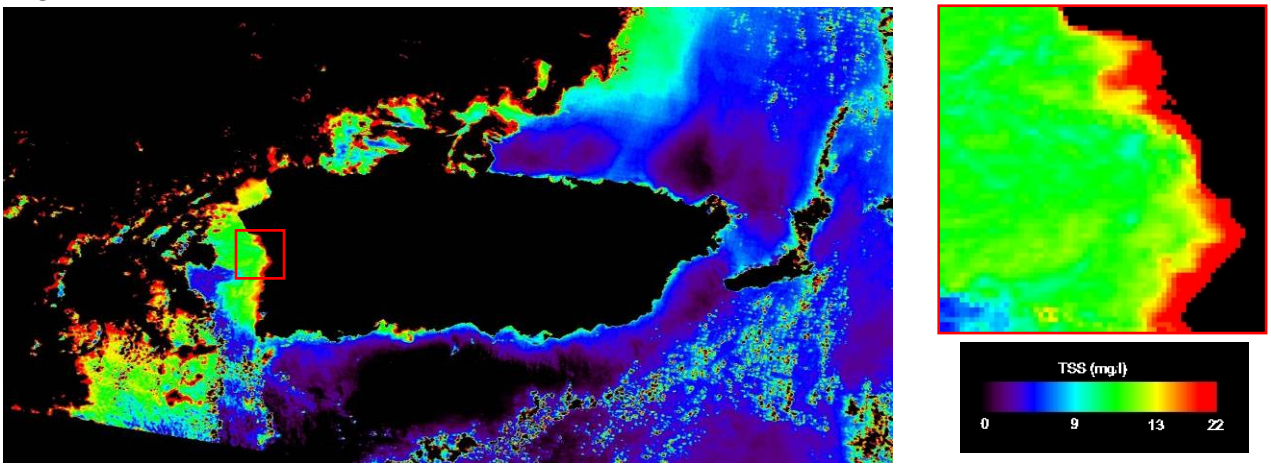

Algorithm 2.2

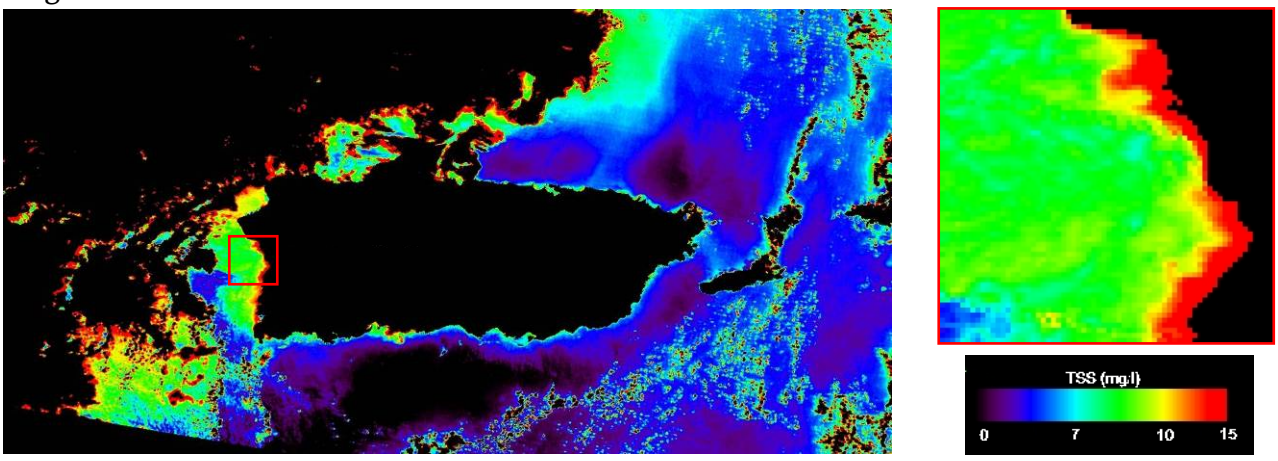

Algorithm 2.3

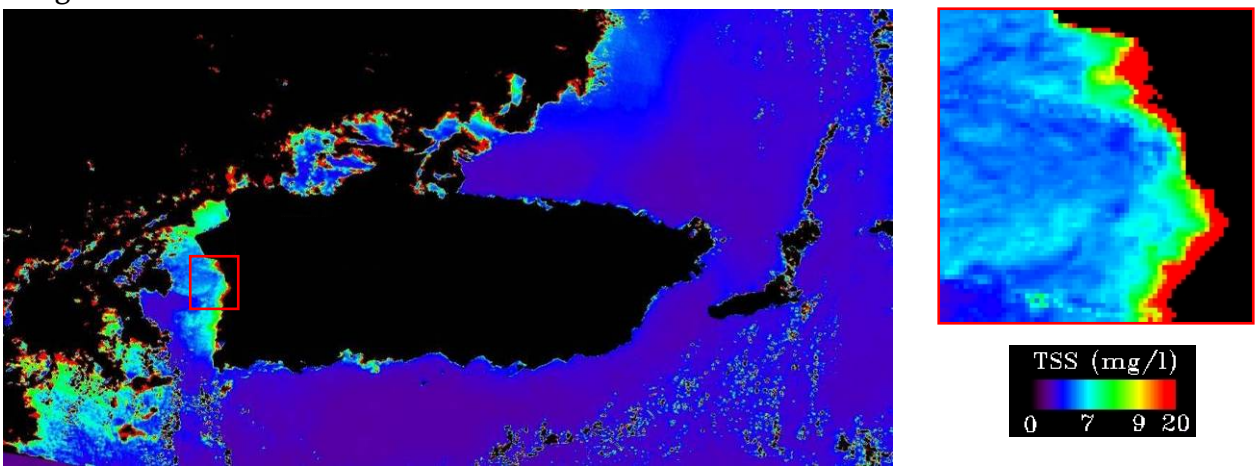

Figure 15 b. TSS products generated using three developed algorithms based on MODIS band 1 data for March 8, 2006. Mayagüez Bay indicated with the red box and a close up is shown on the right side. Note the differences in scale values of the color palettes.

TSS estimated values corresponding to Mayagüez Bay area were extracted and analyzed using basic statistics. Figure 16 illustrates the distribution of TSS values using both field data (Study Period: January 2004-October 2006) and generated TSS products for February 12, 2004. Direct comparison between these data sets has been made considering the following statements: (i) sampling stations are distributed along the bay covering inshore and offshore areas (ii) TSS measurements used in this analysis includes only surface samples (iii) selected date for this analysis (February 12, 2004) presents commonly occurrence conditions in this bay. Mean values for all products (4.6, 5.0, 4.7 mg/l) were highly comparable to *in situ* mean value (5.9 mg/l) and all showed positive skewed distributions (Fig. 16).

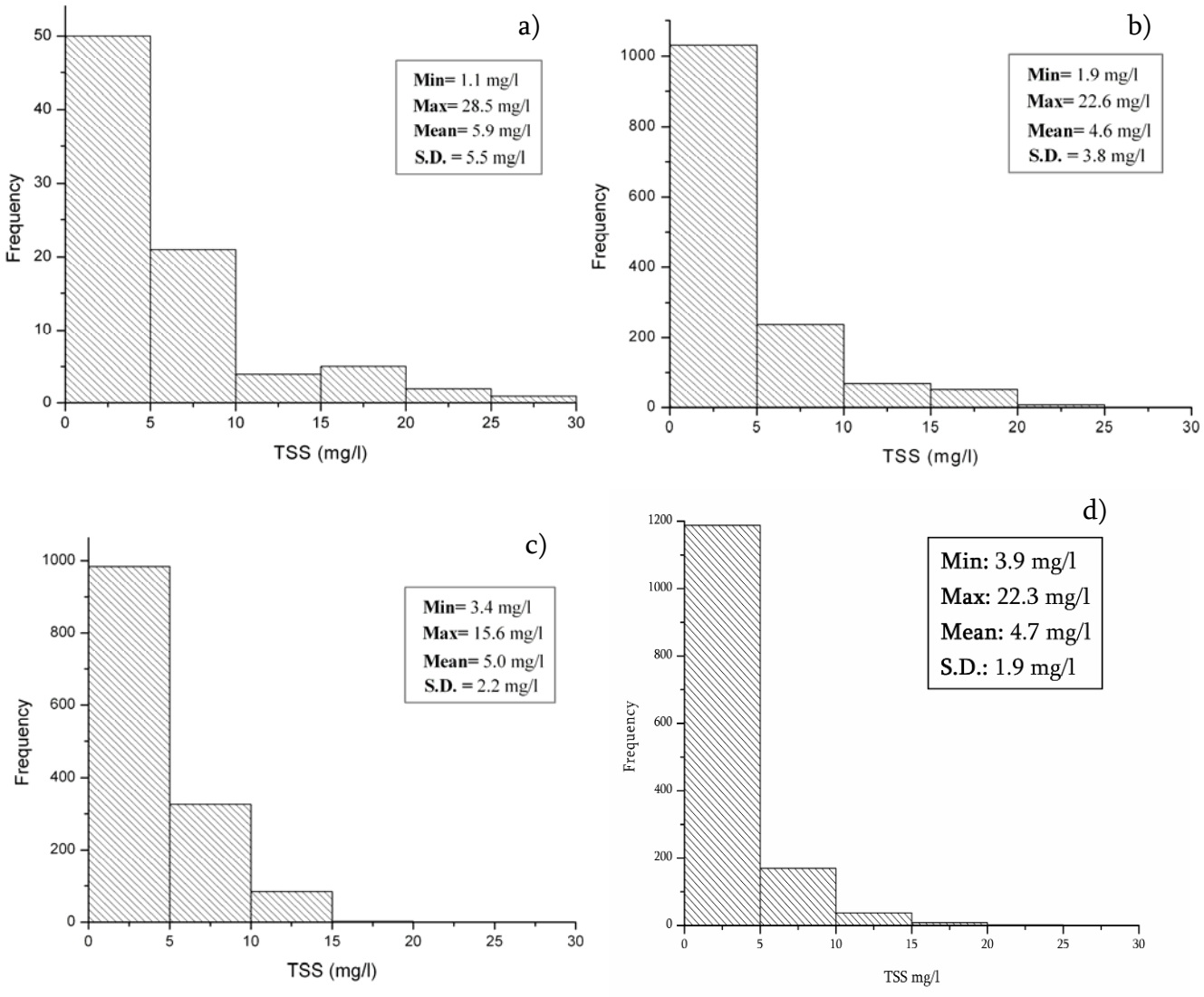

Figure 16. Descriptive statistics and histograms illustrating TSS values distribution for (a) in situ measurements collected within the study period (January 2004-October 2006) and TSS products generated using (b) equation 2.1, (c) equation 2.2 and (d) equation 2.3.

.

Minimum values of algorithms 2 and 3 (> 3.0 mg/l) indicates that these results can be overestimated considering that this analysis includes areas where TSS concentrations are normally lower than 2.0 mg/l (e.g. offshore in the southern part of the bay). Algorithm 1 presented the higher similarity with the distribution of *in situ* TSS measurements (Fig. 16b). However, in order to determine which estimation better

followed real conditions, spatial analysis of *in situ* measurement of that particular day should be incorporated.

2.4 CONCLUSION

Geometric and radiometric corrections utilized during image pre-processing routines are crucial for this type of analysis. Atmospheric correction included in L2gen command (SeaDAS) is not suitable for application in Mayagüez Bay waters. This same result is expected to find in other tropical bays. Fairly good empirical relationship were defined between *in situ* R_{rs}, TSS and MODIS band 1 data using linear and exponential equations. Application of developed equations resulted on TSS products able to detect spatial variations associated with typical patterns of coastal environments. Algorithm 3 showed the higher correspondence between observed and estimated values (RMSE 4.76 mg/l). However, all three algorithms resulted in reasonable TSS pixel values when compared with data from *in situ* measurements. Therefore at this point none of the algorithms is excluded for future application. More testing of all of them is needed. Using an exponential equation resulted in a more suitable approach for this study purpose, since the algorithm including this equation was more effective estimating low values which are the dominant conditions in the studied bay. Validation results can be improved by addressing limiting factors such as lack of data corresponding to high concentrations, and contamination by the remaining atmospheric effect in the derived reflectance of the sensor. This study provided baseline results to develop TSS operational products for tropical coastal waters by developing preliminary products and identifying potential errors and limiting factors occurring during the process.

CHAPTER 3:

Estimating annual suspended sediment load in Mayagüez Bay using GIS and Remote Sensing techniques

Abstract-

The development of methods to integrate inland and coastal products using GIS and remote sensing techniques provides an enormous advance in the study of coastal environments. The Revised Universal Soil Loss Equation (RUSLE) was applied to Mayagüez Bay watershed by defining raster layers (pixel size = 10 m) of associated factors in a GIS based model. Spatially variable soil erosion rates and sediment yields estimations, from 2001 to 2005, were estimated for this basin. Validation results indicated that the equation published by Boyce (1975) to calculate sediment delivery ratios (SDR) responded to conditions of the area, while the other two equations evaluated for the same purposes (Vanoni, 1975 and USDA, 1972) tended to overestimate this parameter. Sediment yield estimations generated for year 2004 for Rosario river sub-watershed (32,365 Mg/yr) were highly comparable to field measurements at USGS gauge station (33,622 Mg/yr) showing the great potential of the developed model. MODIS data for twenty dates of 2004 were used to generate suspended sediment load products corresponding to northern and southern parts of the bay. Results of the northern area showed a fairly good relationship (R^2=0.71) with Añasco river discharge measurements, but additional values of high river discharge are required to strengthen this association. This study presents a new approach with excellent baseline results for parallel applications in this bay and other tropical coastal systems.

3.1 INTRODUCTION

Dynamics of coastal environments is highly influenced by inland fluvial processes, such as soil erosion and sediment deposition and transport. Soil erosion by water has been identified as the most important land degradation problem Worldwide (Eswaran et al., 2001). Increase in sediment yields from river basins causes by different forms of catchments disturbance have been increasingly recognized as a major environmental problem in many areas of the World (Walling, 1997). For instance, high erosion could cause loss of soil fertility and a reduction in reservoirs water storage capacity. The amount of material eroded and transported influences channel morphology (Alvarez, 2005) and sediment deposition rates in reservoirs and ponds (Soler, 1999; Soler et al., 1999). Also, special concern exists on transportation of sediments associated with nutrients, pesticides and heavy metals from agricultural areas (Behera and Panda, 2006; Corvera 2005). Different types of sources contributing to the sediment budget of a watershed includes: landslides, debrisflows, gullies, treethrow and animal burrows. Defining and describing sediment production is a complex process that involves many considerations such as type of erosion, sources of sediments and its relative contribution, grain-size distribution associated with these sources, approximate volume and grain size of sediments stored along the streams and the transport rate through the fluvial system (Reid and Dunne, 1996). However, it is difficult to account for all these aspects in a single model, especially if the study area has a large extension. This is the case of Mayagüez Bay watershed which has an area of 915 km^2 which include Añasco, Guanajibo and Yagüez rivers watersheds (Fig. 17). Empirical models facilitate predictions and perform with the same quality as complex distributed models (Jetten et al., 2003; López-Vicente and Navas, 2009). The Revised Soil Loss Equation (RUSLE) is the most accepted empirical model to predict average soil loss by water at plot and catchments scale (Renard et al., 1997). This model predicts the amount of soil loss, caused by sheet and rill erosion, occurring within a

determined area for one year (Wischmeier, 1976). Predictions of this equation are commonly used to identify areas with higher potentiality of soil erosion and determine the effect of land use changes in sediment production in small watersheds (Onyando et al., 2005; López et al, 1998; Cartwright, 2002). Originally this equation was not intended for application in non agricultural areas and complex watersheds (Wischmeier, 1976), but various studies have presented its potential for soil loss prediction in large and complex watersheds (Simms et al., 2003).

Remote Sensing and Geographic Information System (GIS) technologies provide tools that allow the incorporation of spatial variations of physical, climatologic and topographic factors affecting erosion potentiality in a watershed. Chapter 2 shows how spectral analysis tools permits the estimation of suspended loads in absolute terms (mg/L) in coastal waters. In this chapter additional products will be derived in order to compare them with parallel results generated using a GIS based model. GIS is a computer based system designed to collect, analyze, store, manage and display geographic data. The application of these technologies has facilitated the implementation of this type of models raising more uses and applications for sediment studies in larger spatial scales. Renard (1997) has proposed the used of RUSLE to estimate sediment delivered down slope by combining calculated soil loss and sediment delivery ratios (SDRs) functions. This approach is essential for the current study purposes since one of the main objectives is to associate coastal sediment variations to inland processes.

3.2 METHODS

3.2.1 Watershed Erosion Modeling

A GIS based model was developed to estimate soil erosion in the Mayagüez Bay watershed (Fig. 17) using principles of the most widely used empirical model to predict soil erosion by water. This model was first developed by Wischmeier (1976)

and named as the Universal Soil Loss Equation (USLE), then in 1985 the Natural Resources Conservation Service of the United States Department of Agriculture (USDA-NRCS) decided to develop a revision to incorporate additional research resulting in a adapted version known as RUSLE- Revised USLE (Renard et al., 1997) This equation predicts annual soil loss, in units of tons/acre/year, as the products of different factors associated with erosion by water using the following equation:

$$A = R * K * L S * C * P \qquad 3.1$$

Where,

A= Soil erosion (Tons/Acre/Year); **R**= Rainfall factor; **K**= soil erodability factor; **L**= Slope length factor; **S**= Slope steepness factor; **C**= Cover and management factor; **P**= erosion control practice factor. Figure 18 illustrates information related to the origin of the data used to define all these factors.

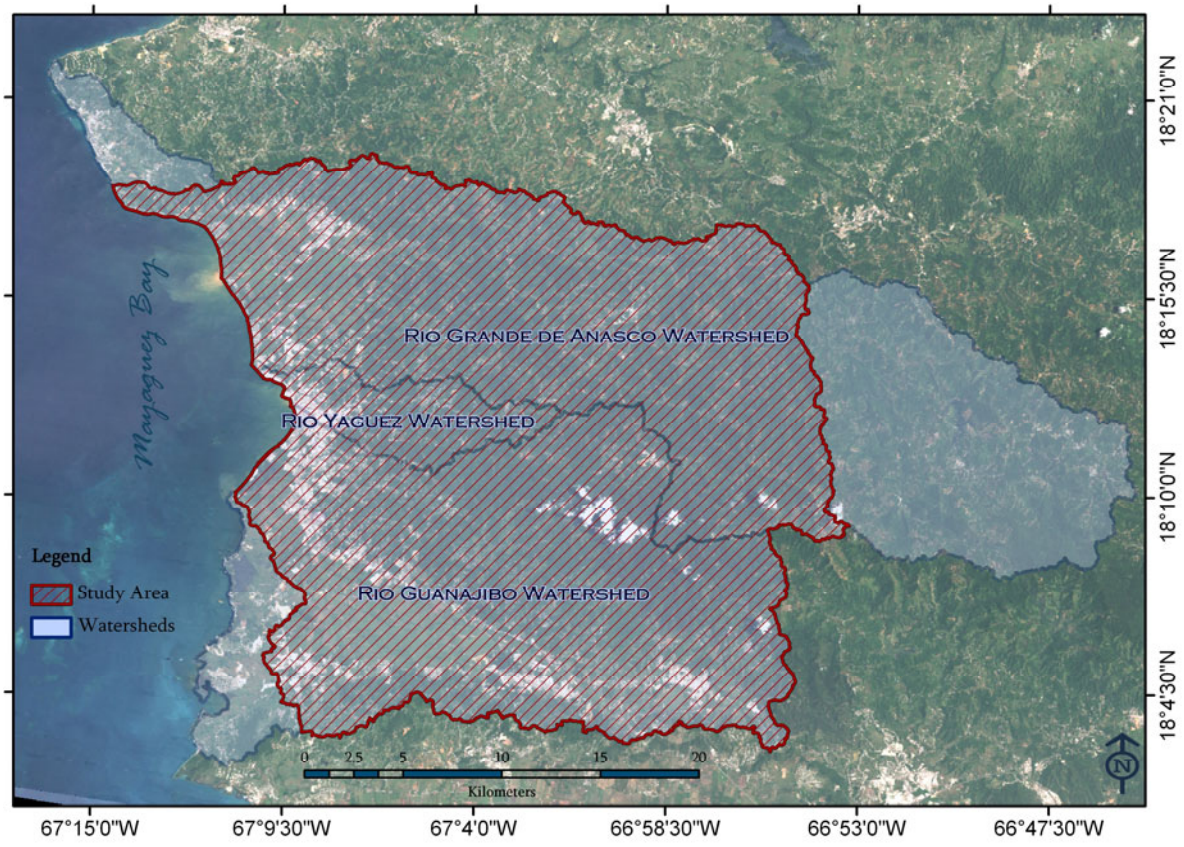

Figure 17. Mayagüez Bay and three watersheds associated with this coastal system. Region in red indicates area included in the GIS model.

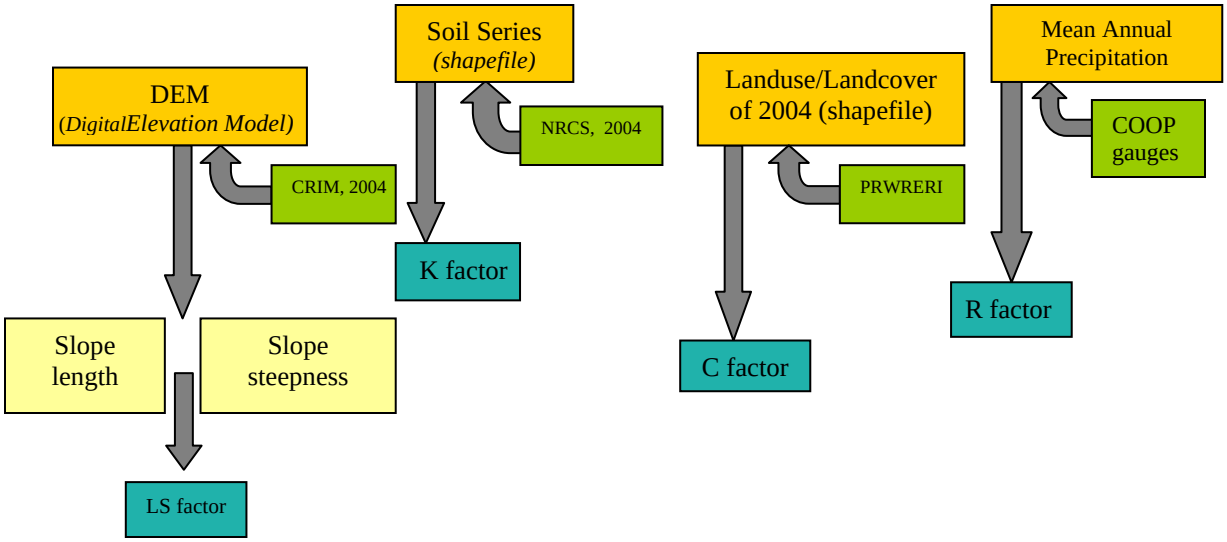

Figure 18. Schematic diagram showing information about the origin of all layers defined in the model. Information of land management practices within the study area was not available; therefore, the P factor was set as 1.

Units of RUSLE factors are originally derived in English units and the direct conversion of each unit to the International System is not recommended (Renard et al., 1997), instead the resultant product was converted from ton/acre/year to Mg/ha/yr.

The assemblage of this model required defining RUSLE factors for all the study area using raster format. The raster format is a cell-based representation of map features that better allows overlay analyses in a GIS (ESRI, 2002). This part of the study also aimed to detect significant temporal variations in five consequent years (2001-2005). Therefore, independent annual estimations of soil loss were generated for each year within that period. However, the only component that was changed in all five simulations was the rainfall factor because non-significant changes were expected in Soil Erodibility and Slope Steepness/Length factors, and no additional land cover data was available for the time period evaluated. Annual soil loss estimates consist of a new grid layer generated as the product of six factors defined in the next sections:

3.2.2 Soil Erodibility factor (K)

The K factor represents an annual average value (ton*acre*hour/hundreds of acre *foot*ton*inch) that integrates variation of soil profiles in terms of detachment and transport properties by raindrop impact and surface flow (Renard et al., 1997). K values for the study area were retrieved from the RUSLE attribute table available in the USDA-NRCS Soil Data Mart Portal. Finally, this information was joined to a soil thematic layer and converted to raster format for incorporation in the GIS model.

3.2.3 Cover Management factor (C)

The C factor (dimensionless) integrates the effect of cropping and management practices on soil erosion rates. López et al. (1998) made use of land use variations in terms of vegetation coverage and land uses to define the C factor based on local values published in RUSLE Handbook developed for the Caribbean Area (NRCS, 1995).

For this study the input layer to derive C factor was a land-use thematic layer developed by the Puerto Rico Water Resources and Environmental Research Institute (PRWRERI) in 2004. This thematic layer originally consists on 32 categories (classes) and then it was reclassified to eight categories to which unique C values were assigned (Table 6).

Table 6. Eight landuse classes included in the model and their area extent. Defined classes and C factors were based on López et al. (1998).

Landuse Class	Area (Km²)	Total Cover	C Factor
Agriculture	26.8	3.6%	0.050
Bare Soil	12.5	1.7%	1.000
Closed Canopy Forest	143.9	19.3%	0.014
Dense Urban	94.7	12.7%	0.001
Less Dense Urban	12.1	1.6%	0.020
Open Canopy Forest	198.7	26.7%	0.023
Pasture	253.5	34.0%	0.032
Water	3.1	0.4%	0.000
TOTAL	**745.3**		

NRCS 1995; López et al. (1998)

3.2.4 Slope Steepness and Length Factor (LS)

The slope and length factor represents the effect of topography in sheet and rill erosion by combining the slope length and steepness of an area. A set of high resolution (10 m) DEMs were processed to produce a single elevation grid for all the area to use as input information to define the slope steepness/length factor. This grid was used to generate raster layers indicating slope (percent) and flow accumulation by a routine available in the Spatial Analyst extension of ArcGIS 9.2 (©ESRI Inc., 1999-2006). Flow accumulation is the number of cells contributing to the flow of a specific cell. The following equation was adapted from Morgan (2005) to calculate the LS factor:

$$LS = \sqrt{\frac{(Flow\ accumulation + 0.5) * L}{22.13}}(0.065 + 0.045 * S + 0.0065 * S^2) \qquad 3.2$$

where,

L is the cell size (m) and S is slope (%).

3.2.5 Rainfall Erosivity factor (R)

The input data used to define the Rainfall factor was total annual precipitation measured in 16 weather stations located within the Mayagüez Bay watershed and surrounding areas (Fig. 19). All these stations are part of the Cooperative Observer Network Program which includes thousands of weather stations that collect data along all US 50 states, Puerto Rico, and the Virgin Islands. Table 7 shows location, stations names IDs and precipitation data of all weather stations used in this study. Total annual precipitation was used to calculate the R factor for each location where precipitation data was available for each year by using the following linear equation:

$$R = 0.2629 * X - 11.06 \qquad 3.3$$

where,

R is the rainfall factor (hundreds of ft. ton. in. acre-'. yr^{-1}) and X was defined as annual precipitation (mm). This linear equation was defined by López et al. (1998) and consists of an empirical relationship between mean annual precipitation (1981-1995) of 11 weather stations distributed along Puerto Rico and the R factor values extracted from an iso-erosivity map.

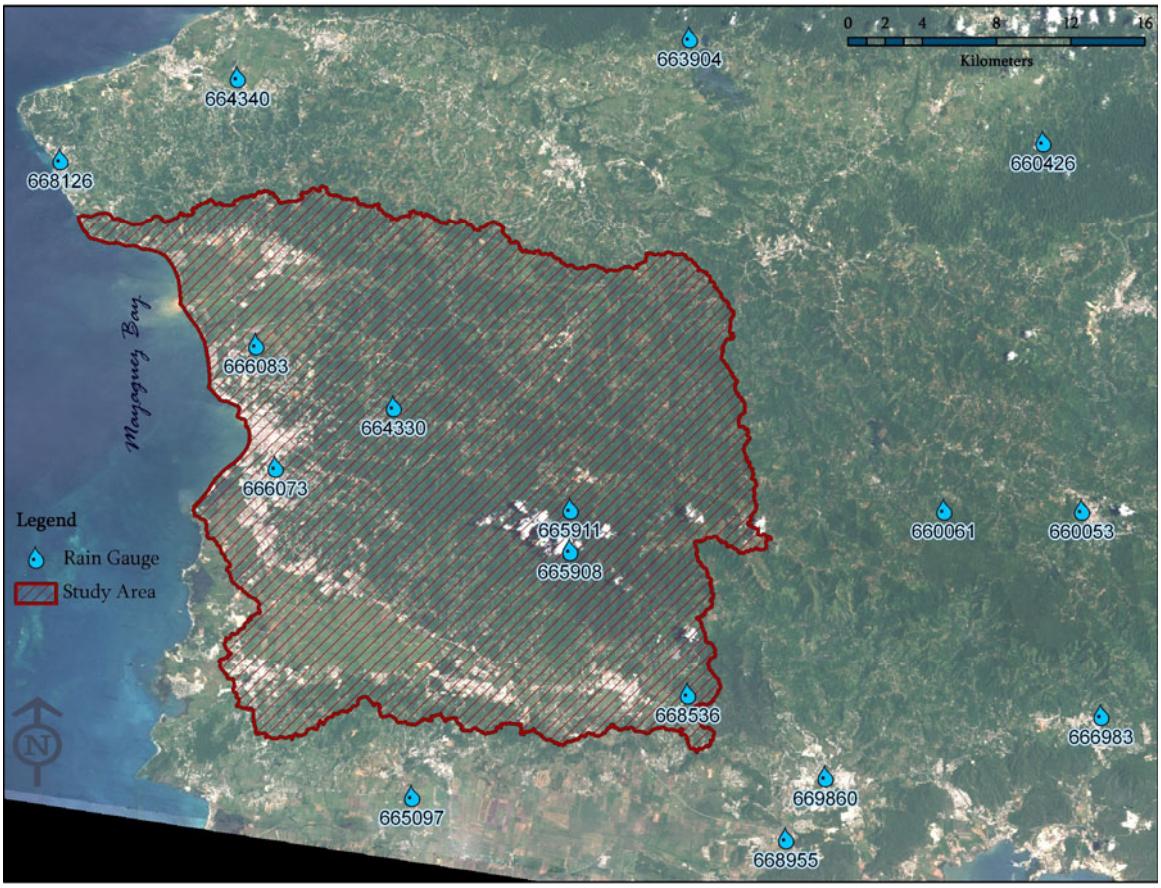

Figure 19. Sixteen weather stations from which precipitation data was obtained to estimate R factor.

Table 7. Descriptive information of sixteen stations and annual precipitation totals (mm) for five years (2001, 2002, 2003, 2004 and 2005). See figure 19 for station locations.

Station Name	COOP ID	Latitude	Longitude	Annual Precipitation (mm)				
				2001	2002	2003	2004	2005
ADJUNTAS 1 NW	660053	18.16801	-66.72957	1883	1640	2358	2648	2653
ADJUNTAS SUBSTATION	660061	18.16802	-66.79961	1960	1728	2264	2462	2176
COLOSO	664340	18.37799	-67.15966	2300	2031	2294	1730	2007
HACIENDA CONSTANZA	664330	18.21801	-67.07961	No Data	No Data	1542	1883	1862
LAJAS SUBSTATION	665097	18.02803	-67.06963	1067	894	1704	1308	1293
MARICAO 2 SSW	665908	18.14802	-66.98962	2653	2385	2242	2666	2609
MARICAO FISH HATCHERY	665911	18.16801	-66.98964	2280	2432	2665	2731	2606
MAYAGUEZ AIRPORT	666083	18.24803	-67.14963	3092	2557	940	1476	3412
MAYAGUEZ CITY	666073	18.18798	-67.13962	2033	1274	1190	1542	944
PENUELAS 1 NE	666983	18.06803	-66.71964	1196	1172	2177	No Data	No Data
RINCON	668126	18.33803	-67.24965	1561	No Data	No Data	716	869
SABANA GRANDE 2 ENE	668536	18.07804	-66.92964	1787	1756	2123	1819	1419
SANTA RITA	668955	18.00802	-66.87962	No Data	605	1216	935	1129
YAUCO 1 NW	669860	18.03804	-66.85965	1097	No Data	1571	1513	1540
ARECIBO OBSERVATORY	660426	18.34802	-66.74963	2163	1959	2260	2065	2309
GUAJATACA DAM	663904	18.39800	-66.92962	1773	1592	1655	1804	1832

The Spatial Analyst extension of ArcGIS 9.2 (©ESRI Inc., 1999-2006) was used to produce the R factor raster grid (Cell size= 10 m) for all the study area. This extension has four interpolation methods: Inverse Distance Weighted, Spline, Kriging and Natural Neighbors. All interpolation methods available were evaluated using as an input calculated R factor values for 2004, and it was determined that the interpolation method which better distributed calculated values was the Spline method using the tension option (Fig. 20). The Spline method is a general-purpose interpolation that fits a minimum-curvature surface trough the input points (ESRI, 2002).

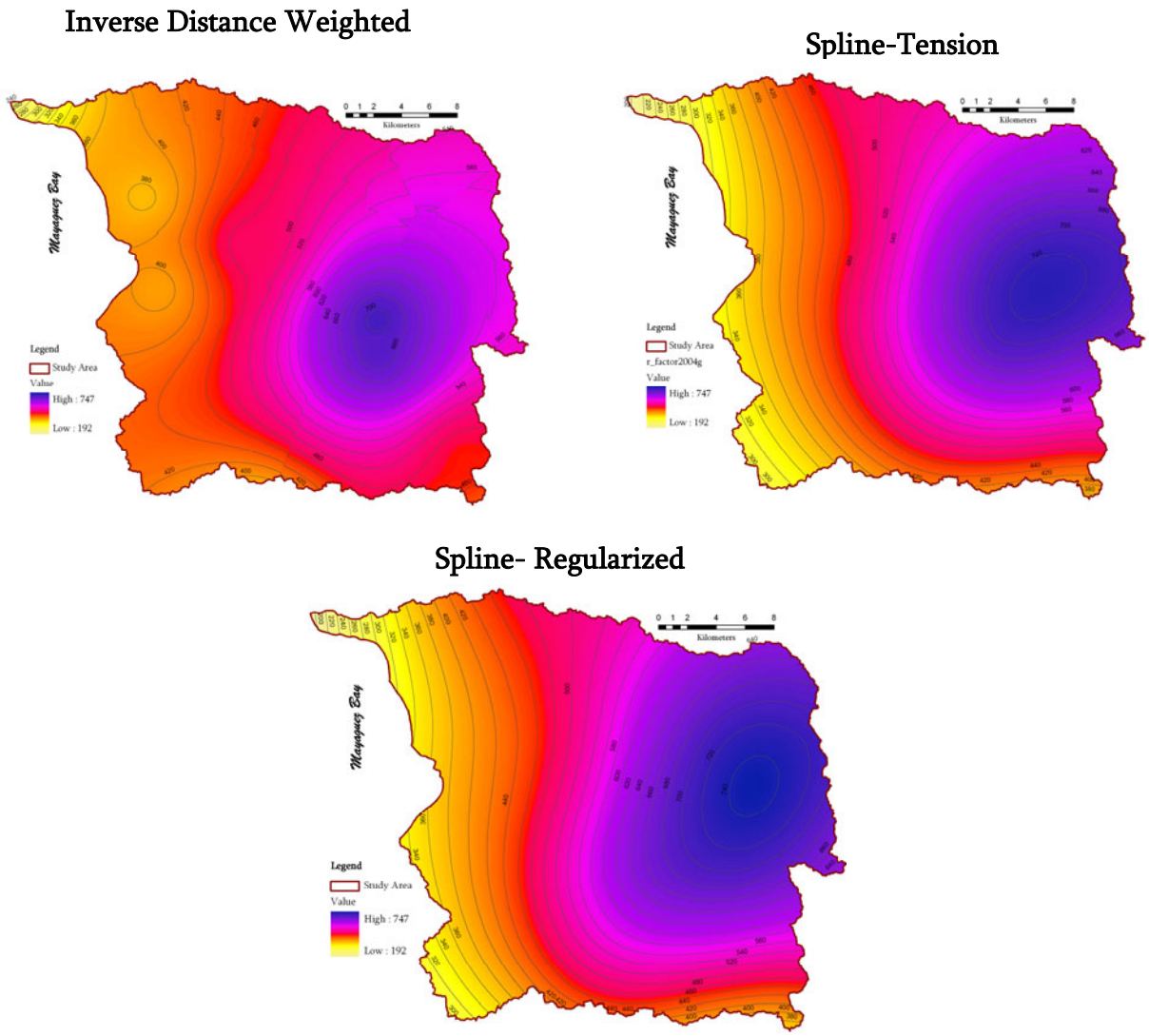

Figure 20. Output raster layers showing spatial distribution of R factor values for 2004 using three of the evaluated interpolation methods: Inverse Distance Weight, Spline using tension option and Spline using regularized option

3.2.6 Support Practice factor (P)

The support or land management practice factor expresses how surface and management practices (eg. contouring, strip-cropping and terracing) are used to reduce soil erosion. This information was not available for this study; therefore, the P factor was set as 1 assuming no control or none management practices in the area.

3.2.7 Masking Streams

One additional layer was created in order to mask, from resultant products, pixels corresponding to streams. The threshold value used to identify streams using the flow accumulation layer was 500 cells, which was determined by visual interpretation of the raster layer. All pixels with values higher or equal to 500 were assigned to 0 using the reclassification tool. These pixels corresponded to water flow channels and were not considered in the soil erosion products since used equation (RUSLE) is not designed to estimate soil loss in stream channels (Fig. 21).

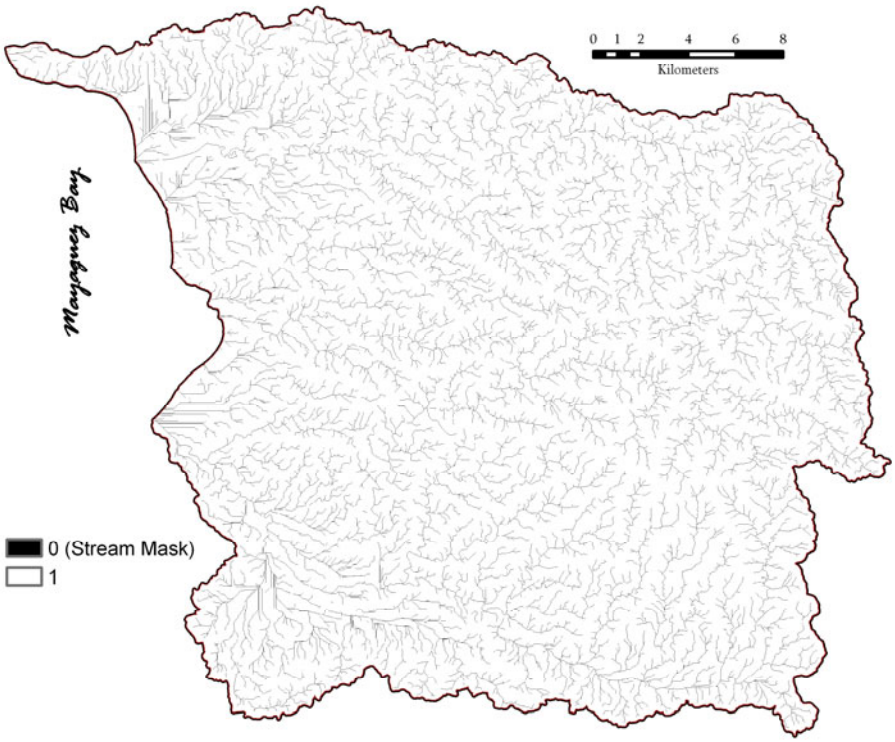

Figure 21. Stream mask layer incorporated in the GIS model in order to exclude erosion estimations corresponding to channels.

3.2.8 Soil Erosion Products

The raster calculator tool in ArcGIS 9.3 (©ESRI Inc., 1999-2006) was used to multiply all layers defined by RUSLE factors and generate a new raster layer indicating erosion rate predictions. Original resulting units of this model are tons/acre/yr however a

conversion factor of 2.242 was incorporated in equation in order to have all products in Mg/ha/yr (Renard et al., 1997).

3.2.9 Sediment Delivery Ratios

Four sub-watersheds were independently analyzed corresponding to Añasco, Yagüez and Guanajibo Rivers (Fig. 22-a) in order to generate sediment yields from contrasting areas of the entire watershed. For this approach, raster layers of soil loss rates (*A,* Mg/ha/yr) were used as input data to derive sediment yields in a sub-watershed level. The first step was to divide this product by 100 considering each pixel covers an area of 100 m^2 (cell size= 10 m); after this procedure working units were Mg/yr. Although the sum of pixels within a predetermined area corresponded to total soil loss in a year for that area, this information should not be interpreted as sediment contribution to a river flow system because it does not account for deposition occurring in the path. Sediment delivery ratios (SDR) represents the fraction of total soil loss of an area that contributes to the sediment budget in a determined point of a water flow system. It is well known that SDRs are inversely related to drainage area (Boyce, 1975). Three equations defining this relationship were evaluated:

$$SDR = 0.4724\ A^{-0.125}$$

Vanoni, 1975 **(3.4)**

$$SDR = 0.3750\ A^{-0.2832}$$

Boyce, 1975 **(3.5)**

$$SDR = 0.5656\ A^{-0.11}$$

USDA, 1972 **(3.6)**

where,

A= Watershed Area (Km^2).

Results of these equations were compared and evaluated in order to select the one with higher potential to estimate sediment yields in Mayagüez Bay watershed and sub-areas. This evaluation consisted in the analysis of a sub-watershed associated

with a USGS gauge station (50136400) from which suspended sediment discharge data was available (Fig. 22b). This station is located at Río Rosario and its catchment area was delimited using the watershed tool available in ArcGIS 9.3.

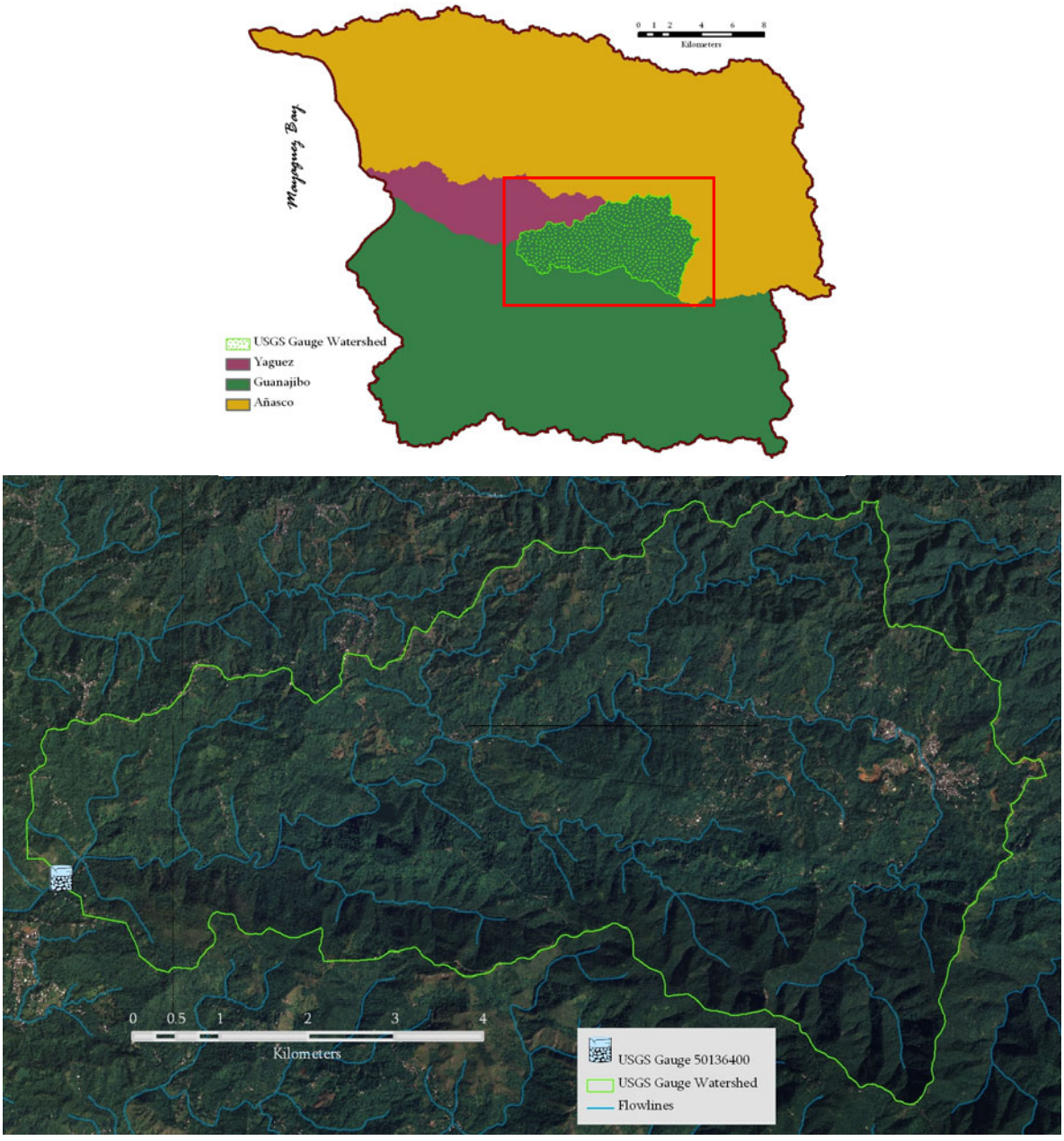

Figure 22. Sub-watersheds independently analyzed to obtain suspended yield products. At top the basis of Añasco River (yellow), Yagüez River (Magenta), Guanajibo River (Green) and Rosario river (dotted light green) are shown. At bottom the zoom of an orthorectified aerial photo (2006) showing flowlines, USGS gauge station (50136400) location and its corresponding subwartshed.

3.2.10 Suspended Sediment Load

A total of 20 MODIS images corresponding to year 2004 were processed to generate suspended sediment load products (Table 8). First, all images were processed using the same methodology described in previous chapter and then it was applied the algorithm developed to estimate TSS. Since these products provide estimations of TSS concentration, they were hardly comparable to inland sediment yield estimations from the GIS based model. In order to derive suspended sediment load products from TSS concentration, the following equation was applied to all pixels:

$$SS\ load\ (Kg) = \frac{TSS\ est\ (mg/l)}{1{,}000} * 62{,}500\, m^3 \qquad (3.7)$$

All pixel values were divided by 1,000 to change units to Kg/m^3, and then multiplied by 62,500 m^3, corresponding to the estimated volume per pixel where sediment presence can be mainly attributed to river discharge. This volume was determined by two parameters: MODIS pixel size (250 m) and depth. A preliminary analysis was made using equation defined in Table 3 in section 1.3.4 (TSS = 64.895 * ($b_{bp}620$) + 2.5188) to determine how deep TSS material is mostly influenced by river discharge. Backscattering data collected on August 17 of 2005 was used to estimate TSS and develop vertical profiles showing variations in water column associated with this parameter (Fig. 23). During this date were recorded the highest TSS concentration values within the study period (24.1 and 28.5 mg/l), therefore it was representative of water conditions dominated by TSS material. Resultant vertical profiles showed that in northern stations (I1 and O1) higher values are concentrated in the surface (0-1m), while in southern stations (I6 and O4) are in deeper areas. Considering that remote sensors mostly detect surface water and that observed high values in deep areas can be mainly attributed to bottom sediment re-suspension, it was determined that 1 m was an appropriate threshold value to set pixel volume for this analysis.

Table 8. Dates corresponding to good quality MODIS images used in the analysis of suspended sediment load.

Dates	
7-Jan-04	17-Apr-04
9-Jan-04	26-Apr-04
16-Jan-04	23-Aug-04
27-Jan-04	7-Sep-04
1-Feb-04	12-Oct-04
8-Feb-04	14-Oct-04
28-Feb-04	6-Nov-04
7-Apr-04	19-Nov-04
9-Apr-04	24-Nov-04
16-Apr-04	15-Dec-04

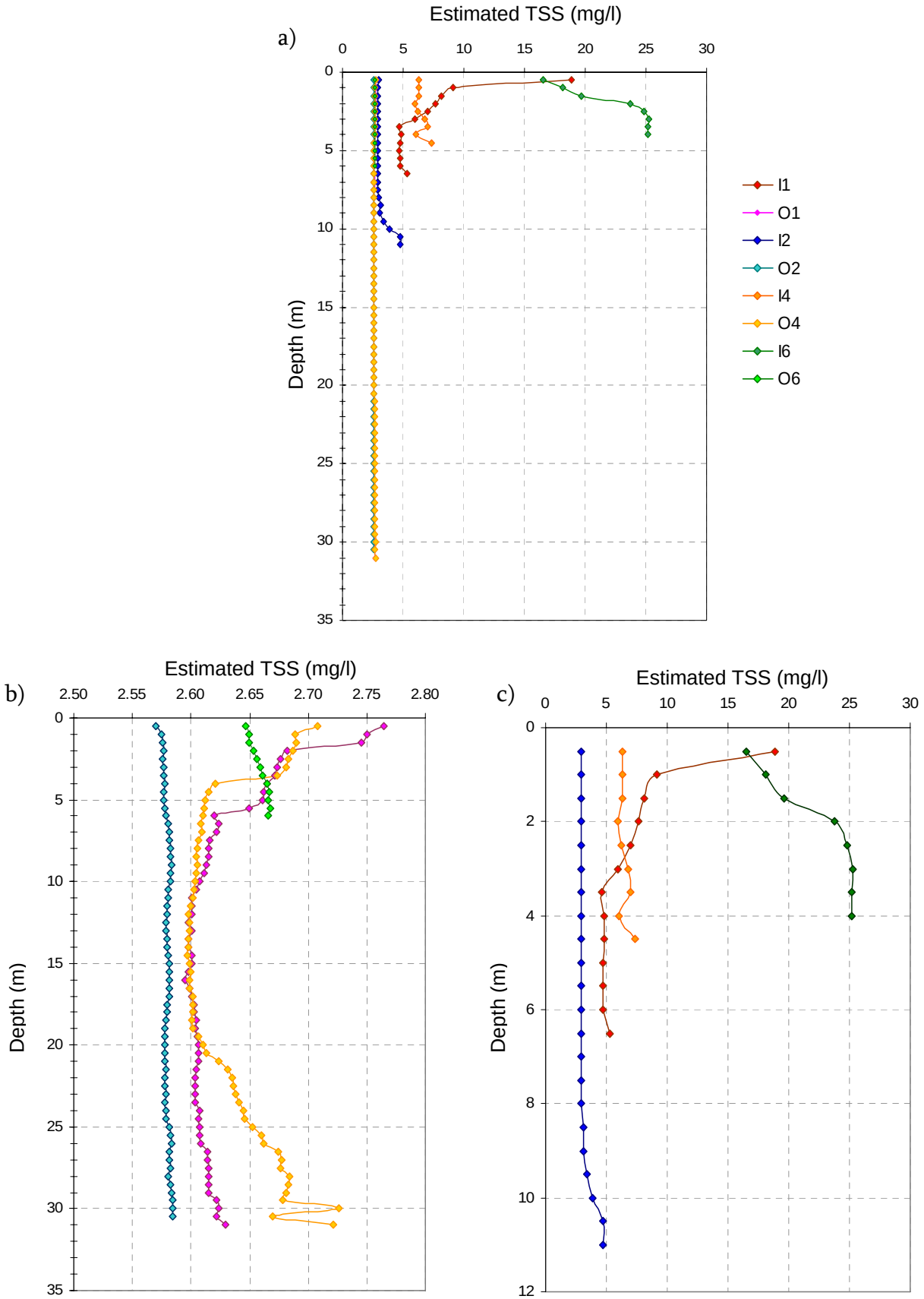

Figure 23. Vertical profiles of TSS concentration derived from particle backscattering at 620 nm. a) all stations, b) offshore stations and c) inshore stations

Finally, after applying equation 3.7 to all images, pixel values with higher potential of being influenced by suspended sediment discharge were extracted for their comparison with inland sediment yield products. Mayagüez Bay was divided in two main regions: northern and southern region (Fig. 24). After extracting pixel values corresponding to these areas in all images, it was assumed that pixels with more effect of inland processes were those higher to the mean (a single value for each image and region). Figure 24 shows an example of two areas selected in one image (January 7, 2004) using described methodology.

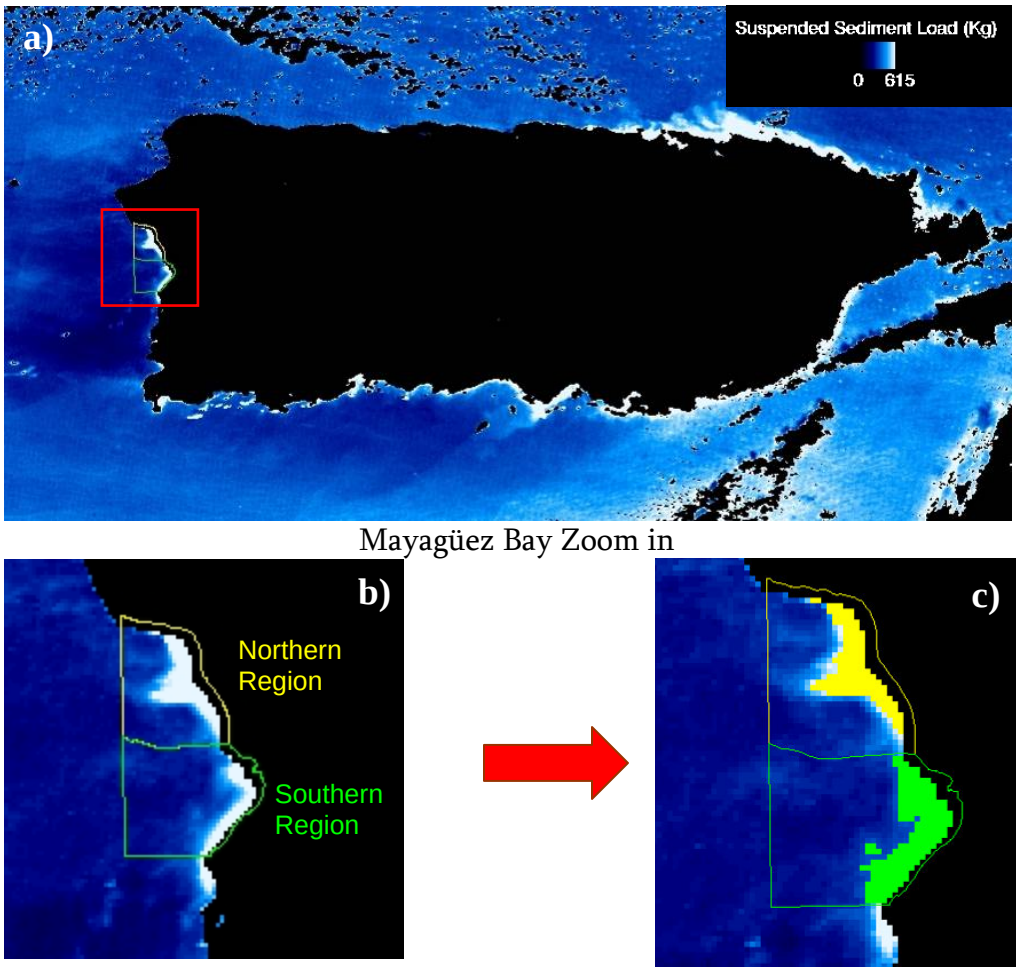

Figure 24. Illustrative description of methodology used to extract pixel values with higher effect of rivers discharge. a) Suspended sediment load product generated for Puerto Rico coastal waters in January 7 of 2004, b) Polygons delimiting northern and southern regions in Mayagüez Bay and c) Pixels in yellow and green represents selected values for analysis corresponding to the northern and southern regions, respectively.

3.3 Results and Discussion

3.3.1 Temporal and Spatial Variability of Soil Erosion Rates

RUSLE factors values were estimated and spatially defined for Mayagüez Bay watershed area resulting in four raster layers that were use as input data for the model (Fig. 25 a). The mean value of the K factor was around 0.06 ton acre hour hundreds of $acre^{-1}$ $foot^{-1}$ ton^{-1} $inch^{-1}$ with a maximum of 0.24 ton acre hour hundreds of $acre^{-1}$ $foot^{-1}$ ton^{-1} $inch^{-1}$. Soil thematic layer identified a large area (63.7 Km^2/8.5 %) in the northern area of Guanajibo watershed dominated by serpeninite outcrops, and within all this area the erodibility factor (K) was set to 0. The most common type of soil was Consumo (CoF2) which covered an area of 123.2 km^2 (16.5 %) mostly within the Añasco watershed, this series contains 26.1 percent sand, 28.9 percent silt and 45.0 percent clay and a K factor of 0.1 indicating relatively low detachment properties. Similar physical properties are observed in Mucara Series (MxE2), which covers 40.8 Km^2 (5.5 %) of the watershed mostly in Guanajibo area. Both of these soils series are derived from weathered volcanic material which has been associated with low sediment yield in eastern subwatersheds of Puerto Rico (Larsen, 1997). Soils series with highest K factor value (0.24 ton acre hour hundreds of $acre^{-1}$ $foot^{-1}$ ton^{-1} $inch^{-1}$) were Coloso (Cn) and Caguabo (CbF2) series that were distributed along the northern and southern areas of the watershed covering 33.2 km^2 (4.5 %) and 57.0 Km^2 (7.6 %) of area extent, respectively. Coloso series are mainly composed of alluvial sediment characteristic of river flood plains and low terraces; it contains 16.9 percent of sand, 48.1 percent of silt and 35.0 percent of clay, while Caguabo series is derived from basaltic material and contains 35.4 percent of sand, 33.6 percent of silt and 31.1 percent of clay. Higher K factor values are associated with loam and sandy loam textures and blocky and massive structures while combination of silty loam textures and medium or coarse granular structures are associated with low values (López-Vicente and Navas, 2009).

The most common land use in the study area are pastures with a C factor value of 0.32 which is the third highest value of this layer subsequent of bare soils (C factor= 1.0) and agricultural land (C factor = 0.5). Spatial distribution of C factors does not show significant difference between Añasco and Guanajibo watershed, with the exception of agricultural lands which are mainly located in the northern region (Añasco watershed).

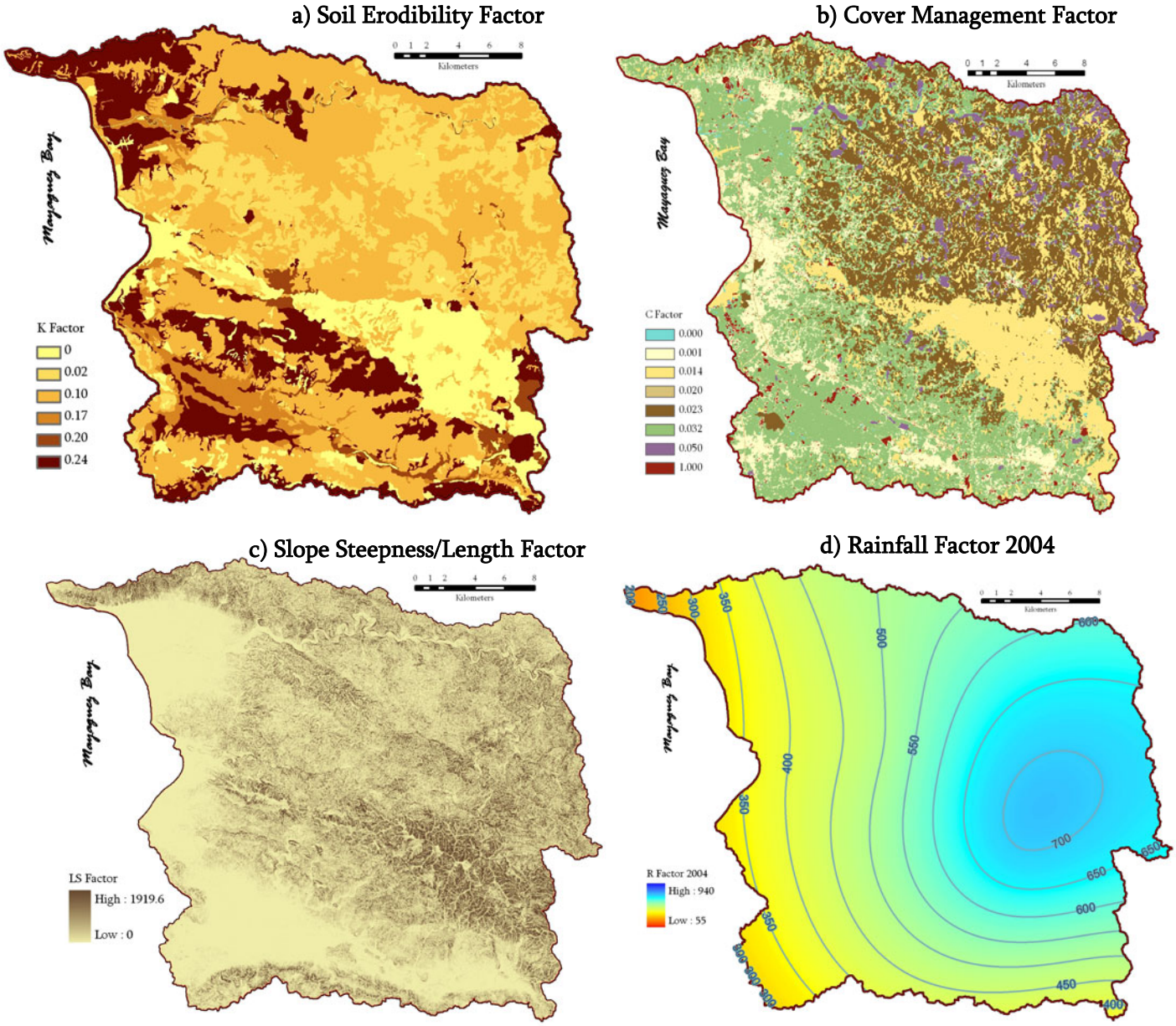

Figure 25 a. Raster layers generated to use as input data for the GIS model a) K Factor, b) C Factor, c) LS Factor, d) R Factor in 2004.

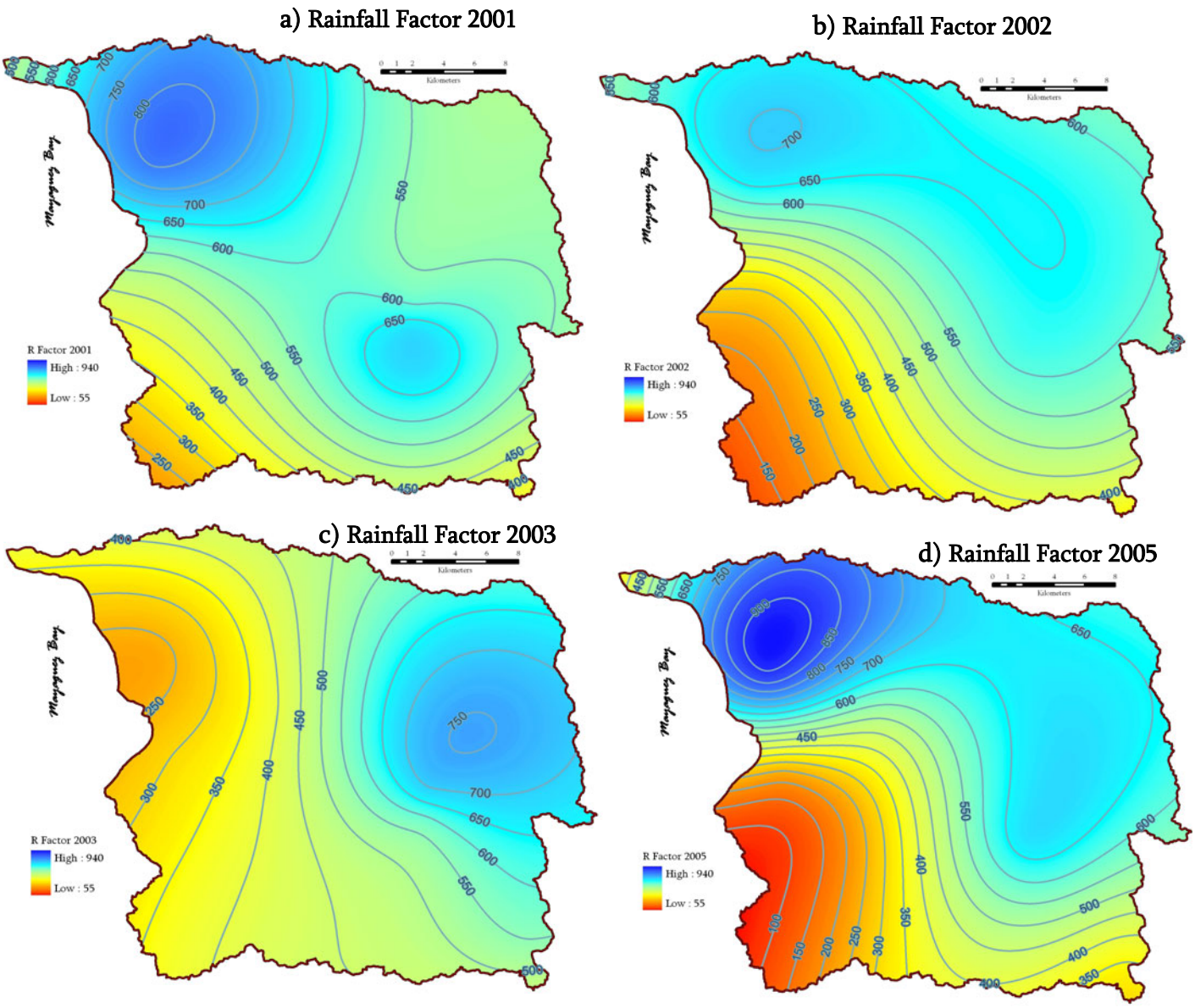

Figure 25 b. Additional raster layers of the Rainfall factor generated to perform soil erosion simulations representative of years: a) 2001 b) 2002, c) 2003 d) 2005.

Resultant LS factor values ranges from 0 to 1,919.6, with a mean value of 15.5. This large range is caused by some areas that presented slope percent greater than 100 combined with large flow accumulation values, most of these pixels were located in mountainous areas closed to stream channels. Having slope values higher than 100

percent is equivalent to a slope higher than 45 degrees corresponding to common steepness in mountainous areas of the island (Acevedo, 2009).

The R factor values were defined in raster format for the entire area using annual precipitation corresponding to five years (2001, 2002, 2003, 2004 and 2005) (Fig. 25 a, 25 b). These layers provided information with sufficient spatial and temporal resolution to perform annual simulations of developed model. Spatial variation varies along years but values tended to be higher in north-west and north-interior of the watershed. During 2005 the highest contrasting precipitation data between stations was observed, resulting in a highly variable raster layer which includes all range of R factor values (56-936 hundreds of ft * ton * inch / acre * hour * yr^{-1}) obtained within the study period. Higher values of the rainfall erosivity (R) factor were observed closed to Mayagüez Airport weather station; annual precipitation measured during this year was 3,412 mm which is almost two times higher than mean annual precipitation in this station (=1,770 mm; National Weather Service using data from 1971 to 2000). Lower R factor values were observed around Joyuda area (Cabo Rojo, Puerto Rico) mainly due to low annual precipitation registered at Mayagüez City station (944 mm), this total can be underestimated if considered that several months did not reported precipitation during that year.

Five products indicating spatial variations of erosion rate (Mg/ha*yr) were generated for the study area corresponding to 5 years from 2001 to 2005. The assemblage of this model establishes that any quantitative or spatial differences in soil erosion detected between these years will be completely controlled by the precipitation factor. Products comparison showed quantitatively variations, but not spatial significant differences were observed. Table 9 summarizes statistics of A values obtained during these years and Figure 26 shows raster layer generated for 2004. Not significant

differences were observed in soil erosion rates predictions for evaluated years. The highest mean value was observed in 2001 (55.7 Mg/ha*yr) while lowest value corresponded to 2003 (47.5 Mg/ha*yr). High erosion rates are associated with high R factor values located in steep areas. Obtained mean values are within the range of reported rates in Australia natural areas and in USA and Ivory Coast cultivated regions (Morgan, 2005). Estimations in Guadiana watershed, which is an area dominated by closed canopy forests, indicated a mean soil erosion rate of 37.9 Mg/ha*yr between 1991-1995 (López et al., 1998). Coverage data layer indicated that pastures and open canopy forests covered the highest extent of Mayagüez Bay watershed; therefore, as expected for these land uses, erosion rates predicted for this area are considerably high. Two critical regions in terms of erosion vulnerability were identified in Mayagüez Bay watershed by two factors: large amount of high A values, and closeness to a stream channel flowing into the bay. One of these areas is "Barrio Hatillo" in Rincón, a zone with very steep slopes and a high soil erodibility factor (K) value of 0.24. The other critical zone is located at Rosario Alto, which presented high erosion rates (> 100 Mg/ha*yr) in a large area closed to Rio Rosario, and important channel connected to the Guanajibo river. This area also presented steep slopes and high K Factor. Patches with extremely high erosion rates (> 500 Mg/ha * yr) mainly corresponded to areas that originally were very steep and therefore contains high values of the LS factor, but then disturbed for construction or agricultural purposes and also have high values of C factor. Although predictions in these areas responded to unreal conditions, no automatic method could be distinguished to mitigate this effect.

Table 9. Basic statistics of predicted soil erosion rates in Mayagüez Bay for the five studied years

Year	Soil Erosion (Mg/ha*year)			
	Max	Min	Mean	SD
2001	93637.1	0	55.7	405.0
2002	87536	0	51.8	374.8
2003	80030.7	0	47.5	302.4
2004	79750.7	0	49.2	297.8
2005	97772.3	0	53.1	403.1

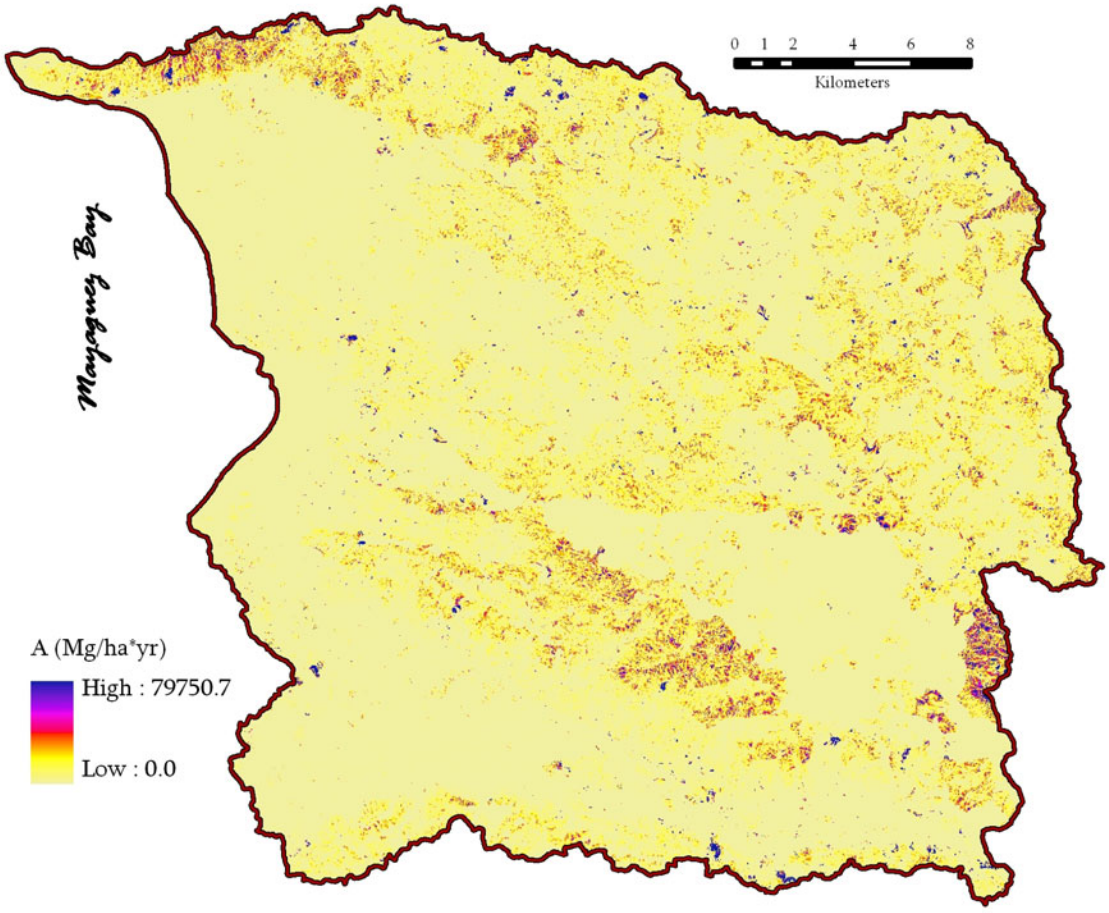

Figure 26. Soil Erosion, A, (Mg/ha*yr) as predicted using GIS model for 2004. Similar spatial variations were observed in all additional years evaluated (2001, 2002, 2003 and 2005).

3.3.2 Sediment Yield as the product of Soil Erosion Rates Multiplied by Sediment Delivery Ratios

Predictions of total erosion were obtained by summing all pixels of soil erosion (A) within specified watersheds delimited areas. Añasco and Guanajibo rivers have similar area extent, however the Guanajibo river watershed presented less amount of eroded material (mean equals to 1,479,814 Mg/yr) when compared with the Añasco river. Añasco river watershed showed the highest values during all years with a mean value of 2,333,692 Mg/yr representing a 61 percent of the total mean value estimated for the entire watershed (3,835,307 Mg/yr; Table 11). Factors affecting erosion were spatially and individually analyzed in order to explain the difference in soil erosion between these two watersheds. It was encountered that rainfall erosivity (R) factor and slope steepness/length (LS) factor were the only two factors with higher values in the Añasco river watershed while the other two factors (K,C) were higher in Guanajibo river watershed. Although southern area of this watershed presents soils with high K values, these areas were also characterized by small precipitation and short slopes with low relief. Also, there is a large area in Guanajibo watershed dominated by serpentinite outcrops (defined as 0) which reduces significantly sediment contribution from this area. On the other hand, the northern region has soils with high erodibility (e.g. Caguabo) located very close to the coast combined with high precipitation measurements and very long-steep slopes. Lower total erosion values resulted in smaller watersheds such as Yagüez and Rosario rivers, with mean estimations of 144,125 Mg/yr and 200,952 Mg/yr, respectively. Difference in soil erosion between these two areas can be attributed mainly to contrasting land uses. Yagüez river watershed has a large percent of urban areas resulting on minimal erosion potentiality while Rosario River is dominated by open canopy forests and various patches of agriculture, producing land uses with relatively high C values (Fig. 27).

All erosion rates predictions described above give an idea of variations in soil erosion potentiality between these watersheds but are theoretically incomparable to suspended sediment load to the bay since they represent the total amount eroded material and do not account for deposition occurring in the path. Sediment yield is the most suitable parameter associated with suspended sediment dynamics in the bay since it corresponds to total amount of sediment moving out of a watershed in a given time interval. In order to predict sediment yield (Mg/yr) in a watershed, it was required to multiply products of total soil erosion by sediment delivery rations (SDR).

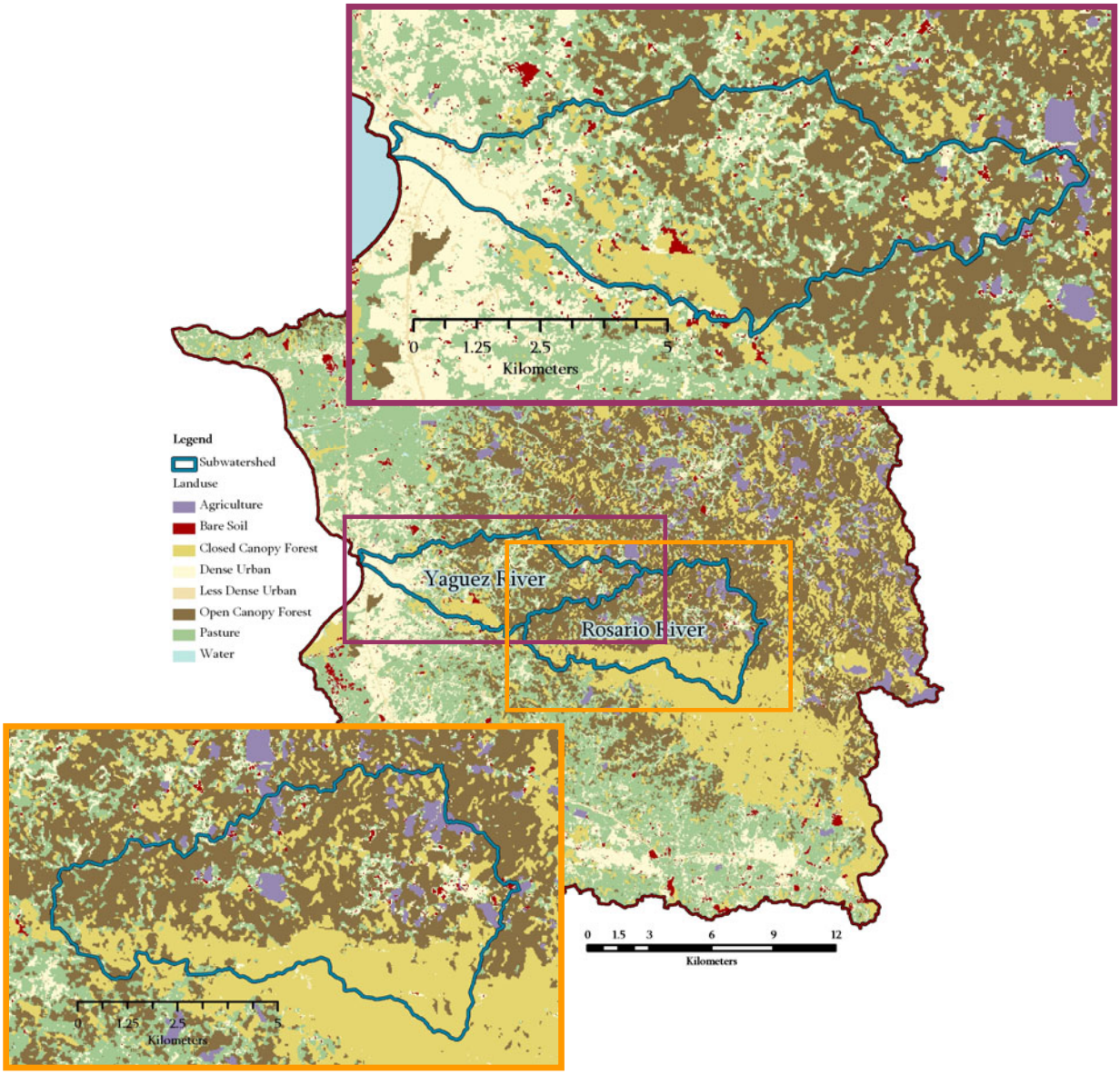

Figure 27. Zoom of Yagüez R. and Rosario R. sub-watersheds showing variation in land uses occurring in these areas.

Three equations developed to estimate SDR based on area extent (Km^2) were evaluated and compared for various sub-watersheds within the Mayagüez Bay catchment area. Equation published by USDA (1972) presented higher ratios (0.27-0.37), Boyce (1975) equation resulted on lower values (0.08-0.15), while intermediate ratios were observed using Vanoni (1975) equation (0.21-0.30). Table 10 shows the comparison of the results from these three equations. Total erosion predictions were

multiplied by corresponding SDR in order to calculate sediment yield (Table 11). Generally, relative differences in sediment yields between watersheds are equivalent to those discussed for soil erosion totals. Marked variations in sediment yield were observed between Boyce estimations and products of Vanoni and USDA equations. Three mean sediment yield products were predicted for the study period (2001-2005) resulting on 297,621 Mg/yr by Boyce, 792,647 Mg/yr by Vanoni and 1,048,004 Mg/yr by USDA; in terms of sediment yield per unit area all these values are correspondent to 399, 1,064 and 1,406 $Mg/Km^2/yr$, respectively (Table 11). Based on data collected at river gauges from October 1990 to September 2000, the US Geological Survey (USGS) reported a mean annual suspended sediment discharge for Puerto Rico western region (783 Km^2) of 960,000 Mg/yr, equivalent to 1,200 $Mg/Km^{2*}yr$ (Warne et al, 2005). These values are highly comparable to presented predictions of sediment yield when applying Vanoni and USDA formulas. On the other hand, Boyce equation resulted on lower values for this area when compared with USGS report. However, the study period of this report (1990-2000) included all mass movement occurred during Hurricane Georges event (September 21-22, 1998). Combination of an extreme value in a relatively short time period suggests that mentioned mean value (960,000 Mg/yr) is not necessarily representative of normal conditions of the area. Further in this discussion, Rosario river gauge data will be incorporated in the analysis in order to account for this consideration.

Table10. Results of calculated sediment delivery ratios for five watersheds of different extent associated with Mayagüez Bay.

Watershed	Area (Km^2)	Sediment Delivery Ratio		
		Boyce	Vanoni	USDA
Río Yagüez	41.95	0.15	0.30	0.37
Río Guanajibo	350.16	0.09	0.23	0.30
Río Añasco	353.03	0.09	0.23	0.30
Río Rosario	46.25	0.15	0.29	0.37
Mayagüez Bay	***745.15***	*0.08*	*0.21*	*0.27*

These results were compared to additional reported estimations in other areas of Puerto Rico and the World. Soil erosion predictions were estimated using a similar model at Perkerra River in Kenya (Onyando et al., 2005). Their model was developed for a large catchment area (1,207 Km^2) where it was defined a SDR of 0.83 estimating a total sediment yield of 1,430,000 Mg/yr, equivalent to 1,185 $Mg/Km^{2*}yr$. Although Perkerra River is located in a very different geographic area, this publication reported similar results to the present study when there were used SDR between 0.21 and 0.27. Similar sediment yield values with very different SDR suggests higher soil erosion rates in our area. In local areas, there have been reported sediment yields of 757 $Mg/Km^{2*}yr$ and 857 $Mg/Km^{2*}yr$ for Yahuecas and Guayo Lakes, respectively (Soler, 1999; Soler et al., 1999). These results are between estimated values when using Boyce and Vanoni's equation, and suggested that USDA equation is overestimating significantly sediment yields for this area. Annual sediment yields per unit area were estimated for four watersheds in the eastern part of Puerto Rico. Larsen (1999) reported mean fluvial sediment yields of 225, 1,163, 954, 227 $Mg/Km^{2*}yr$ for Canóvanas, Cayaguás, Icacos and Mameyes watershed, respectively. Mass-wasting erosion and fluvial sediment transport rates reported for Cayaguás and Icacos watersheds are the highest for the island of Puerto Rico (Larsen, 1999). They were mainly attributed to large coverage of pasture and agricultural lands overlain by intrusive material, which has

been associated to extreme denudation rates. Considering that the west part of Puerto Rico is dominated by volcanoclastic derived material and contains large areas with land uses characterized for low sediment production (e.g. Closed Canopy Forest, Urban, etc.), values obtained by Vanoni and USDA equations can be overestimating sediment yield in evaluated catchments.

Table 11. GIS model predictions during five simulations corresponding to years 2001, 2002, 2003, 2004 and 2005.

Watershed	[1]Total Soil Erosion (Mg/yr)	Sediment Yield (Mg/yr)			Sediment Yield per unit Area (Mg/Km^{2*}yr)		
		Boyce	Vanoni	USDA	Boyce	Vanoni	USDA
2001							
Yagüez River	169,995	26,173.31	50,334.50	63,739.83	623.92	1199.88	1,519.43
Guanajibo River	1,611,650	149,675.74	366,008.79	478,477.73	427.44	1045.25	1,366.44
Añasco River	2,369,800	219,657.42	537,635.91	702,929.51	622.20	1522.90	1,991.11
Rosario River	199,130	29,869.50	58,251.57	73,678.10	645.827	1259.49	1593.04
Mayagüez Bay	*4,151,445*	*322,152.94*	*857,983.06*	*1,134,388.67*	*432.33*	*1151.427*	*1,522.37*
2002							
Yagüez River	135,265	20,826.10	40,051.15	50,717.77	496.45	954.74	1,209.01
Guanajibo River	1,347,080	125,104.83	305,924.44	399,930.37	357.27	873.66	1,142.12
Añasco River	2,378,350	220,449.92	539,575.64	705,465.61	624.44	1528.40	1,998.29
Rosario River	198,585	29,787.75	58,092.14	73,476.45	644.06	1256.05	1,588.68
Mayagüez Bay	*3,860,695*	*299,590.69*	*797,893.48*	*1,054,940.79*	*402.06*	*1070.79*	*1,415.75*
2003							
Yagüez River	169,995	15,048.20	28,939.55	36,646.87	358.72	689.86	873.59
Guanajibo River	1,611,650	138,518.20	338,724.77	442,809.74	395.58	967.33	1,264.58
Añasco River	2,369,800	180,799.80	442,527.57	578,580.57	512.13	1253.50	1,638.88
Rosario River	202,990	30,448.50	59,380.73	75,106.30	658.35	1283.91	1,623.92
Mayagüez Bay	*3,539,828*	*274,691.32*	*731,579.54*	*967,263.31*	*368.64*	*981.79*	*1,298.08*
2004							
Yagüez River	124,854	19,223.17	36,968.52	46,814.16	458.24	881.26	1,115.96
Guanajibo River	1,593,480	147,988.27	361,882.35	473,083.29	422.63	1033.47	1,351.03
Añasco River	1,950,710	180,811.85	442,557.07	578,619.13	512.17	1253.58	1,638.99
Rosario River	215,759	32,363.85	63,116.05	79,830.83	699.76	1,364.67	1,726.07
Mayagüez Bay	*3,669,044*	*284,718.53*	*758,284.79*	*1,002,571.87*	*382.10*	*1017.63*	*1,345.47*
2005							
Yagüez River	120,515	18,555.12	35,684	45,187.24	442.32	851	1,077.18
Guanajibo River	1,235,210	114,715.33	280,519	366,717.63	327.60	801	1,047.27
Añasco River	2,599,800	240,976.18	589,816	771,152.05	682.59	1,671	2,184.36
Rosario River	188,298	28,244.70	55,083	69,670.26	610.70	1,191	1,506.38
Mayagüez Bay	*3,955,525*	*306,949.51*	*817,492*	*1,080,853.24*	*411.93*	1,097	*1,450.52*
Mean							
Yagüez River	144,125	19,965	38,395	48,621	476	915	1,159
Guanajibo River	1,479,814	135,200	330,612	432,204	386	944	1,234
Añasco River	2,333,692	208,539	510,422	667,349	591	1446	1,890
Rosario River	200,952	30,143	58,785	74,352	652	1271	1,608
Mayagüez Bay	*3,835,307*	*297,621*	*792,647*	*1,048,004*	*399*	*1064*	*1,406*

[1] Based on developed GIS model

Results of this model were also evaluated based on suspended sediment (SS) discharge measurements collected at Rosario River USGS gauge station (50136400) during water years 1991 to 2000 as reported by Warne et al. (2005). According to this report, mean annual SS discharge at Rosario River station is 58,000 Mg, very similar to predicted values when applying Vanoni's equation that resulted on 58,785 Mg/yr (Table 11). An additional analysis was performed including SS discharge data of same origin but specific to years evaluated during model simulations. The highest mean daily SS discharge (122.28 Mg/day) was observed in 2003 while the lowest (29.74 Mg/day) in 2002 (Table 12). Maximum discharge observed along the study period was 24,585 Mg/day and it took placed on November 13 of 2003, within a week where heavy rains over Puerto Rico led numerous mud, land and rock slides with around 45 million dollars in total damages and 19 municipalities declared as a federal disaster (NOAA National Weather Service). This event caused a rise of 4.6 m in Guanajibo River at San German, which was considered the 8th highest river rise of all monitored rivers in Puerto Rico. Although 2003 sediment yield estimation was the second higher for the study period, the model did not identify a significant increase at Rosario watershed (Fig. 28). This can be explained with distribution of high R values for this year that were mainly located in areas of low erosion potential. Mean annual SS discharge from 2001 to 2005 was 26,402.47 Mg, a value significantly lower than reported for this station (1990-2000 mean equals to 58,000 Mg; Warne et al., 2005). Several studies indicated that within a year, 93% of the suspended sediments export from this type of systems is transported during storm events (Pérez-Alegría, personal communication, Díaz, 2004). During 1990 to 2000 three hurricanes (Marilyn in 1995, Hortense in 1996 and Georges in 1998) affected Puerto Rico area causing, within other effects, torrential flooding. Contrasting mean values can be dismissed if considered that annual SS discharge measured in 1998 at this gauge station was 364, 671 Mg, a value 14 time higher than annual mean for the period of 1986 to 1997

(25,820 Mg). Therefore observed values for evaluated time period are representative of normal condition in the watershed and are suitable for adjustment and validation of the model.

Table 12. Summary statistics of suspended sediment discharge data obtained from USGS Río Rosario gauge station (50136400) corresponding to years 2001, 2002, 2003, 2004 and 2005.

Year	Suspended Sediment Discharge (Mg/yr)	Suspended Sediment Discharge (Mg/Km²*yr)	Min (Mg/day)	Max (Mg/day)	Mean (Mg/day)	Median (Mg/day)
2001	18,336.41	431.44	0.07	4,917.02	50.24	0.71
2002	10,853.62	255.38	0.05	1,542.24	29.74	0.65
2003	44,633.04	1,050.19	0.07	24,585.12	122.28	1.09
2004	33,622.17	791.11	0.05	7,484.40	91.86	0.75
2005	24,567.10	578.05	0.05	2,948.40	67.31	1.54
Mean	**26,402.47**	**621.23**				

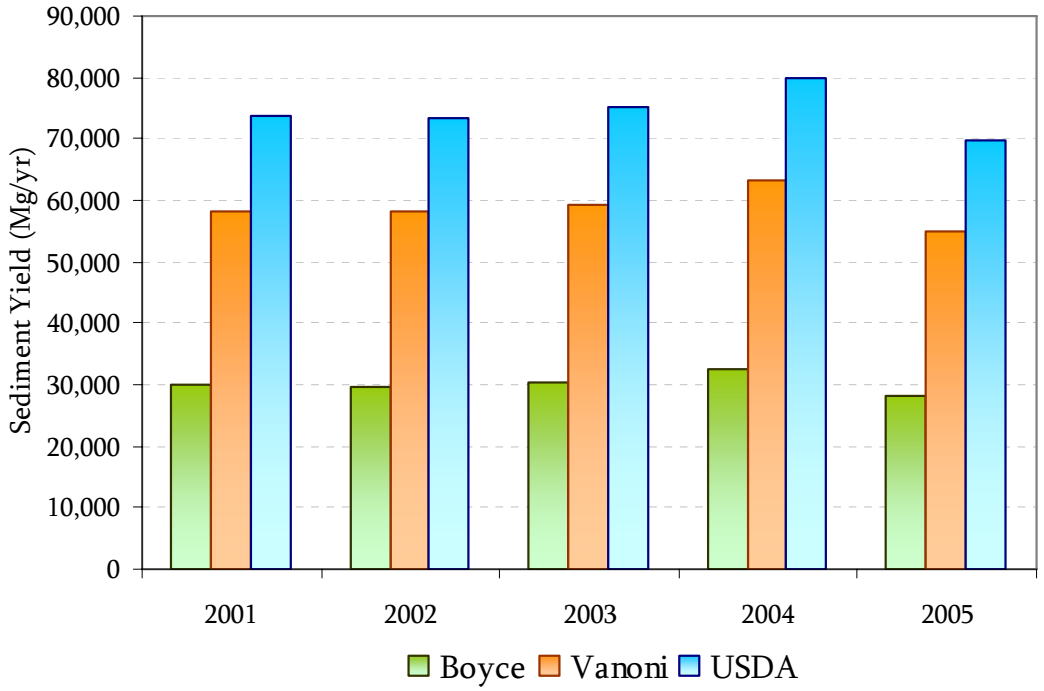

Figure 28. Comparison of Rosario River sediment yield results (Mg/yr) for simulated years (2001, 2002, 2003, 2004 and 2005) by applying three equations based on Boyce, 1975, Vanoni et al., 1975, and USDA, 1972.

In order to select the most appropriate equation to estimate sediment yield in Mayagüez Bay watershed, sediment delivery ratios were calculated by dividing SS discharge (as measured at gauge station 50136400) by sediment yield predictions for this area (Table 13). This analysis resulted in a mean SDR of 0.13, very closed to corresponding calculated ratio using Boyce equation. Comparison between sediment yield estimations for Rosario river watershed after applying Boyce equation and observed SS discharge indicates that model best predictions corresponded to years 2004 and 2005 (Fig. 29). Developed model did not detect temporal variations during the study period but it was able to fairly predict sediment yield for those years from which the land use layer was representative. A sensitivity analysis was conducted in order to determine how much impact all defined factors have in the model, and it was encountered that the LS (Slope Steepness/Length) factor has the highest effect in resultant soil erosion rates values followed by the C (Cover Management) factor (Table 14). Although it is difficult to detect variations in the LS factor when working with a large area, for future studies it is important to account for land use coverage variations additionally to precipitation even when working in a relative short study period. Generally, presented model provide an excellent resource to monitor erosion vulnerability and sediment transport in a watershed. The next section will illustrate how these results can be integrated in a remote sensing based coastal study using results obtained in 2004.

Table 13. Estimated sediment delivery ratios for five simulated years.

Year	[1]Estimated Total Soil Erosion (Mg/yr)	[2]Suspended Sediment Discharge (Mg/yr)	Resultant Sediment Delivery Ratio
2001	199,130.00	18,336.41	0.09
2002	198,585.00	10,853.62	0.05
2003	202,990.00	44,633.04	0.22
2004	215,759.00	33,622.17	0.16
2005	188,298.00	24,567.10	0.13
			Mean = 0.13

[1] Based on developed GIS model; [2] Based on USGS Gauge Station 50136400

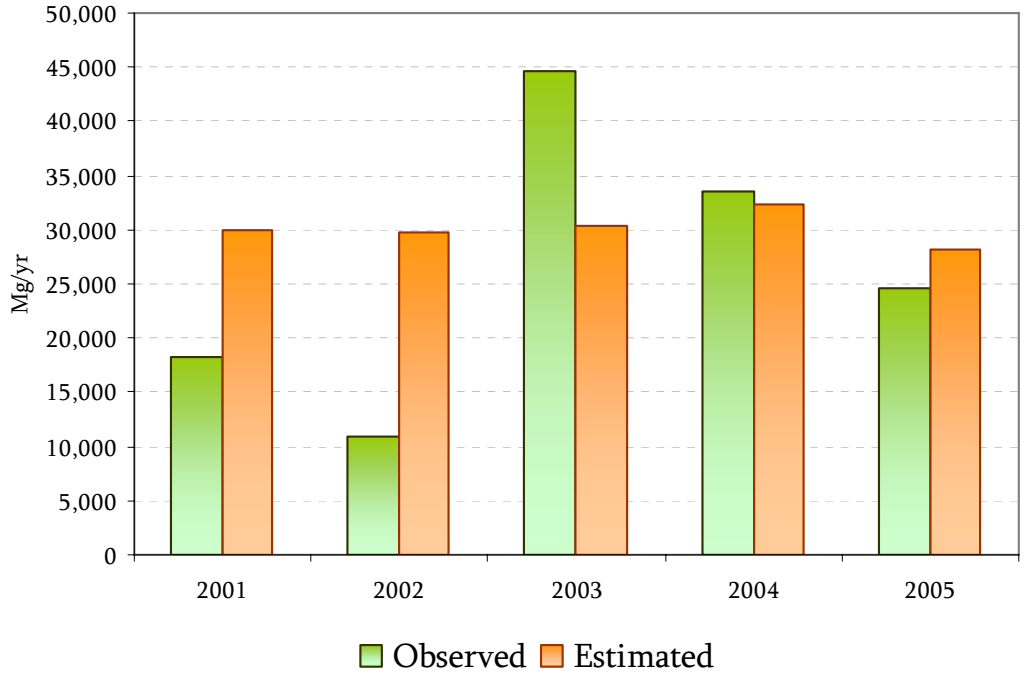

Figure 29. Validation results of GIS model using estimation sediment yield after applying Boyce equation and observed suspended sediment discharge at USGS gauge station (50136400)

Table 14. A sensitivity analysis showing predicted results (A, Soil Erosion Rate) of the GIS model under six different extreme conditions.

Condition	R	K	LS	C	P	A (tons/acre*yr)	A (Mg/ha*yr)
All factors presenting low values	200	0.02	0.05	0.001	1	0.0002	0.0004
All factors presenting high values	600	0.28	72.15	1	1	12121.2000	27175.7304
High Rainfall (R) Factor	600	0.02	0.05	0.001	1	0.0006	0.0013
High Soil Erodibility (K) Factor	200	0.28	0.05	0.001	1	0.0028	0.0063
High Slope Steepness/Length (LS) Factor	200	0.02	72.15	0.001	1	0.2886	0.6470
High Cover and Management (C) Factor	200	0.02	0.05	1	1	0.2000	0.4484

3.3.3. Land-sea interface analysis results

Suspended sediment load products were generated using MODIS data for twenty dates corresponding to year 2004 (Table 8). Independent analyses were made for the northern and southern regions of the bay in order to account for existing differences

in suspended sediment dynamics between these two areas. Relative variations in suspended sediment load were similar with the exception of one date (October 14, 2004) that detected an extreme value (339.5 Mg) at the Añasco plume that was not observed in the southern area (Fig. 30). Geomorphology of this coastal system suggests that the northern part of the bay is mostly influenced by the Añasco River contributing area (353 Km^2) while along southern regions, the higher amount of inland water comes from Yagüez and Guanajibo sub-watersheds (392 Km^2). Variations in water flow systems within these catchments were compared with suspended sediment load products in order to determine the potential of this innovative methodology for land-sea interface studies. An excellent relationship (R^2=0.87) between Guanajibo and Añasco river discharge measurements was encountered for dates included in this analysis (Fig. 31). Good correspondence of river discharge in these stations indicates that there is no major difference in the relative variation between the northern and southern part of the bay in terms of fresh water input, however previous analysis identified one date (October 14, 2004) that certainly did not meet this condition. The suspended sediment load generated for this date detected a large amount of material released by the Guanajibo River but this was all directed to the south, outside the area extracted for this analysis (Fig. 32). Based on these results it was determined that results from this method underestimate the amount of TSS material discharged by the Guanajibo River. This can cause discrepancies of results in this area when compare with sediment yield estimations of the GIS based model. On the other hand, the developed method was able to capture the Añasco River plume values, making this area more suitable for association with inland values.

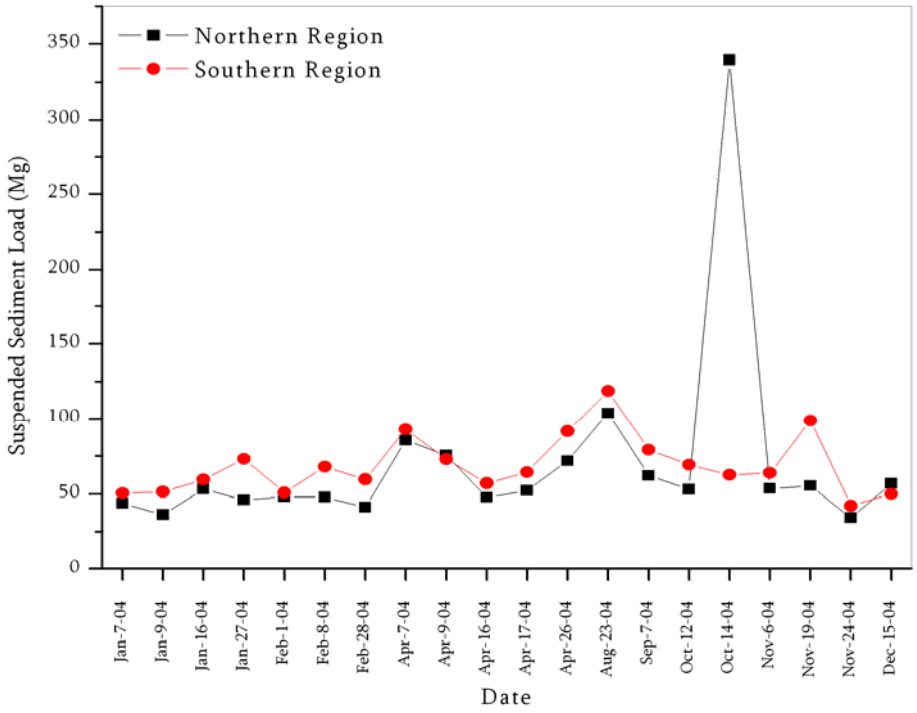

Figure 30. Suspended sediment load for the twenty dates included in the land-sea interface analysis. Note that these are discrete values and lines do not represent a temporal continuity, they were included for illustration purposes only.

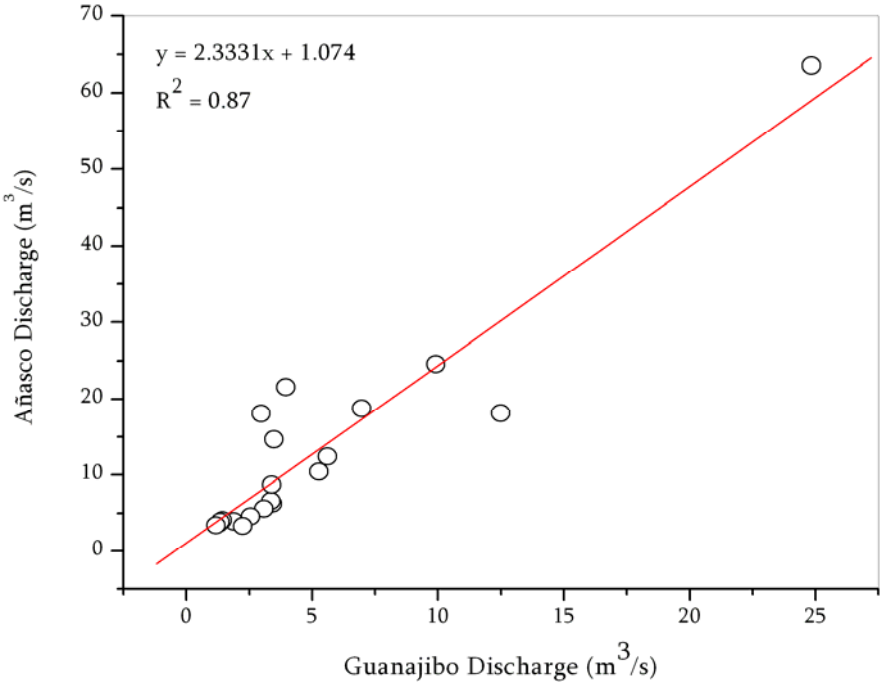

Figure 31. Regression analysis between annual river discharge data collected during dates used for analysis at two USGS gauge stations (50144000 in Añasco watershed and 50138000 in Guanajibo watershed).

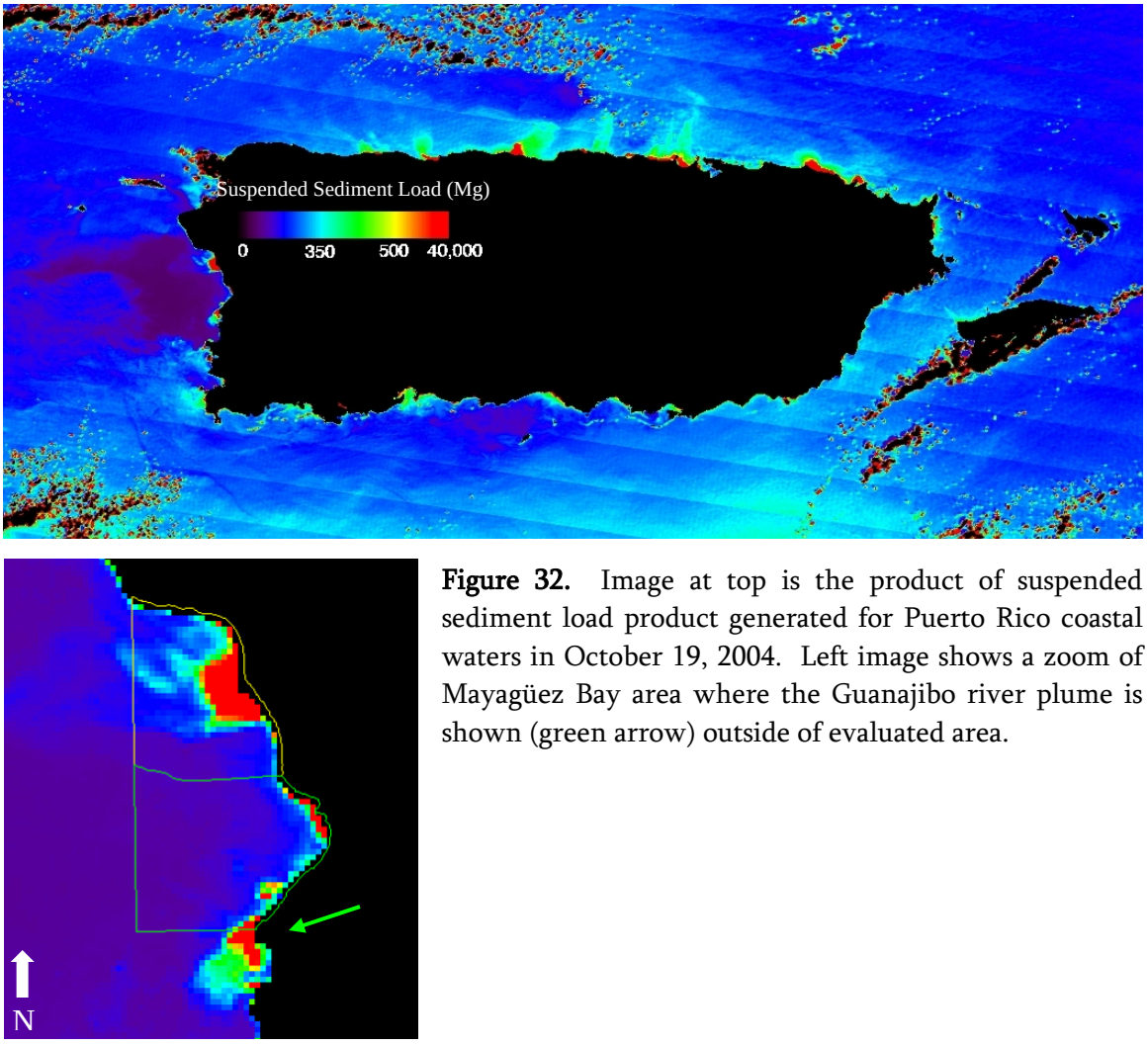

Figure 32. Image at top is the product of suspended sediment load product generated for Puerto Rico coastal waters in October 19, 2004. Left image shows a zoom of Mayagüez Bay area where the Guanajibo river plume is shown (green arrow) outside of evaluated area.

Two relationships were defined between estimated suspended sediment load in the northern part of the bay and river discharge (Añasco River gauge station 50144000) (Fig. 33), because most of the river discharge values remained lower than 25 m^3/s and there was only one extreme value of 63.6 m^3/s. No relationship was encountered when using clustered data (R^2= 0.001), and a fairly good relationship was defined when the high value was included (R^2=0.71). Equivalent results were observed when using Guanajibo River discharge data (USGS gauge station 50138000). In order to have more robust conclusions, it is necessary to incorporate more data corresponding to events with high river discharge. Additional observations will make it easier to detect a threshold value that will determine the minimum river discharge required to

detect a significant reflectance response in the image. Present results, suggest that this value is between 25 and 63 m^3/s but the large gap in the data causes a large uncertainty in the analysis. Days in which these conditions occurred are not rare considering that in 2004 a total of 39 dates resulted in river discharge values greater than 25 m^3/s. A major limitation in this approach is the common high percent of cloud coverage during days with high river discharge. For this study purposes, it was assumed that detected relationship between MODIS-derived suspended sediment load (Mg) and Añasco River discharge (m^3/s) is correct with the extreme value.

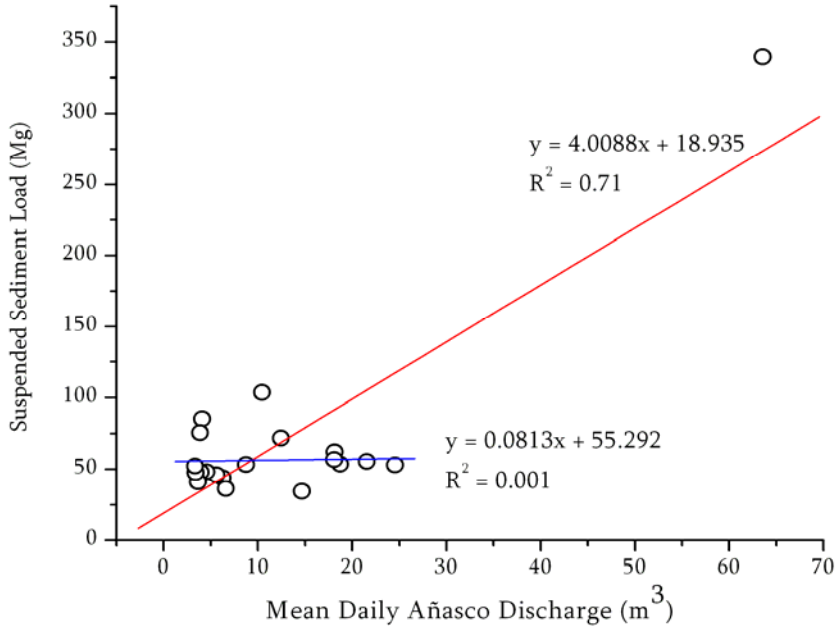

Figure 33. Relationship between Añasco River mean daily discharge (USGS gauge station 50144000) and estimations of suspended sediment load derived from MODIS data. Two straight lines represent the linear fit of these two parameters including all data (red) and clustered data only (blue).

Suspended sediment load values were estimated for every day of 2004 using the defined linear equation (y = 4.0088x + 18.935), and then added to get a total of 26,216 Mg. This estimation is equivalent to annual suspended sediment load for the Añasco river watershed and can be compared with two inland products: sediment yield results from the GIS based model, and a calculation derived from suspended sediment

data from Rosario River gauge station. According to the GIS based model, sediment yield for the Añasco River in 2004 was 180,812 Mg (Table 11). While, when extrapolating annual suspended sediment discharge rate of 2004 (727 Mg/Km^2; calculated from field data of Rosario River 50138000 USGS gauge station) to the Añasco watershed resulted in an annual suspended sediment discharge of 256,278 Mg for this area. A high contrast is observed between inland calculated values and suspended sediment load estimations in the bay, which mainly corresponded to a significant underestimation of remote sensing derived products. This limitation can be diminished by modifying spatial and temporal parameters defined during the process. For instance, if it is assumed that estimated suspended sediment load represents a twelve hours period of river discharge, the annual load will increase to 314,593 Mg. A more complex analysis including sediment deposition rates can be incorporated in future studies to better define this parameter. Another factor that can be causing an underestimation is the exclusion of pixels associated to the Añasco river discharge during the pixel extraction process. An increase in the spatial extension of extracted values will result on higher suspended sediment load estimations; however, this action can reduce correspondence of this parameter to river discharge data. Developed methodology should be extended to additional years in order to refine the definition of parameters and improve the integration of derived products.

3.4. CONCLUSIONS

The developed GIS model was able to identify spatial variations in soil erosion rates in Mayagüez Bay watershed for five years between 2001 and 2005. Two areas, located in the north and middle-south of this basin, were identified as important contributors of TSS material to its water-flow system. Soil erosion rates estimations were within mean values reported for other areas in Puerto Rico, where Añasco and Rosario river sub-watershed had the highest values and Guanajibo river catchment area the lowest.

USGS data reflected that the years evaluated in this study had normal annual suspended sediment discharge values, when compared to parallel data corresponding to period between 1986 and 1997 (mean equals to 25,819.7 Mg/yr). The equation developed by Boyce (1975) to estimate SDR corresponded more closely with the calculated fraction between soil erosion model predictions and USGS suspended sediment discharge data. The other two equations evaluated, Vanoni et al. (1975) and USDA (1972), appeared to overestimate SDR for this area. Simulation corresponding to year 2004 presented the best validation results for the study period, but the model was not able to predict temporal variations, neither a notable increased in mass movement occurred during one of the evaluated years (2003). Modification of the rainfall factor in a yearly basis is not sufficient to detect temporal changes during a five years period in a large catchment when using RUSLE.

The major limitation in the studied area to perform analyses including remote sensing derived data is the large percent of cloud coverage in satellite images. Derived suspended sediment load for the southern part of Mayagüez Bay did not account for spatial variation of TSS associated with Guanajibo River, therefore products for this area were not suitable for a land-sea interface analysis using developed method. Although the relationship defined between SS load in the northern part of the bay and Añasco River discharge was completely controlled by one event, observed correspondence among these parameters suggested that incorporation of more data associated with high river discharge can produce better results in an equivalent analysis. Integration of inland estimates with coastal products indicates a significant underestimation of suspended sediment load values that are based on remote sensing. This does not preclude the use of developed methodologies in future applications, but suggests that several modifications are required in the definition of spatial and temporal parameters during the process.

GENERAL CONCLUSIONS

Results of this study promote the used of remotely derived data to generate total suspended sediment operational products in Mayagüez Bay and provided various conclusions that support this effort:

- The range between 589 nm and 645 nm has the higher potential for remote sensing single band applications. Analyses of *in situ* measurements indicated that within this range TSS dominated the water-leaving signal in this area.

- A positive relationship was detected between particle backscattering and TSS concentration, this analysis also suggested that the southern part of the bay is optically different to the rest of the area since field measurements collected at the station located near Guanajibo River plume (i.e. Station I6) contributed large variability to defined regression.

- When performing regression analyses between satellite sensors and *in situ* measurements it is important to consider that exponential equations may provide better results.

- The higher square correlation coefficient (R^2) observed between TSS concentration and *in situ* R_{rs} was found when using red to green ratios (i.e. 655 nm/545 nm). Additional sensors should be explored in order to incorporate two bands analyses in future assessments.

- MODIS band 1 is appropriate to derive TSS products; however, its spatial resolution (250 m) resulted in a significant limiting factor for the development of required algorithms. This study was able to generate this type of product for Mayagüez Bay area with reasonable validated results, but additional field and remote measurements that represent high TSS concentration should be incorporated in the dataset in order to strengthen the relationships.

- The Dark Subtract method was not very effective for atmospheric correction in this study. Additional atmospheric corrections should be evaluated but considering that global algorithms (e.g. SeaDAS L2gen command) are not suitable for their application in this area.

This study also presented an innovative methodology which integrates inland sediment yield estimations (from a GIS based model) with coastal suspended sediment load products (from satellite images derived data).

- GIS technology facilitated the application of the Revised Universal Soil Loss Equation (RUSLE) to calculate annual soil erosion rates for Mayagüez Bay watershed in a five years period.

- Derived products of annual soil erosion rates were useful to identify areas with higher potential of erosion, but they were not effective detecting temporal variations within the study period. Changing the rainfall factor was not sufficient to detect changes on annual basis, even when working in relatively small period of time (five years).

- According to validation results, it was determined that Boyce (1975) equation to calculate sediment delivery ratios is the best of the three evaluated equations in this area.

- Methodology presented to estimate suspended sediment load products from MODIS band 1 data did not accounted for southward movement of Guanajibo river plume, a different spatial extent defining Mayagüez Bay area is necessary in order to include this region in land-sea interface applications.

- Defined spatial and temporal parameters to estimate suspended sediment load from MODIS data were not the most appropriate, since predicted value for the

Añasco River in 2004 were significantly lower than corresponding inland sediment yield estimated value. Several adjustments in these parameters were suggested in order to improve satellite derived estimates that can be evaluated by including additional years in similar analyses.

CONCLUSIONES GENERALES

Los resultados de este estudio promueven el uso de datos derivados de imágenes de satélite para generar productos operacionales de concentración de sedimento suspendido en la Bahía de Mayagüez y se definieron varias conclusiones que apoyan este esfuerzo:

- El rango espectral entre 589 nm y 645 nm tiene mayor potencial en percepción remota en aplicaciones de una sola banda. Los análisis de las mediadas *in situ* mostraron que en este rango el sedimento suspendido domina la señal que sale del agua en el área estudiada.

- Se detectó una relación positiva entre la retrodispersión de las partículas y la concentración del total de sedimento suspendido (TSS), este análisis sugirió que el área sur de la bahía es ópticamente diferente que el resto de la bahía debido a que las medidas de campo colectadas en la estación localizada cerca de la desembocadura de Río Guanajibo (Station I6) contribuyeron gran parte de la variabilidad observada en la regresión definida.

- Es importante considerar el uso de ecuaciones exponenciales cuando se realizan análisis de regresión entre medidas derivadas de datos de satélite y medidas de campo.

- En el análisis de la concentración de TSS y las medidas *in situ* de reflectancia teledectectada (R_{rs}) se observó un valor más alto en el coeficiente de correlación al cuadrado (R^2) cuando se utilizaron razones de bandas verde y rojo (655 nm/545 nm). En futuros estudios se deberían explorar censores adicionales que permitan incorporar análisis con dos bandas.

- La banda 1 de MODIS es apropiada para derivar productos de TSS; sin embargo, su resolución espacial (250 m) resultó ser un factor limitante durante

el desarrollo de los algoritmos deseados. En este estudio se logró generar este tipo de producto para el área de la Bahía de Mayagüez con resultados razonablemente validados, pero para lograr fortalecer las relaciones definidas es importante incorporar medidas de campo y teledetectadas adicionales que sean representativas de condiciones con concentraciones de TSS altas.

- En este estudio el método de substracción del píxel más oscuro no fue muy efectivo durante la corrección atmosférica. Se deberían evaluar correcciones atmosféricas adicionales considerando que correcciones basadas en algoritmos globales (por ejemplo, comando de SeaDAS L2gen) no son apropiadas para su aplicación en esta área.

Este estudio también presenta una metodología innovadora que integra estimados de producción de sedimento en la zona terrestre (de un modelo basado en Sistemas de Información Geográfica, SIG) y descarga de sedimento en la costa (basados en datos derivados de imágenes satelitales).

- Utilizar la tecnología de SIG facilitó la aplicación de la Ecuación Universal de Pérdida de Suelos Revisada (RUSLE, por sus siglas en Inglés) para calcular tazas de erosión anual en la cuenca de la Bahía de Mayagüez para un periodo de cinco años.

- Los productos de tazas de erosión anual derivados fueron bien útiles para identificar las áreas con mayor potencial de erosión, pero no fueron efectivos detectando variaciones temporales en el periodo de estudio. Aún cuando se trabaja en un periodo de estudio corto (cinco años), cambiar solamente el factor de precipitación (R) para detectar cambios temporales anuales no es suficiente.

- De acuerdo con los resultados de validación, se determinó que la ecuación desarrollada por Boyce (1975) para calcular la razón de descarga de sedimento es la más apropiada de las tres ecuaciones evaluadas para esta área.

- La metodología presentada para estimar productos de TSS utilizando datos de la banda 1 de MODIS no consideró el movimiento hacia Sur observado en la pluma del Río Guanajibo, es necesario definir para la Bahía de Mayagüez una extensión espacial diferente para lograr incluir esta región en futuras aplicaciones que integren productos terrestres y costeros.

- Los parámetros espaciales y temporales definidos para estimar descarga de sedimento suspendido utilizando datos de MODIS no fueron los más apropiados, debido a que los valores estimados para el Río Grande de Añasco en el 2004 fueron significativamente menores a los estimados de producción de sedimento equivalentes generados para esta zona. Para mejorar los estimados derivados de datos de imágenes satelitales se sugirieron varios ajustes que podrían ser aplicados a estos parámetros realizando pruebas similares en años adicionales.

REFERENCES

Acevedo-González, M.J. (2009). The Topography of Puerto Rico. *Encyclopedia of Puerto Rico*. May 27, 2009. http://www.encyclopediapr.org

Althius, IJ. A. (1998). Suspended Particulate Matter detection in the North Sea by hyper spectral airborne remote sensing. *Aquatic Ecology, 32,* 93-98.

Álvarez, A. (2005). Channel planform dynamics of an alluvial tropical river. *Doctoral Dissertation*. Texas A&M University.

Austin, R. (1974). The remote sening of spectral radiance from below the ocean surface. In: N. G. Jerlov, & E. Steemann Nielsen (Eds.), *Optical aspects of oceanography* (pp. 317-344). London, New York: Academic Press.

Arnold, J.G., Williams, J.R., Nicks, A.D. & Sammons, N.B. (1990). SWRRB: A Basin Scale Simmulation Model for Soil and Water Resource Management. User's Manual Texas A&M University Press, College Station.

Arnold, J.G., Williams, J.R., Srinivasan, R., King, K.W. (1996). SWAT: Soil and Water Assessment Tool. User's Manual USDA Agriculture Research Service Grassland, Soil and Water Research Laboratory, 808 East Blackland Road Temple, TX 76502, p. 190.

Baker, E. T., Tennant, R. A., Feely, G. T. & Walker, S. L. (2001). Field and laboratory studies on the effect of particle size and composition on optical backscattering measurements in hydrothermal plumes. *Deep-Sea Research, Part I, 48,* 593-604.

Beasly, D.B. & Hugins, L.F. (1982). ANSWERS: Areal non-point source watershed environmental response simulation. User's Manual, U.S. EPA Report, Chicago, IL, p. 54.

Behera, S. & Panda, R.K. (2006). Evaluation of management alternatives for an agricultural watershed in a sub-humid subtropical region using a physical process based model. Agriculture, *Ecosystem and Environment*, 113, 62-72.

Binding, C.E., Bowers, D. G. & Mithelson-Jacob, E. G. (2003). An algorithm for the retrieval of suspended sediment concentrations in the Irish Sea from SeaWiFS ocean colour satellite imagery. *International Journal of Remote Sensing, 24(19),* 3791–3806.

Binding, C.E., Bowers, D.G. & Mitchelson-Jacob, E.G. (2005). Estimating suspended sediment concentrations from ocean colour measurements in moderately turbid waters: the impact of variable particle scattering properties. *Remote Sensing of Environment, 94*, 373-383.

Boss, E., W. S. Pegau, M. Lee, M. Twardowski, E. Shybanov, G. Korotaev, & F. Baratange (2004a). Particulate backscattering ratio at LEO 15 and its use to study particle composition and distribution. *Journal Geophysical Research, 109,* C01014, doi:10.1029/2002JC001514.

Boss, E., Stramski, D., Bergann T., Pegau, S., & Lewis, M. (2004b). Why should we measure optical backscattering? *Oceanography, 17(2)*, 46-49.

Bowers, D.G. & Binding, C.E. (2006). The optical properties of mineral suspended particles: A review and synthesis. *Estuarine Coastal and Shelf Science, 67,* 219-230.

Bowers, D.G., Evans, D., Thomas, D.N., Ellis K. & Williams, P.J. le B. (2004). Interpreting the colour of an estuary. *Estuarine Coastal and Shelf Science, 59,* 13-20.

Boyce, R.C. (1975). Sediment routing with sediment delivery ratios. Present and Prospective Technology for ARS. USDA, Washington, D.C.

Cameron, A. (2003). Spectral Analyses and Sedimentation of the West Coast Beaches of Puerto Rico . *Undergraduate Research*. University of Puerto Rico at Mayagüez, Department of Geology.

Carter, M., Elsner, J.B. & Bennet, S. (1997). Monthly rainfall climatology for Puerto Rico. Technical attachment: SR/SSD 97040.

Cartwright, J.H. (2002). Identifying potential sedimentation sources through a Remote Sensing and GIS analysis of Landuse/Lancover for the Weeks Bay watershed, Baldwin County, Alabama. *Master Thesis*. Mississippi State University.

Chang G.C. & Gould, R.W. (2006). Comparisons of optical properties of the coastal ocean derived from satellite ocean color and *in situ* measurements. *Optics express, 14 (22)*, 10149-10163.

Chen, Z., Hu, C. & Muller-Karger, F. (2007). Monitoring turbidity in Tampa Bay using MODIS/Aqua 250-m imagery. *Remote Sensing of Environment, 109,* 207–220.

Corvera, R. (2005). Aportación de nitrógeno, fósforo y sedimentos suspendidos durante eventos de tormenta en micro cuencas del Río Grande de Añasco, Puerto Rico. *Master Thesis*. University of Puerto Rico at Mayagüez, Department of Agronomy.

Cruise, J.F. & Miller, R.L. (1994). Hydrologic Modeling of Land Processes in Puerto Rico Using Remotely Sensed Data. *Water Resources Bulletin*, 30(3), 419-428.

Curran, P. & Novo, E.M.M. (1988). The relationship between suspended sediment concentration and remotely sensed spectral radiance: A review. *Journal of Coastal Research, 4 (3)*, 351-368.

Dana, D.R., & Maffione R.A. (2002). Determining the Backward Scattering Coefficient with Fixed-Angle Backscattering Sensors-Revisited. Presented as a poster at Ocean Optics XVI Santa Fe New Mexico.

Díaz, J. (2004). Modeling sediment export potential of the Río Caonillas Watershed. *Master Thesis*. University of Puerto Rico at Mayagüez, Department of Civil Engineering.

Doxaran, D., Froidefond, J., Lavender, S., & Castaing, P. (2002a). Spectral signature of highly turbid waters; application with SPOT data to quantify suspended particulate matter concentrations. *Remote Sensing of Environment, 81,* 149– 161.

Doxaran, D., Froidefond, J., & Castaing, P. (2002b). A reflectance band ratio used to estimate suspended matter concentrations in sediment dominated coastal waters. *International Journal of Remote Sensing, 23 (23)*, 5079– 5085.

Doxaran D., Froidefond, J.M., & Castaing P. (2003). Remote-sensing reflectance of turbid sediment-dominated waters. Reduction of sediment type variations and changing illumination conditions effects by use of reflectance ratios. *Applied Optics, 42 (15),* 2623-2634.

Doxaran, D., Nagur Cherukuru R. C. & Lavander S. J. (2004). Estimation of surface reflection effects on upwelling radiance field measurements in turbid waters. *Journal of Optics: Pure and Applied Optics, 6,* 690-697.

D'Sa, E.J. & Miller R.L. (2003). Bio-optical properties in waters influenced by the Mississippi River during low flow conditions. *Remote Sensing of Environment, 84,* 538–549.

ESRI (2000-2002). Using ArcGIS 3D Analyst (ArcGIS 8.3 user manual), p.72-75.

Eswaran, H., Lal, R. & Reich, P.F. (2001). Land degradation: an overview. In: Bridges, E.M., Hnnam, I.D.,Oldeman, L.R., Penning the Vries, F.W.T., Scherr, S.J., Sombatpanit, S. (Eds.), Response to land degradation. Science Publishers Inc, Enfield, NH, USA, pp. 20-35.

Froidefond J.M, Gardelb L., Guiralb D., Parrab M., Ternonb J.F. (2002). Spectral remote sensing reflectances of coastal waters in French Guiana under the Amazon influence. *Remote Sensing of Environment, 80,* 225-232.

Gardner, T. A., Côté, I. M., Gill, J. A., Grant, A., Watkinson, A. R. (2003). Long-term region-wide declines in Caribbean corals. *Science, 301,* 958–960.

Gilbes, F., López, J.M., & Yoshioka, P.M. (1996). Spatial and temporal variations of phytoplankton chlorophyll-a and suspended particulate matter in Mayagüez Bay, Puerto Rico. *Journal of Plankton Research, 18 (1),* 29-43.

Grove, K. (1977). Sedimentation in Añasco bay and river estuary: Western Puerto Rico. *Master thesis*. University of Puerto Rico at Mayagüez, Department of Marine Sciences.

Guerriero, A., Matarrese, R., Morea, A., Tijani, K. (2007). A Grid Enabled Look-Up Table for Aerosol Optical Thickness Estimation on Coastal Water, *Proc. of the 9th WSEAS Int. Conf. on Mathematical and Computational Methods in Science and Engineering*, Trinidad and Tobago, November 5-7, 137-140.

Hellweger, F. L., Schlosser, P. & Weissel, J. K. (2004). Use of satellite imagery for water quality studies in New York Harbor. *Estuarine, Coastal and Shelf Science, 61,* 437-448.

Hu, C., Chen, Z., Clayton, T.D., Swarzenski, P., Brock J.C., Muller-Karger F.E. (2004). Assessment of estuarine water-quality indicators using MODIS medium-resolution bands: Initial results from Tampa Bay, FL, *Remote Sensing of Environment, 93,* 423-441.

Hubbard, D. K. (1987). A general review of sedimentation as it relates to environmental stress in the Virgin Islands Biosphere Reserve and the eastern Caribbean in general. *Biosphere Reserve Report No. 20, Virgin Islands Resource Management Cooperative*, St. Thomas, US Virgin Islands.

Huot, Y., Morel, A., Twardowski, M. S., Stramski, D., Reynolds, R. A. (2007). Particle optical backscattering along a chlorophyll gradient in the upper layer of the eastern South Pacific Ocean. *Biogeosciences Discussion, 4,* 4571–4604.

HydroScat-6 Spectral Backscattering Sensor: User's Manual (2007). Hydro-Optics, Biology, & Instrumentation Laboratories, Inc.

Jetten, V., Govers, G. & Hessel, R. (2003). Erosion models: Quality of spatial predictions. *Hydrological Processes,* 17 (5), 887-900.

Johanson, R.C. Imhoff, J.C., Davis, H.H., Kittle, J.L., Donigian, A.S. (1984). HSPF: Hydrologic Simulation Program-Fortran. *User's Manual, EPA Environmental Research Laboratory*, Athens, Georgia.

Jordan, T.E. & Flemings, P.B. (1991). Large scale stratigraphic architecture, eustatic variation, and unsteady tectonism: a theorical evaluation. *Journal of Geophysical Research, 96,* 6681-6699.

Karabulut M. & Ceylan N. (2005). The spectral Reflectance Responses of Water with Different Levels of Suspended Sediment in The Presence of Algae. *Turkish J. Eng. Env. Sci, 29 (2005)*, 351-360.

Larsen, M.C. (1997). Tropical geomorphology and geomorphic work: A study of geomorphic processes and sediment and water budgets in montane humid-tropical forested and developed watersheds, Puerto Rico: *Doctoral Dissertation*, University of Colorado Geography Department, 341 p.

Li, R. & Li, J. (2004). Satellite Remote Sensing Technology for Lake Water Clarity Monitoring: An Overview, *Environmental Informatics Archives,2,* 893-901.

López-Vicente, M. & Navas, A. (2009). Predicting soil erosion with RUSLE in Mediterranean agricultural systems at catchment scale. *Soil Science 174 (5),* 272–282.

López, T., Mitchell, A. & Scatena, F.N. (1998). The effect of Land Use on Soil Erosion in the Guadiana Watershed in Puerto Rico. *Caribbean Journal of Science*, 34(3-4): 298-307.

Maffione, R. A. & Dana, D. R. (1997). Instruments and methods for measuring the backward-scattering coefficient of ocean waters, *Applied Optics, 36,* 6057-6067.

Mattson, P. H. (1960). Geology of the Mayagüez area. *Geological Society of America Bulletin* 71:319-362.

McKee, D. & Cunningham, A. (2006). Identification and characterisation of two optical water types in the Irish Sea from in situ inherent optical properties and seawater constituents. *Estuarine, Coastal and Shelf Science, 68,* 305-316.

Menon, H. B., Lotliker, & A., Nayak, S. R. (2005). Pre-monsoon bio-optical properties in estuarine, coastal and Lakshadweep waters. *Estuarine, Coastal and Shelf Science, 63*, 211–223

Miller, R. L., Cruise, J. F., Otero, E., & López, J. M. (1994). Monitoring Suspended Particulate in Puerto Rico: Field measurements and remote sensing, Water Resources *Bulletin: American Water Resources Association, 30 (2),* 271-283.

Miller, R. L. & McKee, B. A. (2004). Using MODIS Terra 250 m imagery to map concentration of total suspended matter in coastal waters. *Remote Sensing of Environment, 93,* 259-366.

Miller, R.L., McKee, B.A. & D'Sa, E.J., (eds.). (2004). Monitoring bottom sediment resuspension and suspended sediments in shallow coastal waters, *Remote Sensing of Coastal Aquatic Environment*, 259-276, Springer, Printed in the Netherlands.

Moore, G. F., Aiken, J., & Lavander, S. J. (1999). The atmospheric correction of water colour and the quanti tative retrieval of suspended particulate matter in Case II waters: application to MERIS. *International Journal of Remote Sensing, 20 (9),* 1713-1733.

Morel, A., Gentili, B., Claustre, H., Babin, M., Bricaud, A., Ras, J., & Tièche, F. (2007). Optical properties of the "clearest" natural waters. *Limnoogy and Oceanograghy, 52 (1),* 217-229.

Morelock, J., Grove, K., & Hernández, M.L. (1983). Oceanography and patterns of shelf sediments Mayagüez, Puerto Rico. *Journal of Sedimentary Petrology, 53 (2),* 0371-0381.

Morgan, R.P.C. (2005). Soil Erosion and Conservation. 3rd ed. Blackwells Publ. Malden, MA.

Mueller, J. L., Morel, A., Frouin, R. T. Davis C., Arnone, R., Carder, K., Lee, Z. P., Steward, R. G., Hooker S., Mobley C. D., McLean S., Holben B., Miller M., Pietras C., Knobelspiesse K. D., Fargion G. S., Porter J., Voss K. (2003). Ocean optics protocols for Satellite Ocean Color validation, Revision 4, Volume III: Radiometric Measurements and Data Analysis Protocols. In Mueller J.L., Fargion G. S. and McClain C.R. (Eds.). *NASA/TM 2003-21621* (pp. 28-29) Greenbelt, MD: NASA Goddard Space Flight Center.

Mueller, J. L., & Austin, R. W. (1995). Ocean optics protocols for SeaWiFS validation, revision 1. In S. B. Hooker, & E. R. Firestone (Eds.), *NASA Tech. Memo. 104566, vol. 25* (pp. 1 – 67). Greenbelt, MD: NASA Goddard Space Flight Center.

Nasr A.H., El Leithy, B.M., Helmy, A.K. (2007). Assessment of Some Water Quality Parameters Using MODIS Data along the Red Sea Coast, Egypt, *Proc. of* 3rd *WSEAS International Conference on Remote Sensing,* Venice, Italy, November 21-23, 570-423.

NOAA National Weather Service. Puerto Rico and U.S. Virgin Islands Severe Rainfall- November 12-14, 2003. January 12, 2009. Retrieved on August 23, 2009. http://www.srh.noaa.gov/sju/?n=2003_flood01

OceanColor Webmaster (2008) http://oceancolor.gsfc.nasa.gov/seadas/doc/l2gen/l2gen.html

Onyando, J. O., Kisoyan, P., & Chemeli, M. C. L. (2005). Estimation of Potential Soil Erosion for River Perkerra Catchment in Kenya. *Water Resources Management, 19,* 133–143.

Peckhman, S.D. (2007). A new method for estimating suspended sediment concentrations and deposition rates from satellite imagery based on the physics of plumes, *Computers Geosciences*, 24, 1198-1222.

Pico, R. (1974). The Geography of Puerto Rico. Chicago Illinois, Aldine Publishing Co., 439.

Piere, R. G. (1967). Clay mineralogy of Bahía de Añasco, western Puerto Rico: Puerto Rico Nuclear center Marine Biology Program, *Progess Summary Report* no. 5, p. 663-642.

Reid, L. M. & Dunne, T. (1996). Rapid evaluation of sediment budgets. *Catena Verlag GMBH.*, D-35447, Reiskirchen, Germany, 164 pp.

Renard, K.G., Foster, G.R., Weesies, G.A., McCool, D.K., Yoser, D.C., 1997. Predicting Soil Erosion by Water: A guide to conservation planning with the Revised Universal Soil Loss Equation (RUSLE). USDA, Agricultural Research Service, Agricultural Handbook Number 703.

Ritchie, J. C., Schiebe, F. R., & McHenry, J. R. (1976). Remote sensing of suspended sediments in surface waters. *Photogrammetric Engineering and Remote Sensing, 42 (12)*, 1539-1545.

Roosta, H., Farhoudi, R., Roosta, M. (2007). Multi Temporal Disaggregation of MODIS Images Using Non-Linear Analysis, *Proc. of 5th WSEAS Int. Conf. on Environment, Ecosystems and Development*, Tenerife, Spain, December 14-16, 2007, 222-227.

Rosado-Torres, M. (2000). Variability in the bio-optical properties of Mayagüez Bay *Master thesis*. University of Puerto Rico at Mayagüez, Department of Marine Sciences.

Rosado-Torres, M. (2008). Evaluation and Development of Bio-optical Algorithms for Chlorophyll Retrieval in Western Puerto Rico. *Doctoral Dissertation*. University of Puerto Rico at Mayagüez, Department of Marine Sciences.

Santos, H. (1999). Stratigraphy and Depositional History of the Upper Cretaceous Strata in the Cabo Rojo–San German Structural Block, southwestern Puerto Rico. *Doctoral Dissertation.* University of Colorado, unp.

Schalles, J. F., Rundquist, D. C. & Schiebe, F. R. (2001). The influence of suspended clays on phytoplankton reflectance signatures and the remote sensing estimation of chlorophyll. *Verh. Internat. Verin. Limnol, 27*, 3619-3625.

Simms, A. D., Woodroffe, C. D. *&* Jones, B. G. (2003). Application of RUSLE for Erosion Management in a Coastal Catchment, Southern NSW. *In Proceedings of MODSIM 2003: International Congress on Modelling and Simulation*, Volume 2, Integrative Modelling of Biophysical, Social and Economic Systems for Resource Managment Solutions, Townsville, Queensland, 14-17 July 2003, 678-683

Soler-López, L.R. (1999). Sedimentation survey of Lago Guayo, Puerto Rico, October 1997. U.S. Department of Interior & U.S. Geological Survey. Water-Resources Investigations Report 99-4053.

Soler-López, L.R., Webb, RM.T. & Pérez-Blair, F. (1999). Sedimentation survey of Lago Yahuecas, Puerto Rico, March 1997. U.S. Department of Interior & U.S. Geological Survey. Water-Resources Investigations Report 98-4259.

Stramski, D., Boss, E., Bogucki, D. & Voss, K.J. (2004). Review: The role of seawater constituents in light backscattering in the ocean. *Progress in Oceanography, 61,* 27–56.

Sydor M. & Arnone, R. A. (1997). Effect of suspended particulate and dissolved organic matter on remote sensing of coastal and riverine waters. *Applied Optics, 36 (27),* 6905-6912.

Teodoro A.C., Veloso-Gomes, F. & Goncalves, H. (2008). Statistical Techniques for Correlating Total Suspended Matter Concentration with Seawater Reflectance Using Multispectral Satellite Data. *Journal of Coastal Research*, *24(4C),* 40-49.

Tzortziou, M., Subramaniam, A., Herman J.R., Gallegos, C.L., Neale, P.J., Lawrence, W.H. (2007). Remote sensing reflectance and inherent optical properties in the mid Chesapeake Bay. *Estuarine, Coastal and Shelf Science, 72,* 16-32.

US Department of Agriculture (1975). Sediment Sources, Yields, and Delivery Ratios. National Engineering Handbook, Section 3 Sedimentation.

US Department of Agriculture Natural Resources Conservation Service. (1995). Revised Universal Soil Loss Equation: Caribbean Area. San Juan, Puerto Rico.

United States Geological Survey (2008). Caribbean Water Science Center Webmaster http://vi.water.usgs.gov/

Vanoni, V.A. (1975). Sedimentation Engineering, *Manual and Report* No. 54. American Society of Civil Engineers, New York, N.Y.

Veve, T. & Taggart, B. (1994). Atlas of ground water resources in Puerto Rico and the U.S. Virgin Islands, *U.S. Geological Survey Water Resources Report* 94-4198. Reston, VA.

Villalta, C. (2004). Selección de funciones de transporte de sedimentos para los ríos de la Bahía de Mayagüez usando SAM. *Master Thesis*. University of Puerto Rico at Mayagüez, Department of Civil Engineering.

Volckmann, R.P. (1983). Geologic map of the Cabo Rojo and Parguera quadrangles,southwest Puerto Rico: U.S. Geological Survey Miscellaneous Investigations Series Map I-1557, 1 sheet, scale 1:20,000.

Walling, D.E. (1997). The response of sediment yields to environmental change. Human Impact on Erosion of Sedimentation, Proceedings of Rabat Symposium S6, April 1997. IAHS Publ. no. 245.

Wang, X., Wang, Q., Liu, G., & Li, H. (2005). A study on the Quantitative Remote Sensing Model for the Suspended Sediment Concentration in Coastal Water with ASTER. *Conference paper, Report no. A290054*.

Warne, A.G, Webb, R.M.T. & Larsen, M.C. (2005). Water, Sediment, and Nutrient Discharge Characteristics of Rivers in Puerto Rico, and their Potential Influence on Coral Reefs. *USGS Scientific Investigations Report 2005-5206*.

Webb, R., Collar, P., Schwab, W., Goenaga, C., García, J. & Castro, R. (2000). Assement of the habitats, biota, sediments, and the water quality near the discharge of primary-treated effluent from the Mayagüez regional wastewater treatment plant, Bahía de Añasco, Puerto Rico. *USGS- Water Resources Investigations Report* 99-4141.

Weil, E. (2004). Coral reef diseases in the wider Caribbean (pp. 35-68) in *Coral Health and Diseases*. Rosenberg, E. & Loya, Y., eds., New York: Springer Verlag.

Wernand, M.R., Shimwell, S.J., Boxall, S., van Aken, H.M. (1998). Evaluation of specific semi-empirical coastal colour algorithms using historic data sets. *Aquatic Ecology, 32,* 73–91.

Wischmeier, W.H. (1976). Use and misuse of the universal soil loss equation. *Journal of Soil and Water Conservation*, *31 (1),* 5-9.

Wild-Allen, K., Lane, A. & Tett, P. (2002). Phytoplankton, sediment and optical observations in Netherlands coastal water in spring. *Journal of Sea Research, 47,* 303– 315.

Williams, J.R., Jones, C.A. & Dyke, P.T. (1984). A modeling approach for determining the relationship between erosion and soil productivity. *Trans. ASAE, 27 (2)*, 168-173.

Witte, W.G., Whitlock, C.H., Morris, W.D., Gurganus, E.A. (1982). Laboratory Upwelled Radiance and Reflectance Spectra of Kerr Reservoir Sediment Waters. *National Aeronautics and Space Administration Technical Paper 1993*, Report No. NASA TP – 1993.

Young, R.A., Onstad, D.D. & Anderson, W.P. (1989). AGNPS: a non-point source of pollution model for evaluating agricultural watersheds. *Journal of Soil and Water Conservation*, 44(2), 168-173.